

Secretion Of Vimentin And Its Influence On Cellular Functionality

Dissertation

zur Erlangung des Grades

des Doktors der Naturwissenschaften

der Naturwissenschaftlich-Technischen Fakultät

der Universität des Saarlandes

von

Divyendu Goud Thalla

Saarbrücken

2023

Tag des Kolloquiums: 14. März 2023

Dekan: Prof. Dr. Ludger Santen

Berichterstatter: Prof. Dr. Franziska Lautenschläger
Dr. Bin Qu

Akad. Mitglied: Dr. Alexis Darras

Vorsitz: Prof. Dr. Alexandra K. Kiemer

TABLE OF CONTENTS

ABSTRACT	5
ZUSAMMENFASSUNG	6
ACKNOWLEDGEMENTS	7
ABBREVIATIONS	8
LIST OF FIGURES	9
1 INTRODUCTION	10
1.1 Cytoskeleton	10
1.1.1 Actin Filaments	11
1.1.2 Microtubules	11
1.1.3 Intermediate Filaments	12
1.2 Vimentin	13
1.2.1 Secreted Vimentin	13
1.2.2 Surface Vimentin	16
1.2.3 Extracellular vimentin and IGF1-R interaction	18
2 AIM	19
3 FINDINGS OF THE THESIS	20
3.1 Influence Of Extracellular Vimentin In Cancer And SARS-Cov-2	21
3.1.1 Extracellular Vimentin Promotes Proliferation in MCF-7 Cells through Activation of IGF-1R	21
3.1.2. Extracellular Vimentin Promotes Stronger Adherence to the Underlying Substrate for MCF-7 Cells	22
3.1.3 Extracellular Vimentin Induces Migration of MCF-10a and MCF-7 Cells	23
3.1.4 Extracellular Vimentin Effects Alterations of Cell Monolayer Integrity Caused by the Receptor Binding Domain of SARS-CoV-2 Spike Protein	25
3.2 Vimentin secretion and its effect on macrophage functionality	27
3.2.1 Activated macrophages express cell-surface vimentin in a polarised manner	27
3.2.2 Extracellular cell-surface vimentin is predominantly expressed at the back of activated macrophages and secreted in the form small fragments	28
3.2.3 Extracellular vimentin enhances migration and phagocytosis of macrophages	30
4 DISCUSSION	32
4.1 Influence on cancer cell functionality	32
4.2 Characteristics of extracellular vimentin	35
5 CONCLUSION AND FUTURE WORK	38
6 REFERENCES	39

7 SCIENTIFIC PUBLICATIONS	46
7.1 Publication 1: Extracellular vimentin is expressed at the rear of activated macrophage-like cells: Potential role in enhancement of migration and phagocytosis	46
7.2 Publication 2: Role of Extracellular Vimentin in Cancer-Cell Functionality and Its Influence on Cell Monolayer Permeability Changes Induced by SARS-CoV-2 Receptor Binding Domain	58
7.3 Publication 3: Actin stabilisation in cell migration	74
7.4 Publication 4: A novel universal algorithm for filament network tracing and.....	83
cytoskeleton analysis.....	83

ABSTRACT

The cytoskeleton is a dynamic network of filaments comprising actin filaments, microtubules, and intermediate filaments in the cytoplasm of cells. Vimentin is an intermediate filament protein that plays a crucial role in adhesion, migration, and signalling. These functions of vimentin have broader implications on inflammation, wound healing, cell physiology, and immune response. Inside the cell, the vimentin network extends from the nucleus to the cell's periphery. However, vimentin gets out to the extracellular environment under the circumstances such as activation, stress, and senescence. However, the influence of such vimentin on general cellular functions and its characteristics is not well established. This thesis demonstrates that extracellular addition of vimentin enhances proliferation, adhesion and migration prominently in cancer cells (MCF-7), overexpressing insulin-like growth factor 1 (IGF1-R). Interestingly, in SARS-CoV-2 infection, the extracellular vimentin pre-incubation with the SARS-CoV-2 receptor binding domain protected the cancer (MCF-7) cell's monolayer integrity. Further investigation on the characteristics of extracellular vimentin found secretion of vimentin from the back of activated macrophages in the form of small fragments, enhancing phagocytosis and migration of activated macrophages. Collectively, this work demonstrates new insights into vimentin secretion and its implications on cellular functionality.

ZUSAMMENFASSUNG

Das Zytoskelett ist ein dynamisches Netz von Filamenten, das aus Aktinfilamenten, Mikrotubuli und Zwischenfilamenten im Zytoplasma von Zellen besteht. Vimentin ist ein Zwischenfilamentprotein, das eine entscheidende Rolle bei Adhäsion, Migration und Signalübertragung spielt. Diese Funktionen von Vimentin haben weitreichende Auswirkungen auf Entzündungen, Wundheilung, Zellphysiologie und Immunreaktion. Innerhalb der Zelle erstreckt sich das Vimentin-Netzwerk vom Zellkern bis zur Peripherie der Zelle. Unter bestimmten Umständen wie Aktivierung, Stress und Seneszenz gelangt Vimentin jedoch auch in die extrazelluläre Umgebung. Der Einfluss dieses Vimentins auf die allgemeinen Zellfunktionen und seine Eigenschaften ist jedoch nicht gut untersucht. Diese Arbeit zeigt, dass die extrazelluläre Zugabe von Vimentin die Proliferation, Adhäsion und Migration in Krebszellen (MCF-7), die den insulinähnlichen Wachstumsfaktor 1 (IGF1-R) überexprimieren, deutlich erhöht. Interessanterweise schützte das extrazelluläre Vimentin bei einer SARS-CoV-2-Infektion vor der Inkubation mit der SARS-CoV-2-Rezeptorbindungsdomäne die Integrität der Krebszellen (MCF-7) in der Monolage. Weitere Untersuchungen zu den Eigenschaften von extrazellulärem Vimentin ergaben, dass Vimentin von der Rückseite aktivierter Makrophagen in Form kleiner Fragmente abgesondert wird, was die Phagozytose und Migration aktivierter Makrophagen fördert. Insgesamt zeigen diese Arbeiten neue Erkenntnisse über die Vimentin-Sekretion und ihre Auswirkungen auf die zelluläre Funktionalität.

ACKNOWLEDGEMENTS

I express my deepest gratitude to Prof. Franziska Lautenschläger for giving me this opportunity to work on such an exciting theme. She had been a great supervisor and inspiration throughout my PhD. Without her support, this endeavour wouldn't have been possible.

I had the pleasure of collaborating with Dr. Jan Philipp Jung and Prof. Markus Bischoff. I am incredibly thankful for their contribution to the FluidFM study and the manuscript.

I am incredibly grateful to this lab's founding members: Luiza Stankevics, Emmanuel Terriac and Daniel Flormann. Who provided a great environment during the initiation phase of my project. They were a great support in giving training, suggestions, and needed help.

I want to thank Ashish Chand Rajwar, Annalena Maria Laurent, Johanna Elisabeth Becher and Lucina Kainka for contributing to the macrophage study. This project would not have been possible without your association.

I want to thank all the former and current lab members; Doriane Vesperini, Zahra Mostajeran, Kevin Kaub, Galia Magela Montalvo Bereau, Carsten Baltes, Erbara Gjana, Christoph Anton and Ramona Grünwald. They provided a great working atmosphere always in the lab. Many thanks to the staff at INM, who offered excellent infrastructure and facilities for carrying out my work without difficulties.

I am extremely grateful to my friends Prashanth Kumar, Guru Prasad and Anil Kanduri, who continuously supported and assisted me during my PhD.

I am deeply indebted to my parents and family, who had been great pillars throughout my life, and without them, I could not have undertaken this journey. Lastly, I would like to express my special thanks to my wife Sripada Samhita Thalla, who had always supported me and stepped up to take care of our daughter during this phase.

ABBREVIATIONS

ACE2	Angiotensin-converting enzyme 2
BSA	Bovine Serum Albumin
CAD	Cell-Surface Vimentin
CSV	Circulating Tumor Cells
CTC	Fluidic Force Microscopy
CTCs	Insulin-Like Growth Factor-1
DENV	Insulin-Like Growth Factor-1 Receptor
ECM	Human Breast Cancer Epithelial Cell Line
EMT	Non-Tumorigenic Epithelial Cell Line
F-actin	3-[4,5-Dimethylthiazole-2-Yl]-2,5-Diphenyltetrazolium Bromide
FluidFM	Phosphate-Buffered Saline
G-actin	Polydimethylsiloxane
GBM	Receptor Binding Domain
HCC	Severe Acute Respiratory Syndrome Coronavirus
IGF-1	Filamentous Actin
IGF-1R	Globular Actin
IL	Epithelial-Mesenchymal Transition
IPF	Idiopathic Pulmonary Fibrosis
MCF-10a	Coronary Artery Disease
MCF-7 cells	Rheumatoid Arthritis
MTT	Hepatocellular Carcinoma
PBS	Protein Kinase C
PDMS	Interleukin
PKC	Tumour Necrosis Factor
RA	Von Willebrand Factor
RBD	Glioblastoma Multiforme
SARS-CoV	Circulating Tumour Cell
SEM	Extracellular Matrix
TNF	Dengue Virus
TPA	12-O-Tetradecanoylphorbol-13-Acetate
VWF	Scanning Electron Microscopy

LIST OF FIGURES

Figure 1: Cytoskeleton's three main components (actin filaments, microtubules, intermediate filaments) in a eukaryotic cell.

Figure 2: Actin filament assembly

Figure 3: Microtubule structure

Figure 4: Structural organisation and assembly of intermediate filaments.

Figure 5: Significance of surface vimentin and secreted vimentin.

Figure 6: Graphical representation of IGF1-R activation by extracellular vimentin.

Figure 7. Proliferation of MCF-10a (control) and MCF-7 (cancer) cells under treatment with recombinant (Rh) vimentin.

Figure 8. Adhesion force measurements of the MCF-7 (cancer) cells under treatment with recombinant (Rh) vimentin

Figure 9. Gap closure assays for the MCF-10a and MCF-7 cells under treatment with recombinant (Rh) vimentin.

Figure 10. Transwell migration assays for the MCF-10a (control) and MCF-7 (cancer) cells under treatment with recombinant (Rh) vimentin.

Figure 11. Stepwise procedures for determination of MCF-10a and MCF-7 cell monolayer permeabilities under SARS-Cov-2 RBD treatments using 3 kDa FITC-dextran.

Figure 12. Monolayer permeabilities of MCF-10a and MCF-7 cells using 3 kDa of FITC-dextran treatment for 1 h.

Figure 13. Polarised expression of extracellular vimentin on the surface of TNF- α -activated macrophages.

Figure 14. Visualisation of surface vimentin on macrophages patterned on one-dimensional lines.

Figure 15. Visualisation of surface vimentin on macrophages differentiated from GFP-vimentin HL60.

Figure 16. Stimulation of migration and phagocytosis of macrophages by addition of recombinant (rh)Vimentin.

Figure17. Illustration of the influence of extracellular vimentin in SARS-CoV-2 viral particle entry into cells.

Figure 18. Proposed model of vimentin secretion.

1 INTRODUCTION

1.1 Cytoskeleton

The cytoskeleton is a three-dimensional network of fibrillar structures within the cytoplasm of cells. It comprises three main classes of filaments: actin filaments, intermediate filaments, and microtubules [1].

The cytoskeleton is dynamic and undergoes rapid reorganisation by assembly and disassembly of cytoskeletal filament proteins. Cytoskeletal fibres can reversibly attach and interact with other cellular organelles. Thus, the cytoskeleton is attributed to a cytoplasmic matrix that embeds and spatially organises cellular organelles. Collectively, the cytoskeleton plays a significant role in providing mechanical support to the cell and maintaining its shape, generating forces for shape change and movement, and controlling the cell's metabolic activity [1, 2].

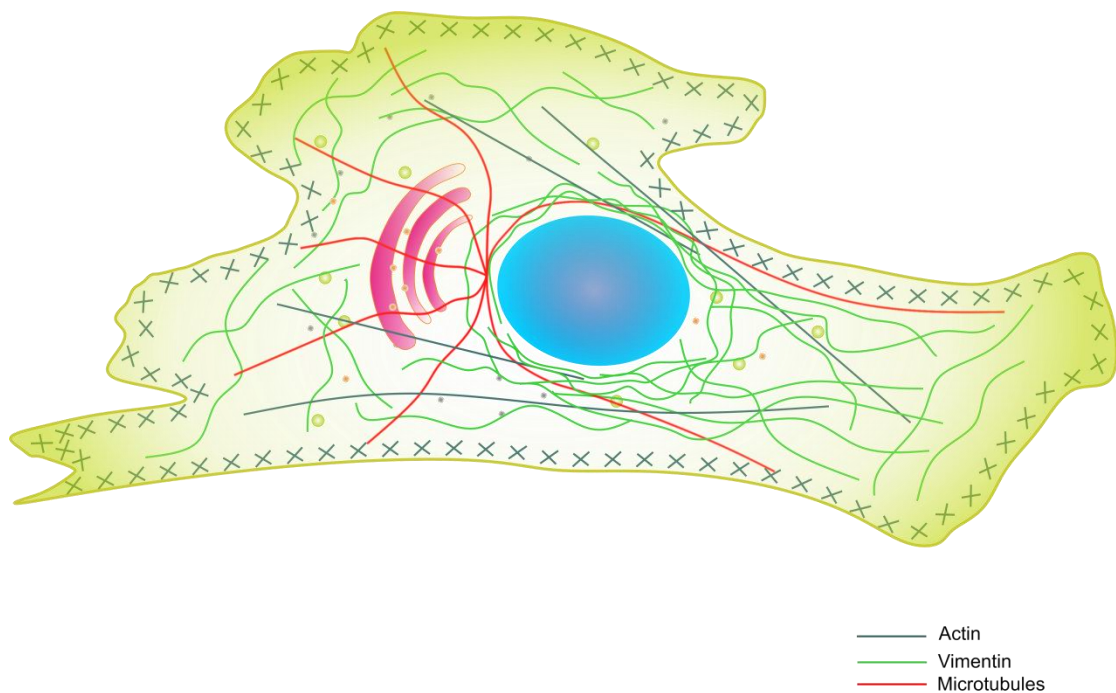


Figure 1: Cytoskeleton's three main components (actin filaments, microtubules, intermediate filaments) in a eukaryotic cell.

1.1.1 Actin Filaments

Actin filaments (F-actin) are thin and flexible microfilaments formed by linear polymerisation of globular actin (G-actin) protein. Individual G-actin monomer binds to two other G-actin monomers via head-to-tail interaction to form double-stranded helical actin filaments typically 7 nm in diameter and 6-7 μm in length [3, 4]. Actin filaments can either form actin bundles or actin networks depending on the circumstances regulated by actin-binding proteins.

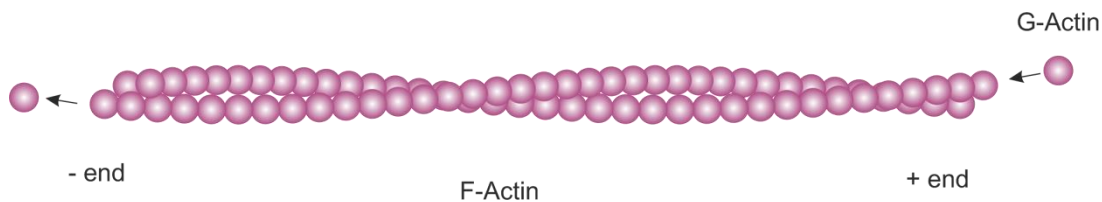


Figure 2: Actin filament assembly

Actin filaments have a wide range of functions related to the cellular shape and motile processes[5, 6]:

- It provides a structural framework for the cells and forms a link between cell components and their surroundings.
- It promotes cell migration by force generation.
- It facilitates intracellular transport.

1.1.2 Microtubules

Microtubules are stiff, hollow cylindrical filaments made of alpha (α) and beta (β) tubulin heterodimers [7]. These heterodimers of α/β -tubulin polymerise linearly to form protofilaments that further associate laterally to form microtubules [7]. They have a diameter of about 25 nm and can reach up to 25 μm in length [8].

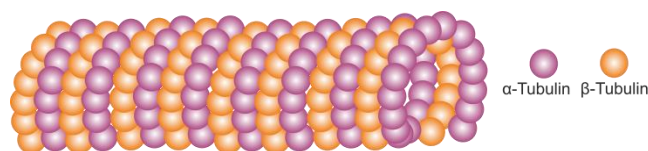


Figure 3: Microtubule structure

Microtubules have four significant functions[9]:

- To maintain the overall polarity of the cell.
- To form mitotic spindle and ensure proper organisation of chromosomes during cell division.
- To provide a structural framework to facilitate movement in cilia and flagella.

- To transport cargo via a transport network.

1.1.3 Intermediate Filaments

Intermediate filaments are a group of cytoskeletal filaments having a diameter of 10 nm, which lie intermediate between microfilaments and microtubules [10]. Intermediate filaments play a significant role in structural organisation, cell adhesion, cell migration, and cell shape [11]. Contrary to actin filaments and microtubules, the intermediate filaments are composed of various proteins. They comprise 65 different genes. Therefore, depending on the amino acid sequences, the intermediate filaments are classified into five groups [12].

- Type I and II: Acidic and basic keratins
- Type III: Desmin, glial fibrillary acidic protein and vimentin,
- Type IV: Neurofilament proteins
- Type V: Nuclear lamins

Despite the heterogeneity, the intermediate filament proteins possess a similar structural organisation. They have an α -helical rod domain along with N- terminal head and C- terminal tail regions [10] (Figure 3). The first step in assembling intermediate filaments is associating two monomers via central domains to form a dimer. Then a tetramer is formed by associating this dimer with another dimer in an antiparallel way, which further assembles end to end into protofilaments. Finally, eight protofilaments wound around each other to form an intermediate filament which is highly flexible and stress-resistant [13].

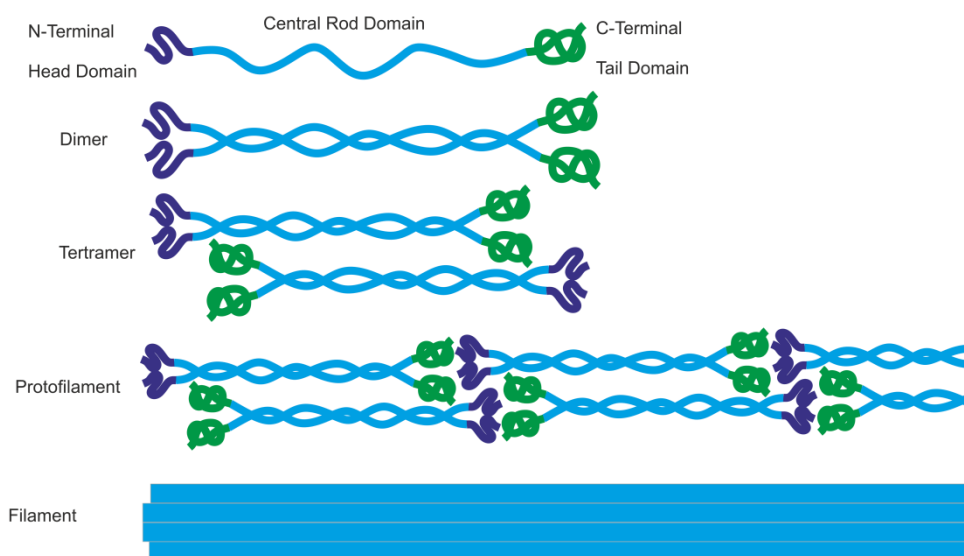


Figure 4: Structural organisation and assembly of intermediate filaments.

Even though intermediate filaments comprise several proteins, the focus is more on the vimentin intermediate filament protein in the current thesis.

1.2 Vimentin

Vimentin is a type III intermediate filament that plays a vital role in cell adhesion, migration and signalling due to its ability to interact with various other proteins. These functions of vimentin have broader consequences in wound healing, cell physiology, inflammation, and immune response [14]. It acts as an epithelial-mesenchymal transition (EMT) marker and gets overexpressed in various cancer cells. Vimentin filament network extends from the perinucleus to the cell membrane [14]. However, besides its presence in the cytoplasm, recent studies have demonstrated its presence in the extracellular spaces around several cells. Activation, inflammation, senescence, and stress are attributed to the secretion of vimentin into extracellular space [15, 16]. Such extracellular vimentin can either bind to the cellular surface or be present in an unbound form in the extracellular matrix (Figure 5).

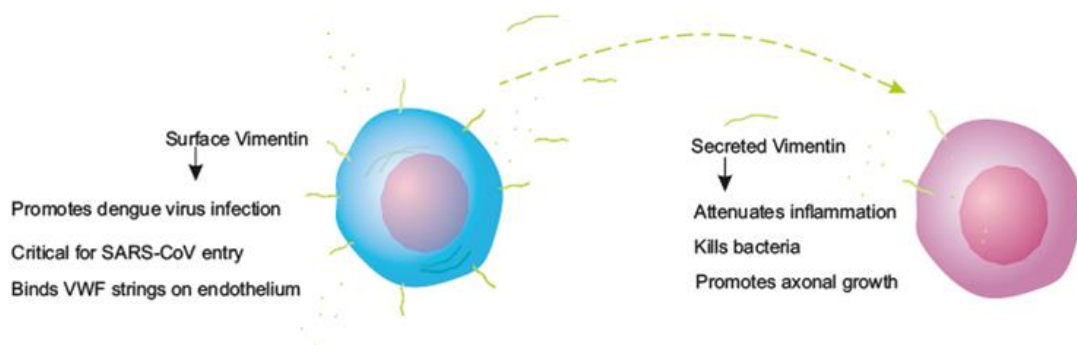


Figure 5: Significance of surface vimentin and secreted vimentin. Taken from original publication [17].

1.2.1 Secreted Vimentin

The unbound form of vimentin can be termed "secreted vimentin", which has the potential to interact with surface receptors on various cells and influence their functions. Different cell types secrete vimentin, for example, astrocytes, endothelial cells, macrophages, monocytes, neutrophils, and apoptotic lymphocytes [15, 18-21]. The secreted form of vimentin has a multifaceted functional role in wound healing, immune function and biomarker for the diagnosis of various diseases.

Biomarkers for many diseases

In particular diseases, vimentin secreted from a vast population of cells gets transfused into the circulating human blood. In such conditions, secreted vimentin serves as a biomarker and can be used to analyse the presence or severity of such diseases.

- In atherosclerosis, vimentin mediates cholesterol accumulation by activating the Dectin-1 receptor [22]. Idiopathic pulmonary fibrosis (IPF) patients have detectable levels of vimentin in their exhaled breath condensate. TGF- β 1 triggers vimentin secretion in CD4 (T cells) dose-dependently. Interestingly, the amount of anti-vimentin antibodies observed in the plasma of IPF patients is inversely proportional to the disease severity [23].
- Serum from patients suffering from systemic lupus erythematosus expressed high antibodies against vimentin [24]. The patients suffering from coronary artery disease (CAD), serum levels of vimentin are increased and correlate with the CAD severity [25]. Neutrophils release the citrullinated form of vimentin in rheumatoid arthritis (RA) patients; antibodies produced against citrullinated vimentin are used for diagnosing the severity of the disease in such patients [26]. In organ transplant patients, antibodies against vimentin are used to assess the risk of rejection or organ transplant failure [27-29].
- Serum vimentin plays a crucial role in detecting cancers. Serum vimentin is more highly detectable in colon cancer than normal sera [30]. Small hepatocellular carcinoma tumors (HCC) can be cured if they are diagnosed early. Serum vimentin is over-expressed in HCC patients. Combined with the conventional alpha-fetoprotein marker, its an effective marker for detecting HCC tumours [31].

Wound healing

- Understanding the functional role of extracellular vimentin in wound healing was limited compared to its intracellular counterpart. However, recent studies have provided insights into extracellular vimentin as a potential candidate for tissue repair. It enters the extracellular milieu, binds to mesenchymal leader cells, and contributes to wound closure. In leader cells, it promotes mesenchymal to myofibroblast differentiation [32].

- After trauma, attaining functional recovery of the central nervous system is still a challenging task in neuroscience. The recent development of a novel compound, denosomin, facilitated spinal cord injury treatment in mice [33]. During treatment, astrocytes secrete vimentin at the injury site. This secreted vimentin stimulates axonal growth via activation of insulin-like growth factor 1 receptor (IGF1-R) and aids spinal cord injured mice's functional recovery [34].
- Extracellular vimentin binds to P-selectin in vascular endothelial cells to block neutrophil adhesion to the vascular endothelium. Due to this, the interaction between P-selectin glycoprotein ligand-1 and P-selectin gets inhibited, resulting in obstruction of acute inflammatory response. It turns out to be beneficial in the case of acute lung injury, as it attenuates unwanted inflammation and decreases the histologic signs of the disease [35].

Immune function

- In activated macrophages, the secretion of vimentin was induced by tumour necrosis factor α (TNF- α , pro-inflammatory cytokine) and inhibited upon treatment with interleukin-10 (IL-10, anti-inflammatory cytokine). Moreover, monensin inhibited the vimentin secretion by blocking the Golgi apparatus. Here, secreted vimentin is involved in immune function by generating oxidative metabolites and eliminating the bacteria [15].
- Neutrophils are crucial for developing adaptive immune responses. In RA disease conditions, neutrophils secrete citrullinated vimentin while releasing neutrophil extracellular traps for immobilising pathogens and promoting immune responses [19, 26].
- In the case of Mycobacterium tuberculosis, vimentin bound to the natural killer cell surface receptor NKp46 contributes to infected cell lyses [36].
- LPS-activated dendritic cells reduce the differentiation of naïve T cells into Th1 cells due to the decreased IL-6 and IL-12 secretion and increased IL-10 secretion triggered by extracellular vimentin. This mechanism helps in bacterial elimination, thereby preventing tissue damage and a low probability of autoimmunity [37].

1.2.2 Surface Vimentin

Surface vimentin is a form of extracellular vimentin which is bound to the cell surface and has the potential to act as a receptor or co-receptor for proteins or pathogens on the cell surface. Surface vimentin on platelets serves as a binding protein for Von Willebrand Factor (VWF), resulting in the translocation of platelets to vascular injury sites [38]. Further, it also contributes to anchoring VWF strings to the endothelial surface by interacting with the A2 domain of VWF [39].

Target and marker for EMT cancer cells

- Epithelial-mesenchymal transition (EMT) occurs in the tumour cells as cancer progresses to metastases. During this transition, cells lose their polarity and adhesion while gaining mesenchymal cells' migratory and invasive properties. Vimentin translocates to the cell surface during EMT. This distinctive property allows for identifying and isolating aggressive cancer cells and further targeting them [40].
- Glioblastoma multiforme (GBM) cancer stem cells are tumour-initiating cells with surface vimentin and tend to form spheroids. By targeting the GBM cells using cell surface vimentin antibody, surface vimentin is internalised, resulting in apoptosis and tumour inhibition [41].
- Human circulating tumour cells (CTC) are identified using a CSV-specific antibody. Surface vimentin is also recognised in neuroblastoma, osteosarcoma and rhabdomyosarcoma cells [42]. In further studies, EMT-induced CD45⁻ CTCs from metastatic colorectal cancer patients and CD133⁻ CTCs from hepatocellular carcinoma cells were isolated [43, 44]. Isolating the CSV positive CTCs have numerous advantages in clinical decision making, providing novel diagnostics, therapeutic target in sarcoma patients and analysing metastatic precursor subpopulation.

Pathogen interaction and internalisation

Surface vimentin is involved in the binding and internalising various bacterial pathogens and viruses.

- *Listeria monocytogenes* (*L. monocytogenes*) belong to a group of bacterial pathogens which causes meningitis by invading the brain. In vivo study revealed that *L. monocytogenes* forms colonies by intruding into the brain by exploiting the surface vimentin alongside internalin surface receptor InIF [45]. Another study on the invasion of *L. monocytogenes* in human microvascular endothelial cells showed that infection was modulated by matrix stiffness and mediated by surface vimentin expression. Expression of surface vimentin and subsequent bacterial uptake increases when extracellular matrix (ECM) stiffness increases and visa-versa when the ECM stiffness is decreased [46].
- Dengue virus (DENV) infection in vascular endothelial cells is mediated by surface vimentin by serving as a co-receptor on the surface. Rod domain of the vimentin interacts with DENV EDIII and facilitates internalisation of DENV[47].
- Group A streptococci (GAS) is a deadly infection resulting from the skeletal-muscle injury. After the skeletal-muscle damage, an excessive amount of surface vimentin is expressed in the skeletal-muscle cells and acts as a binding receptor for streptococcus pyogenes [48].

The years, 2002 and 2003 have seen a niched panic in the name of severe acute respiratory syndrome coronavirus (SARS-CoV), which increased morbidity and mortality. This viral spreading is due to the angiotensin-converting enzyme 2 (ACE2), acting as a functional cellular receptor in vitro and in vivo [49]. Although ACE2 has a significant role as per various findings, further investigations using Vero E6 cells relieved that surface vimentin was directly binding to the spike protein of SARS-CoV. Therefore, surface vimentin is a co-receptor for SARS-CoV and mediates its entry [50]. Furthermore, in 2020, SARS-CoV-2 led us into a pandemic. Interestingly, extracellular vimentin acts as a co-receptor for the SARS-CoV-2 infection[51].

From the above literature, it is evident that extracellular vimentin is not just a mislocalised protein in the extracellular spaces, let it be in a bound or unbound form. Extracellular vimentin has functional roles in wound healing, immune function, diagnosis of various diseases, detecting and targeting cancer cells and pathogen interactions. Further studies on extracellular vimentin would broaden our understanding of this protein and could provide the basis for developing preventive strategies and therapies for numerous disease conditions.

1.2.3 Extracellular vimentin and IGF1-R interaction

As discussed above, extracellular vimentin binds to surface receptors Dectin-1, Nkp46 and insulin-like growth factor 1 (IGF1-R). Out of these, IGF1-R plays a vital role in tissue development and gets activated by the hormone insulin-like growth factor 1(IGF1). IGF1-R binds to IGF1 with high affinity [52]. This pathway plays a significant role in cell cycle progression, translation of proteins, apoptosis, and pathogenesis of autoimmune diseases [53]. Cancer cells overexpress the IGF1-R. They can become sensitive to apoptosis by down-regulation of IGF1-R. And its suppression in adenocarcinoma A549 cells significantly affects various cellular functions [54]. IGF1 induces migration in MCF-7 human breast epithelial cancer cells, where IGF1-R is overexpressed [55].

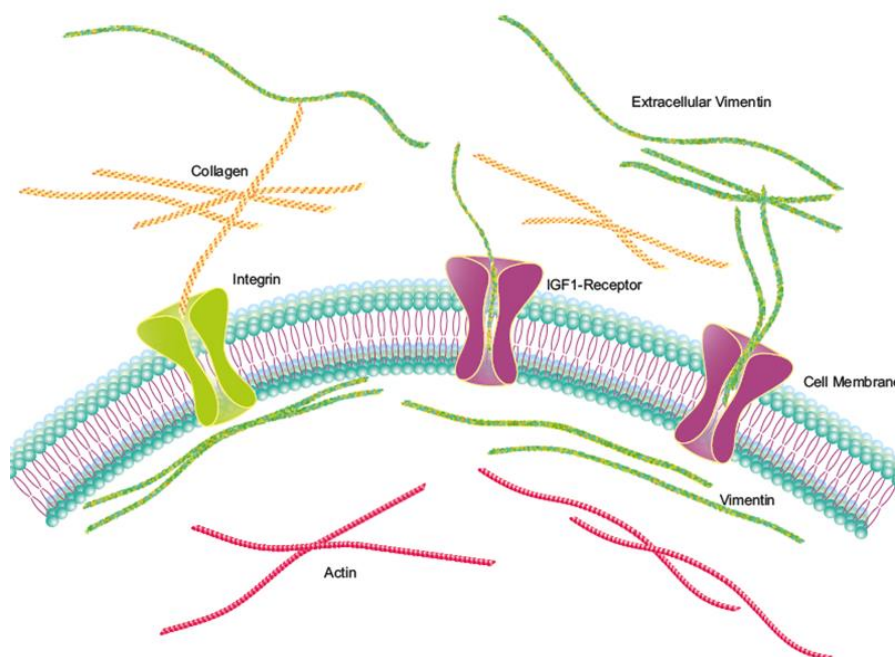


Figure 6: Graphical representation of IGF1-R activation by extracellular vimentin. Taken from original publication[17].

A recent study on spinal cord-injured mice demonstrated that extracellular vimentin activates IGF1-R in the same signalling pathway as IGF1. Therefore, the hypothesis for the current study is that extracellular vimentin could share functional similarities with IGF1 and play a significant role in general cellular functions in IGF1-R expressing cells. Hence, it can potentially alter and stimulate these cellular functions.

2 AIM

The current thesis is divided into two parts. The first part demonstrates the role of extracellular vimentin in the context of these cellular functions in cancer cells. Further, the influence of extracellular vimentin in monolayer permeability caused by SARS-CoV-2 is investigated. In the second part, the thesis focuses on the characteristics of extracellular vimentin.

Part 1

- To study the influence of extracellular vimentin on general cellular functions in cancerous and non-cancerous cells.
- To investigate the influence of extracellular vimentin on cell monolayer permeability changes induced by SARS-CoV-2 Receptor Binding Domain.

Part 2

- To study the characteristics of extracellular vimentin

3 FINDINGS OF THE THESIS

The significant outcomes of this thesis are directly transferred from the following original publications:

- Thalla, D.G.; Jung, P.; Bischoff, M.; Lautenschläger, F. Role of Extracellular Vimentin in Cancer-Cell Functionality and Its Influence on Cell Monolayer Permeability Changes Induced by SARS-CoV-2 Receptor Binding Domain. *Int. J. Mol. Sci.* 2021, 22, 7469. <https://doi.org/10.3390/ijms22147469>

My contribution: 1) Performed all the experiments except the Fluid FM measurements.

2) Writing the original draft.

- Thalla, D.G, Rajwar AC, Laurent AM, Becher JE, Kainka L and Lautenschläger F (2022) Extracellular vimentin is expressed at the rear of activated macrophage-like cells: Potential role in enhancement of migration and phagocytosis. *Front. Cell Dev. Biol.* 10:891281. doi: 10.3389/fcell.2022.891281

My contribution: 1) Supervision and conceptualisation of the project

2) Writing the original draft.

I was further involved in other projects where I contributed by teaching techniques I used in my original publications and supervising. Data from the those published works are not included in this thesis's outcomes but are attached at the end of the thesis.

3.1 Influence Of Extracellular Vimentin In Cancer And SARS-Cov-2

3.1.1 Extracellular Vimentin Promotes Proliferation in MCF-7 Cells through Activation of IGF-1R

To investigate the proliferation of MCF-10a and MCF-7 cells under the influence of extracellular vimentin, we carried out proliferation assays using 3-[4,5-dimethylthiazole-2-yl]-2,5-diphenyltetrazolium bromide (MTT). The cells were treated with increasing concentrations of recombinant human vimentin (0, 50, 100, 200 ng/mL) for 72 h. The absorbance was then measured using a plate reader, to define the viable cells.

These data for the MCF-7 cells show that the absorbance, and therefore the cell metabolic activity, with addition of recombinant vimentin was greater than for the control cells (Figure 7B). At 100 ng/mL recombinant vimentin, MCF-7 cells showed increased proliferation rates, by $\geq 20\%$. For the MCF-10a cells, those treated with recombinant vimentin did not show significant change compared to untreated cells at both 48 and 72 h time points (Figure 7B,D).

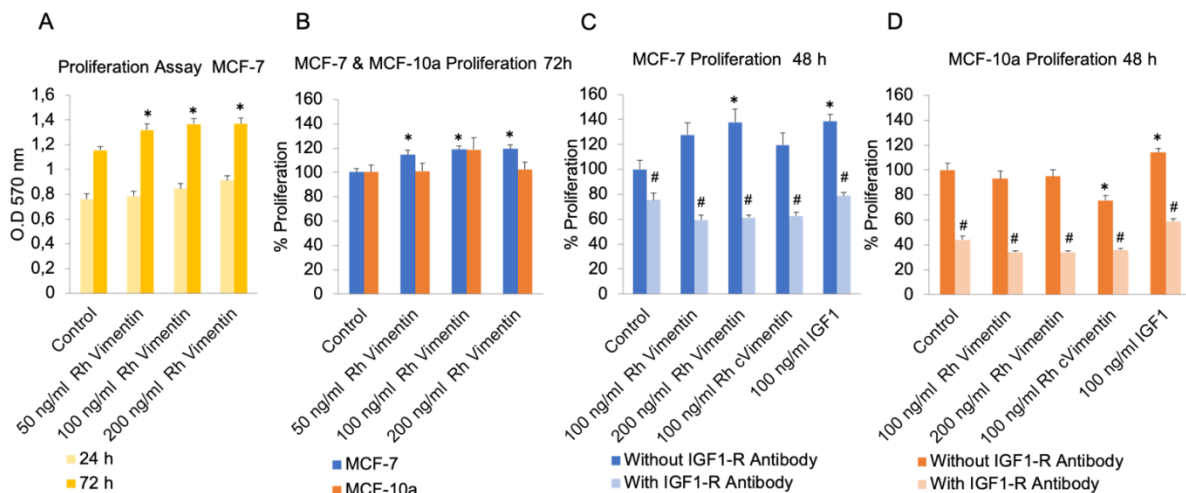


*Figure 7. Proliferation of MCF-10a (control) and MCF-7 (cancer) cells under treatment with recombinant (Rh) vimentin. (A) Raw data for absorbance at 570 nm in the MTT assay for MCF-7 cells after 24 and 72 h. (B) Cell proliferation following 72 h treatments of Rh vimentin. (C,D) Proliferation upon blocking of IGF-1R with pretreatment with an anti-IGF-1R antibody along with Rh vimentin; IGF-1; Rh cVimentin (recombinant citrullinated form of vimentin). * $p < 0.05$, compared to control (unpaired t -tests). # $p < 0.05$, compared to corresponding counterparts without IGF-1R antibody (unpaired t -tests). Experiments were performed at least two times in triplicates. Error bars indicate SEM.*

It has been suggested in the literature that vimentin binds directly to and activates IGF-1R [34]. To determine whether or not cell proliferation was stimulated by a direct interaction between vimentin and IGF-1R, a 15-min pre-incubation with an anti-IGF-1R antibody (ARG51076; anti-IGF1 Receptor antibody; Arigobio) was used to block IGF-1R in the MCF-10a and MCF-7 cells, with cell proliferation monitored over 48 h (Figure 7C,D). Indeed,

blocking IGF-1R inhibited 200 ng/mL vimentin-stimulated cell proliferation in MCF-7 cells. Here, we also treated cells with citrullinated vimentin, which is the form of vimentin that is secreted in patients suffering from rheumatoid arthritis, to see whether the effects seen here are different to those of recombinant vimentin. These data also indicated that addition of extracellular citrullinated vimentin did not improve proliferation in MCF-7 cancer cells through the activation of IGF-1R (Figure 7C). However, proliferation was significantly reduced in MCF-10a cells upon Rh cVimentin treatment (Figure 7D).

3.1.2. Extracellular Vimentin Promotes Stronger Adherence to the Underlying Substrate for MCF-7 Cells

As mesenchymal cell migration is strongly dependent on cell adhesion, we wanted to quantify the adhesion forces between these cells and their underlying substrate. Therefore, we investigated the force necessary to detach the MCF-10a and MCF-7 cells from the fibronectin-coated glass substrate without and with the vimentin treatments, to quantify the adhesion strengths of the cells to this substrate. This was achieved using fluidic force microscopy (FluidFM). This is a particular single-cell force spectroscopy set-up with hollow cantilevers, which, in addition to the measurement of conventional cell mechanical properties, can be used to hold, immobilise, or move cells by negative pressure (Figure 8A,B) [56]. Unfortunately, the force spectroscopy measurements with the MCF-10a control cells led to cell disruption or disengagement of the attachment between the cells and micropipette, which thus overstrained the experimental set-up. Therefore, only the effects of vimentin on the adhesion forces of the MCF-7 cells were considered here. The untreated MCF-7 cells had a maximum detachment force of 14.7 ± 2.1 nN, while with 200 ng/mL vimentin treatment, this was significantly increased to 21.0 ± 1.5 nN (Figure 8C). This was also reflected in the modest increase (not statistically significant) to the young's modulus of these cells upon vimentin treatment (Figure 8D). We also concluded that the adhesion force of the MCF-10a cells was particularly high and appeared to exceed the adhesion force of MCF-7 cells, although it cannot be quantified using this method.

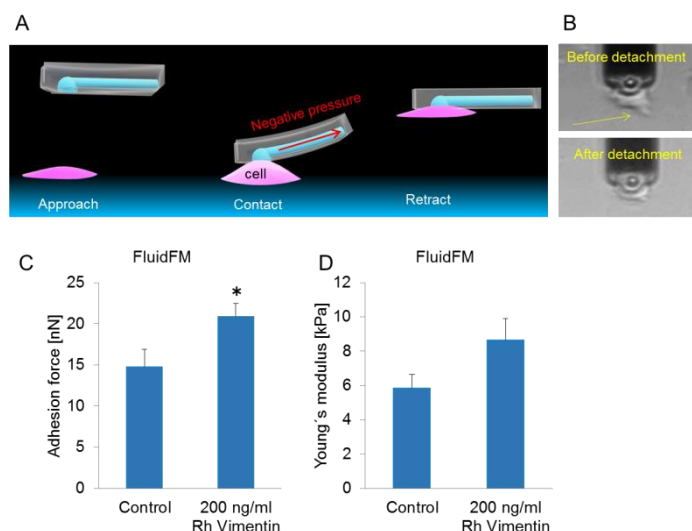


Figure 8. Adhesion force measurements of the MCF-7 (cancer) cells under treatment with recombinant (Rh) vimentin. (A) Illustration of the approach, with cell contact establishment and probe retraction during the FluidFM-based single-cell force spectroscopy. (B) Representative images showing an MCF-7 cell treated with 200 ng/mL recombinant vimentin which was detached by the retraction movement of the FluidFM probe. (C,D) Adhesion force (C) and stiffness (D) measured during the detachment of MCF-7 cells ($n \leq 7$ cells per condition) after 24 h without and with 200 ng/mL vimentin. * $p < 0.05$, compared to control (0) (unpaired *t*-tests). Error bars indicate SEM.

3.1.3 Extracellular Vimentin Induces Migration of MCF-10a and MCF-7 Cells

To further define the role of extracellular vimentin in the functions of these cells, its effects on cell migration were investigated using migration assays. To exclude the possibility that increased cell proliferation after vimentin treatment can obscure a migration result, the cells were initially serum-starved for 24 h. For the migration assays, a circular gap was prepared using soft polydimethylsiloxane (PDMS) pillars of 500 μm diameter on cell culture dishes (Figure 9A). Once the seeded cells had reached confluency, the PDMS pillars were removed, and cell migration was recorded over 24 h using video microscopy.

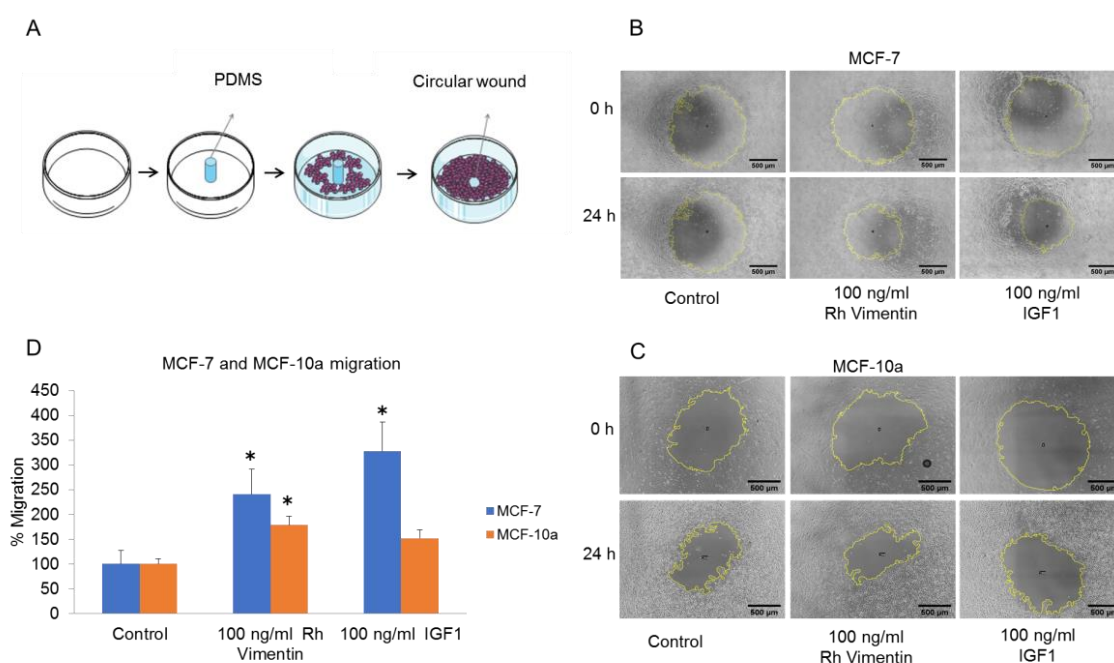


Figure 9. Gap closure assays for the MCF-10a and MCF-7 cells under treatment with recombinant (Rh) vimentin. (A) Schematic representation of the creation of the circular gaps using a PDMS column. (B,C) Representative images of the gap closure of MCF-10a cells (B) and MCF-7 cells (C) without and with treatments with vimentin and IGF-1 (scale bar 500 μm , yellow line indicates the edge of gap closure). (D) Migration rate is calculated by measuring gap closure (area covered by cell monolayer) over the time in terms of $\mu\text{m}^2/\text{h}$ and then it is normalised to control. To exclude effects of cell proliferation on cell migration, the cells were initially starved for 24 h in serum-free medium. * $p < 0.05$, compared to relevant control (unpaired *t*-tests). Error bars indicate SEM.

We analysed the sizes of the gaps directly after removing the PDMS pillar using the ImageJ software, with calculation of the area (μm^2) of gap closure per hour (Figure 9). Migration rate for MCF-10a cells treated with 100 ng/mL vimentin and 100 ng/mL IGF-1 were approximately 1.8 and 1.5 times higher compared to the untreated cells (Figure 4D). In the MCF-7 cancer cells, the migration rate upon 100 ng/mL vimentin and 100 ng/mL IGF-1 treatments, these reached 2.5 and 3 times higher than control respectively (Figure 9D). Gap closure was therefore faster after the treatment with extracellular vimentin in both the MCF-10a and MCF-7 cells. This suggests that activation of these cells with extracellular vimentin enhances cell migration, which results in faster closure of these wounds. Interestingly, the effects of added recombinant vimentin were again stronger in the MCF-7 cancer cells compared to the MCF-10a cells.

In addition to gap closure assay, we also carried out transwell migration assays. The MCF-10a and MCF-7 cells were placed in the upper reservoirs of individual systems and cultured in the presence or absence of Rh vimentin and IGF-1. The number of cells that moved through the porous membranes was then quantified at 48 h post-seeding (Figure 10).

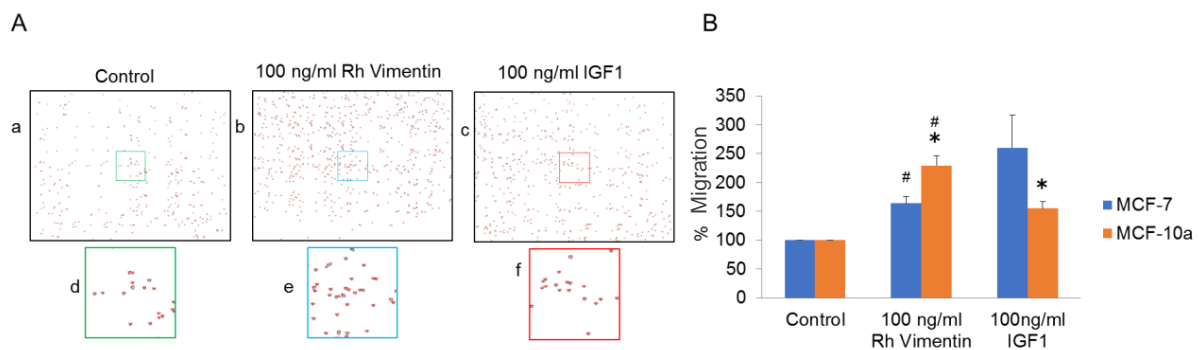


Figure 10. Transwell migration assays for the MCF-10a (control) and MCF-7 (cancer) cells under treatment with recombinant (Rh) vimentin. **(A)** Representative images used for the quantification of the MCF-10a cells that had migrated through the transwell membranes. **(B)** Quantification of the migrated cells without and with vimentin and IGF-1. Individual experiment was normalised to control and then mean values of three experiments were calculated. [#] * $p < 0.05$, compared to group indicating same symbol (unpaired *t*-tests). Error bars indicate SEM.

Both the MCF-10a and MCF-7 cells showed enhanced migration through the porous membranes upon vimentin treatment, and for their adherence to the well plate, as compared to the untreated control cells (Figure 10). Interestingly, the IGF-1-treated MCF-7 cells showed higher migration rates when compared to the vimentin-treated cells, with the converse seen for the IGF-1-treated MCF-10a cells (Figure 10B). This effect complements our findings for gap closure (Figure 10D).

3.1.4 Extracellular Vimentin Effects Alterations of Cell Monolayer Integrity Caused by the Receptor Binding Domain of SARS-CoV-2 Spike Protein

Alterations to epithelial cell monolayer permeability are an indicator of disease conditions in epithelial tissues, as well as a marker of oncogenesis [57-59]. Such alterations might have a role in tumor invasiveness, and also in viral invasion into various organs. Indeed, it was shown in a recent study that SARS-CoV-2 receptor binding domain can affect the endothelial cell monolayer permeability [60]. Here, we measured the fluorescence intensity of 3 kDa FITC-dextran that passed through MCF-10a and MCF-7 cell monolayers upon addition of 10 nM recombinant vimentin and 10 nM SARS-CoV-2 RBD, using a protocol that is illustrated in Figure 11.

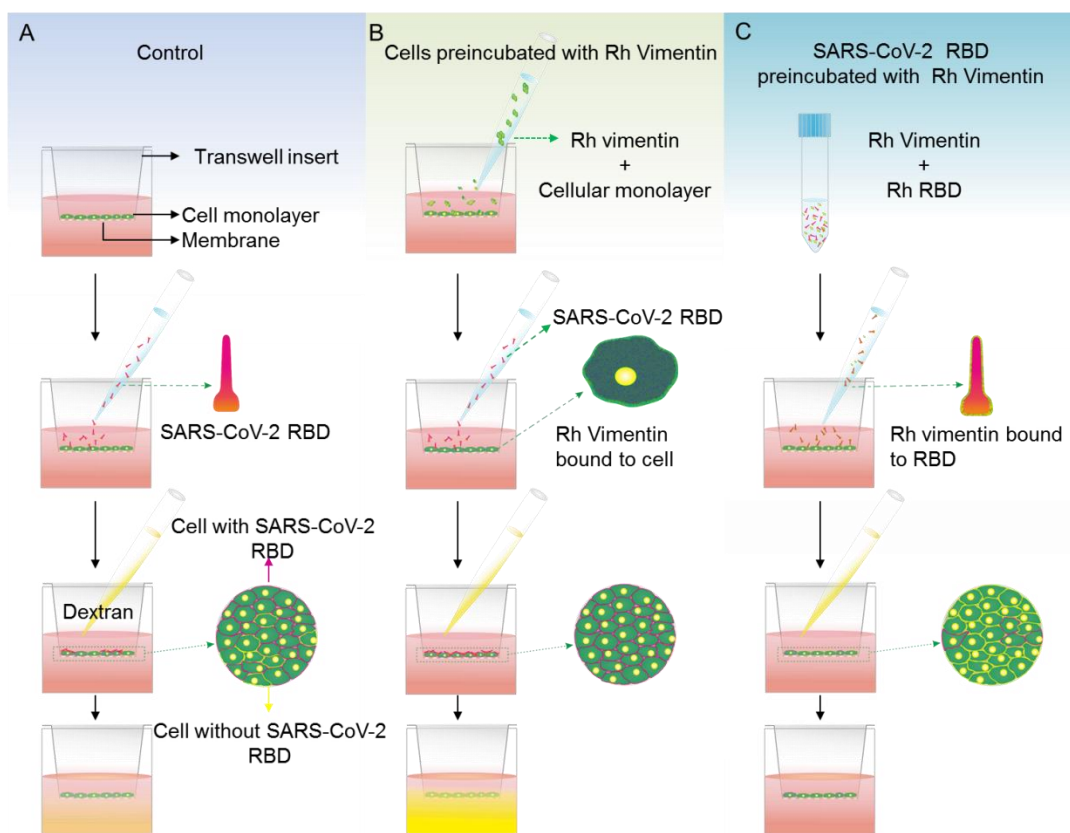
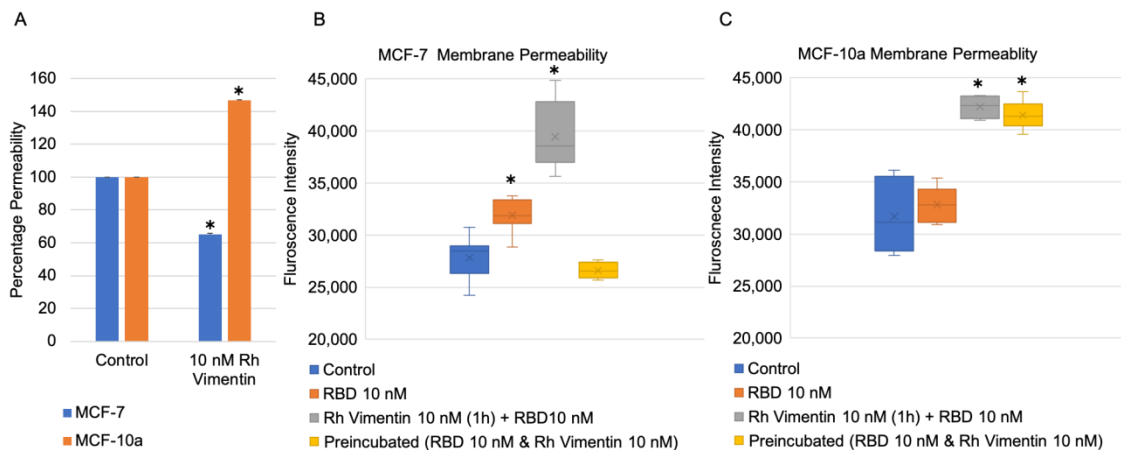


Figure 11. Stepwise procedures for determination of MCF-10a and MCF-7 cell monolayer permeabilities under SARS-Cov-2 RBD treatments using 3 kDa FITC-dextran. (A–C) Cell monolayers were treated for 24 h with SARS-CoV-2 RBD, either alone (A) or after treatment with recombinant (Rh) vimentin for 1 h (B), and with SARS-CoV-2 RBD that had been preincubated with Rh vimentin for 1 h (C).

First, the effects of recombinant vimentin on the permeability of MCF-10a and MCF-7 cell monolayers were determined. MCF-10a control cell monolayers treated with vimentin showed a 45% increase in the monolayer permeability compared to untreated MCF-10a control monolayers. Instead, monolayers of MCF-7 cells treated with recombinant vimentin showed the inverse trend, as a 35% decrease in monolayer permeability compared to the MCF-7 control monolayers (Figure 12A).



*Figure 12. Monolayer permeabilities of MCF-10a and MCF-7 cells using 3 kDa of FITC-dextran treatment for 1 h. (A) Cell monolayers treated with 10 nM of recombinant (Rh) vimentin for 24 h, with data normalised to the controls. (B,C) Treatments of MCF-10a (B) and MCF-7 (C) cell monolayers without (control) and with SARS-CoV-2 RBD for 24 h (RBD), including 10 nM of vimentin monolayer pre-treatment for 1 h followed by SARS-CoV-2 RBD for 24 h; or 10 nM of vimentin and SARS-CoV-2 RBD pre-incubated together for 1 h, followed by SARS-CoV-2 RBD for 24 h. * $p < 0.05$, compared to control (unpaired t -tests).*

We then checked whether recombinant vimentin has an influence on MCF-10a and MCF-7 cell monolayer permeability when the monolayers are also exposed to SARS-CoV-2 RBD. Two different conditions for the recombinant vimentin treatment were used here. In the first (Figure 12B,C), the cell monolayers were pretreated with 10 nM of recombinant vimentin for 1 h prior to addition of 10 nM of SARS-CoV-2 RBD. After 24 h, for both MCF-10a and MCF-7 cells, their monolayer permeabilities were increased significantly compared to treatment of the monolayers with 10 nM of SARS-CoV-2 RBD alone. For the second condition, 10 nM of SARS-CoV-2 RBD and 10 nM of vimentin were preincubated together for 1 h, and then added to the cell monolayers. Interestingly, with the SARS-CoV-2 RBD and 10 nM of vimentin pre-incubation, the monolayer permeability alteration was not affected for the MCF-10a control cells, but it was inhibited for the MCF-7 cancer cells.

To summarise these data in general, we have shown that recombinant vimentin has effects on cell proliferation, adhesion, and migration, and on epithelial cell monolayer permeability in MCF-10a control cells and MCF-7 cancer cells. Vimentin also affects the cell monolayer permeability changes triggered by SARS-CoV-2 RBD.

3.2 Vimentin secretion and its effect on macrophage functionality

3.2.1 Activated macrophages express cell-surface vimentin in a polarised manner

First, we asked whether vimentin is expressed isotopically on the surface of cells. For this, we differentiated HL-60 cells into macrophages by treating them with 12-O-tetradecanoylphorbol-13-acetate (TPA). After 24 h, these macrophages were activated with TNF- α . Interestingly, TNF- α also induces HL-60 macrophage differentiation [61]. However, we used TPA to differentiate our cells.

With permeabilisation of the cell membrane during immunofluorescence staining omitted, this ensured that the images acquired using the fluorescently labelled V9 anti-vimentin antibody only showed vimentin on the surface of the cells.

Upon treatment of the HL-60 cells with TPA for 24 h, they were seen to differentiate into macrophages (Fig. 13A). TNF- α treatment of these macrophages triggered the appearance of cell-surface vimentin in a polarised manner, as seen using the V9 anti-vimentin antibody; i.e. the vimentin expressed was not equally distributed over the cell surface. The vimentin expressed on the extracellular surface of these macrophages was instead polarised, as it was predominantly seen over particular areas of the cell surface (Fig. 13B). The proportion of the cells that expressed vimentin in this polarised manner was determined by cell counting. There was a >2-fold increase in the polarisation of extracellular cell-surface vimentin in these TNF- α -activated macrophages compared to the non-activated macrophages. During TNF- α activation for up to 6 days, greater proportions macrophages with polarised surface vimentin were seen after 1 day and 2 days (Fig. 13C). These data thus show that extracellular cell-surface vimentin is expressed in a polarised manner on these TNF- α -activated macrophages.

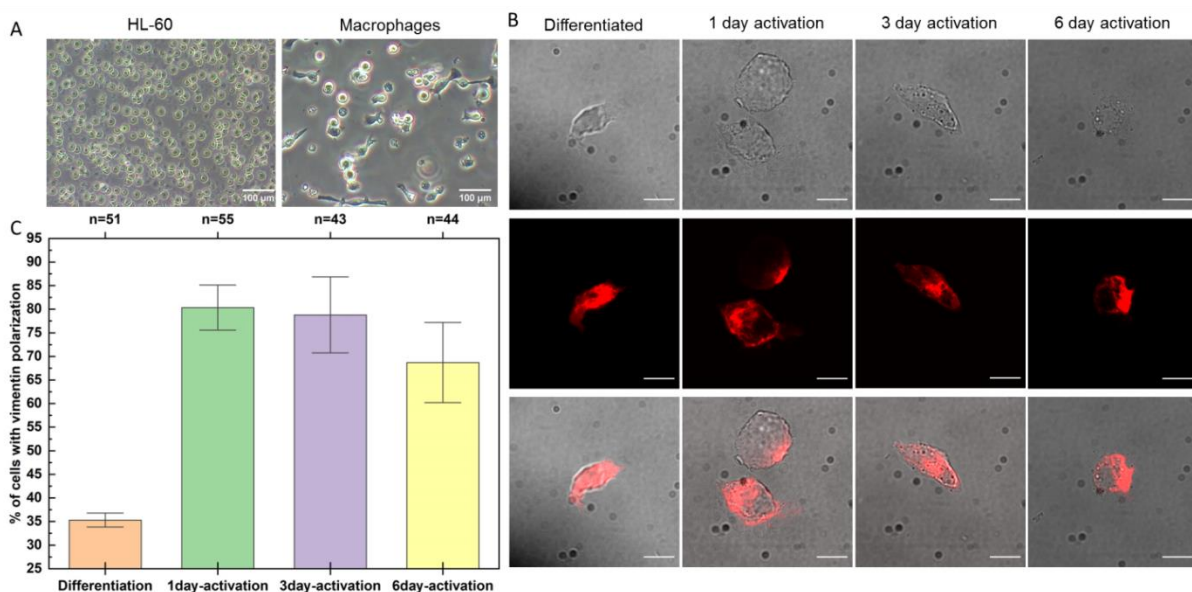


Figure 13. Polarised expression of extracellular vimentin on the surface of TNF- α -activated macrophages. (A) Representative HL-60 cells before (left) and after (right) differentiation with TPA.

(B) Representative non-permeabilised fixed samples of macrophages (Differentiated) stained with the V9 anti-vimentin antibody, showing expression of vimentin on their surface after 1, 3 and 6 days of TNF- α activation. Top row: Phase contrast images. Middle row: Fluorescent images for vimentin (red). Bottom row: Overlay of phase contrast and fluorescent images. Scale bar, 10 μ m. **(C)** Quantification of the proportion of macrophages expressing extracellular cell-surface vimentin in a polarised manner over the 6 days of TNF- α activation. *n* denotes the total number of cells analysed, error bars correspond to standard deviation.

3.2.2 Extracellular cell-surface vimentin is predominantly expressed at the back of activated macrophages and secreted in the form small fragments

Although the vimentin was polarised on the surface of these TNF- α -activated macrophages, as the 'front' and 'back' of these cells were not easily differentiable in these 2D fixed samples, its exact positioning was unknown (Fig. 14A). To solve this problem, patterned migration lines on glass coverslips were used, whereby the front and back of the cells can be distinguished by recording time-lapse movies. By following the macrophage migration on patterned lines coated with fibronectin, a simplified cell shape can be defined that allows visualisation of the position on the extracellular cell surface of the vimentin upon TNF- α activation (Fig. 14B).

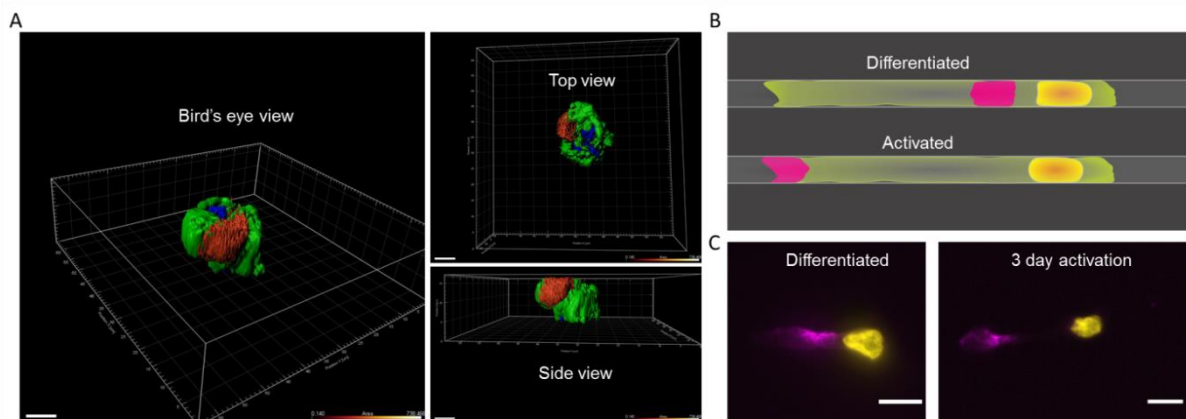


Figure 14. Visualisation of surface vimentin on macrophages patterned on one-dimensional lines. **(A)** Representative three-dimensional projections of a TNF- α -activated macrophage (red, surface vimentin; green, cell membrane), demonstrated using IMARIS. Scale bar, 7 μ m. **(B)** Illustration of the vimentin secretion sites (red) for the differentiated and TNF- α -activated macrophages using patterned lines. Yellow, nucleus; green, cell membrane. **(C)** Representative differentiated and TNF- α -activated macrophage attached and elongated along the pattern on a glass coverslip, revealing the site of vimentin secretion (yellow, nucleus; magenta, extracellular cell-surface vimentin). Scale bar, 10 μ m.

Here, the nucleus was always at the front end of these macrophages during migration. The position of the nucleus was then used as the reference to define the front of the fixed cells. Using this method, the surface vimentin was seen to be polarised at the back of the activated macrophages, allowing us to conclude that vimentin was secreted from the back of these TNF- α -activated macrophages. In contrast, prior to TNF- α activation, the differentiated

macrophages were seen to secrete vimentin at a site close to the nucleus (Fig. 14C). As, 1 day and 3 day activation showed comparable vimentin polarisation (Fig.13 C), here we used 3 day activation in 1D pattern experiment (Fig. 14C).

To further resolve the structure of the polarised vimentin on the cell surface, we used confocal microscopy for imaging. For this, genetically transformed HL-60 cells with vimentin tagged with green fluorescent protein (GFP-vimentin HL60 cells) were differentiated and activated. Here, images of elongated macrophages were acquired in order to evaluate the structure as well as the position of the surface vimentin. We observed small fragments of vimentin at the secretion sites of both differentiated and TNF- α -activated macrophages (Fig. 15A). In order to confirm the small fragments are on the outside of the cell, images of differentiated and TNF- α -activated macrophages were acquired using scanning electron microscopy (SEM) (Fig. 15B). Further, we confirmed the presence of vimentin on the dot like structure by visualising the same cell in both confocal and SEM by using coverslip with grid (Fig. 15C).

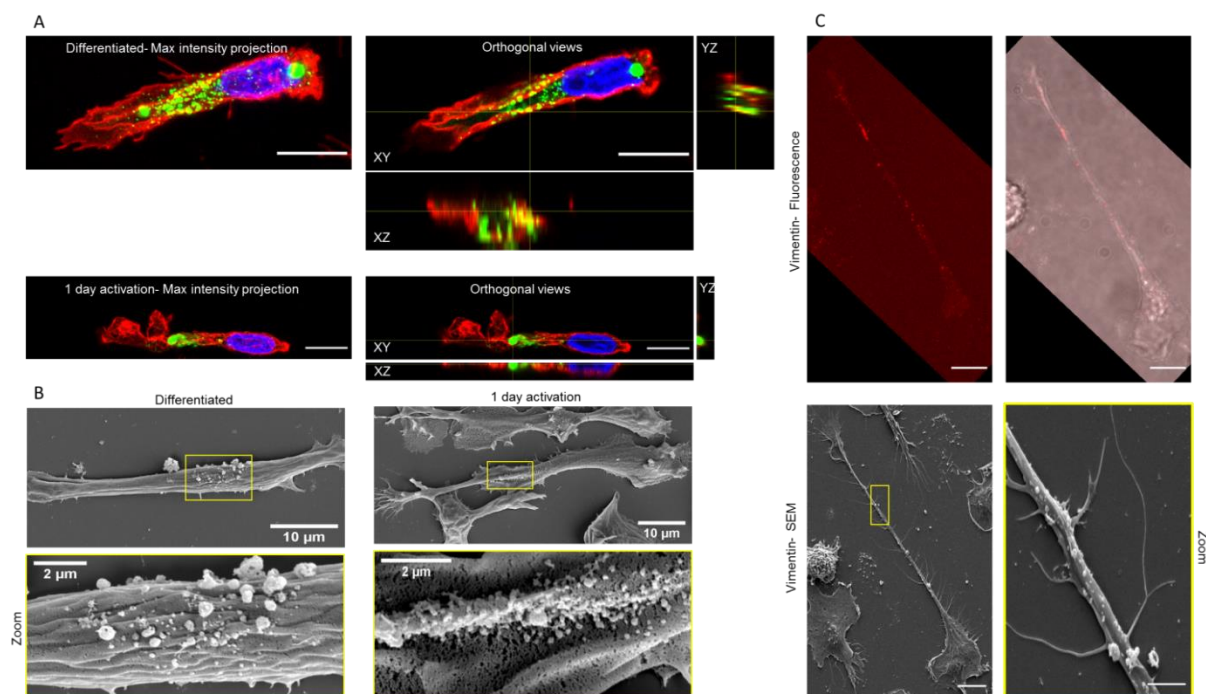


Figure 15. Visualisation of surface vimentin on macrophages differentiated from GFP-vimentin HL60. (A) Maximum intensity projection and orthogonal views of differentiated and TNF- α -activated macrophage (red, membrane; green, surface vimentin; blue, nucleus), acquired with confocal microscopy. Scale bar, 10 μ m. (B) Scanning electron microscopy images of vimentin secretion sites for the differentiated and TNF- α -activated macrophages. Bottom row: higher magnification of vimentin secretion site marked with yellow rectangle. This study was performed on 2D (glass coverslips) not on fibronectin coated 1D patterns. In order to have more residual cells after differentiation and activation, we used 1 day activation of both confocal LSM900 (A) and SEM imaging (B). (C) Confocal and SEM imaging using coverslips with grid. Top: Fluorescence images of vimentin (red; V9 antibody) stained in non-permeabilised activated macrophages. Scale bar 10 μ m. Bottom: SEM images of the same cell where the dot like structure can be seen at the same site of vimentin staining. Bottom (Right): magnified image of area marked in yellow of left. Scale bar 2 μ m.

3.2.3 Extracellular vimentin enhances migration and phagocytosis of macrophages

Macrophages are known to have a vital role in the immune system through phagocytosis of cellular debris and elimination of bacterial pathogens. We thus next investigated this extracellular cell-surface vimentin on the functionality of macrophages, in terms of their migration and phagocytosis.

The migration speeds of the macrophages were measured using a 2D migration assay (Fig. 16A). As the media from the TNF- α -activated macrophages that contained secreted vimentin is expected to have some residual TNF- α , recombinant vimentin was used here. Addition of recombinant vimentin to the differentiated macrophages significantly increased their migration speed. Further, the migration speed of the TNF- α -activated macrophages was significantly reduced when they were pre-incubated with the CSV antibody (Fig. 16B).

To investigate the phagocytic activity of macrophages under the influence of extracellular vimentin, phagocytosis assays using fluorescently-labeled latex beads were carried out to measure the phagocytic process in vitro. With phagocytosis analysed according to the phagocytotic index defined by the intracellular fluorescence intensities following phagocytosis of fluorescent beads (Fig. 16C), this was seen to be significantly increased in the TNF- α -activated macrophages compared to the differentiated macrophages (Fig. 16D). Further, this effect was mimicked by addition of 100 ng/mL recombinant vimentin to the differentiated macrophages, while it was blocked by the V9 anti-vimentin antibody in the TNF- α -activated macrophages (Fig. 16D). As for the migration effect, this enhanced phagocytosis might be due to the high expression levels of vimentin in the TNF- α -activated macrophages. Thus, from these data, we can conclude that extracellular addition of recombinant vimentin enhances both the migration and phagocytosis of these macrophages.

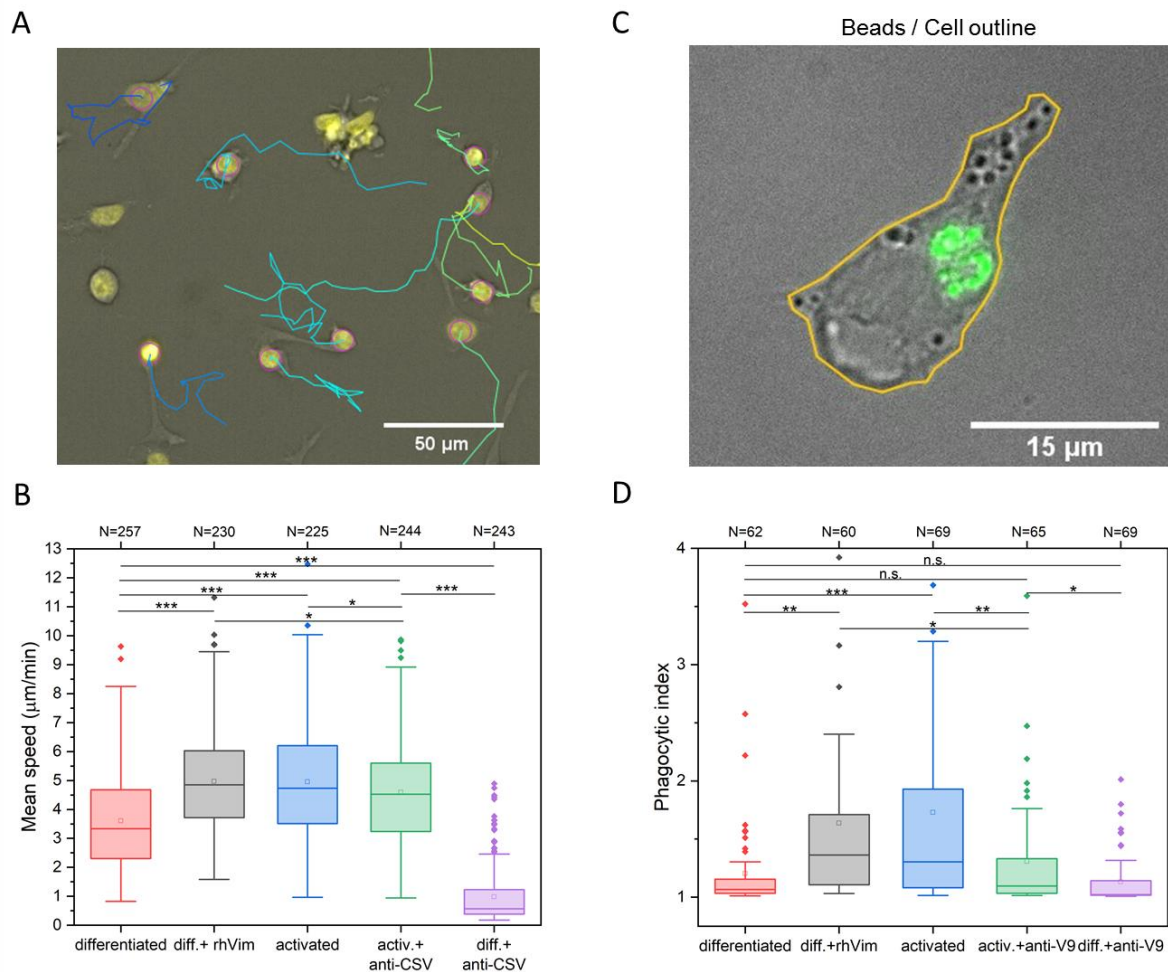


Figure 16. Stimulation of migration and phagocytosis of macrophages by addition of recombinant (*rh*)Vimentin. **(A)** Migration tracks of $TNF-\alpha$ -activated macrophages visualised using TrackMate ImageJ plugin. **(B)** Quantification of migration speeds of differentiated macrophages without and with addition to the medium of 100 ng/mL *rh*Vimentin and anti-cell-surface vimentin antibody, and of $TNF-\alpha$ -activated macrophages without and with addition of the anti-cell-surface vimentin antibody (CSV). **(C)** Visualisation of fluorescent beads (green) phagocytosed by a $TNF-\alpha$ -activated macrophage using fluorescence microscopy. Cell outline (yellow) defined from phase contrast image. **(D)** Phagocytic index determined by the fluorescence intensity within the differentiated macrophages without and with addition of 100 ng/mL *rh*Vimentin and anti-vimentin antibody (V9), and of $TNF-\alpha$ -activated macrophages without and with addition of the anti-vimentin antibody (V9). *, $p < 0.05$; **, $p < 0.01$; ***, $p < 0.001$. n.s. not significant (Student's *t*-tests). All experiments were repeated three times. The data is presented as box plots with whiskers drawn within the 1.5 IQR value. *N* indicates the total number of cells analysed. All experiments were done three times.

4 DISCUSSION

This section is directly transferred from the following two original publications.

- Thalla, D.G.; Jung, P.; Bischoff, M.; Lautenschläger, F. Role of Extracellular Vimentin in Cancer-Cell Functionality and Its Influence on Cell Monolayer Permeability Changes Induced by SARS-CoV-2 Receptor Binding Domain. *Int. J. Mol. Sci.* 2021, 22, 7469. <https://doi.org/10.3390/ijms22147469>
- Thalla, D.G, Rajwar AC, Laurent AM, Becher JE, Kainka L and Lautenschläger F (2022) Extracellular vimentin is expressed at the rear of activated macrophage-like cells: Potential role in enhancement of migration and phagocytosis. *Front. Cell Dev. Biol.* 10:891281. doi: 10.3389/fcell.2022.891281

4.1 Influence on cancer cell functionality

For about a decade, the existence of extracellular vimentin has been questioned by the scientific community, and even by researchers working on vimentin. However, recent studies have shown that vimentin can indeed be secreted into the extracellular space under several physiological conditions, such as cell activation, inflammation, senescence, and stress [3,4,33]. Vimentin is secreted by various cell types, such as macrophages, astrocytes, neutrophils, monocytes, apoptotic lymphocytes, and endothelial cells [15, 18-21, 62]. Mor-Vaknin et al. (2003) reported that activated macrophages secrete vimentin when treated with okadaic acid. Recently, it was shown that oxidised low-density lipoprotein induced vimentin secretion via CD36 in macrophages [63]. Recent studies have also provided evidence that extracellular vimentin is involved in several diseases, in repair mechanisms for spinal cord injury, and in the infection mechanisms of viruses [64]. We also described some of these roles of extracellular vimentin in health and disease in a recent review[14]. The functions of extracellular vimentin are still under debate, however, and these functions appear to depend on the form of this extracellular vimentin.

Secreted vimentin could have a potential role in wound healing, although to date, the role of vimentin in wound healing has mainly focussed on cytoplasmic vimentin. Nevertheless, recent studies have explored the possibility of extracellular vimentin as a potential remedy for tissue repair in many injuries [14]. Post-injury, vimentin released into the extracellular milieu facilitates wound closure by binding to mesenchymal leader cells. This extracellular vimentin promotes mesenchymal to myofibroblast differentiation of leader cells [32]. However, here the interaction of extracellular vimentin with receptors on leader cells that lead to wound healing remains an open question.

Vimentin has also been shown to have a role in wound healing during functional recovery after trauma in the central nervous system, which is a challenge that is still faced in the field of neuroscience [65]. In this context, a newly described compound, denosomin, was shown to provide added benefits in the treatment of mice for spinal cord injury [33]. During the course of these treatments, it was noted that the astrocytes tended to secrete vimentin at the site of the injury. This secreted vimentin promoted axonal growth by activation of IGF-1R, to thus promote improved functional recovery of the spinal cord in mice [34]. However, this previous study was focused mainly on the promotion of axonal growth via the vimentin interaction with IGF-1R, so in the present study we specifically explored the role of the extracellular vimentin and IGF-1R interaction across a range of cellular functions, as cell proliferation, adhesion, and migration; these are all crucial for tumor progression.

In cancers, the collective migration of cells is a critical event for establishment of metastases, and this indicates how cells contribute to cancer invasion [66]. Extracellular vimentin was shown previously to be involved in cancer-cell invasion [67]. In another study, the interaction between surface vimentin and GlcNAc-polymers led to an increase in migration and invasion of MDCK and MCF-7 cells [68]. In the present study, we showed that addition of recombinant vimentin promoted wound closure for both MCF-10a and MCF-7 cells, presumably through increased migratory speed of the cells following activation of the IGF-1R cell-surface receptor. We also showed that recombinant vimentin stimulated a greater increase in cell migration rate in the MCF-7 cancer cells than for the MCF-10a cells. Here, we also compared the effect of vimentin on cell migration with that of IGF-1 itself, as it is well known that IGF-1 induces cell migration in breast epithelial cells [55]. Interestingly, in the MCF-10a cells, the addition of vimentin resulted in greater migratory speed for these cells compared to the addition of IGF-1. We also saw similar effects by using the transwell migration assay here, which was greater with treatment with vimentin, and even higher than for the IGF-1 treatment for the MCF-10a cells.

In invasion by cancer cells, cell adhesion is one of the first steps during metastasis [69]. In addition, cell migration and proliferation are regulated by cell adhesion to the extracellular matrix [70]. Therefore, we additionally investigated cell adhesion upon vimentin treatment in the present study, which showed that vimentin treatment increased the adhesion strength in MCF-7 cancer cells. Interestingly, we also showed that the vimentin-treated MCF-7 cells showed a higher trend towards Young's modulus during these FluidFM measurements. This suggests that the stiffness of the MCF-7 cells was increased by vimentin.

Higher circulating IGF-1 levels are indicative of higher risk of breast cancer in premenopausal women [71, 72], and it has been reported that IGF-1 stimulates proliferation of breast cancer cells [73, 74]. Although serum vimentin expression has been reported for various cancers, these previous studies did not emphasise the significant role of extracellular vimentin in cell proliferation [30, 31]. Therefore, we also tested whether this extracellular (soluble) vimentin had similar effects as IGF-1 on cell proliferation. Interestingly, treatment with vimentin promoted increased proliferation rates in the MCF-7 cancer cells but not in MCF-10a cells. This effect was diminished when IGF-1R was blocked (using an anti-IGF-1R antibody),

which further supports our hypothesis that vimentin binding to IGF-1R is involved in general cellular functions.

Conclusively, as the migration rate of the MCF-10a cancer cells was higher in the presence of vimentin than the migration rate of MCF-7 cells in transwell assays under the same conditions, we hypothesised that transwell migration assays in the presence of vimentin can be used for sorting cancer cells. From this study, we concluded that cancer cells tend to be more sensitive to extracellular vimentin, and hence that extracellular vimentin has an effect on general cellular functions. Taking these parameters into consideration during clinical decision making can have a major role in the treatment of patients with cancers in general, and also under specific disease conditions.

Extracellular vimentin has a vital role in various viral and bacterial infections [64]. A recent study that used a pseudo virus showed that surface vimentin is involved in SARS-CoV-2 infection, through its binding by the viral spike protein. Using an antibody against extracellular vimentin, they showed that vimentin can be used as a potential target to inhibit viral particle entry into cells [75]. In the present study, in the cell permeability assays, vimentin decreased the barrier permeability in MCF-7 cancer cells and increased it in MCF-10a cells. These MCF-7 cancer cells overexpress IGF-1R, which might lead to more binding of vimentin to the cell membrane, and a block (i.e., decreased permeability) of the paracellular junctions. The permeability increases in the cell monolayers of both MCF-10a and MCF-7 cells induced by SARS-CoV-2 RBD and was further enhanced when the cells were pretreated with vimentin. This effect might be because extracellular vimentin can act as a co-receptor for the SARS-CoV and SARS-CoV-2 spike proteins [50]. This role for vimentin as a co-receptor will lead to more attachment of the SARS-CoV2 RBD to the cells treated with vimentin, and will also affect the cell monolayer permeability. This might result in enhanced viral particle invasion into tissues and internalisation into cells (Figure 17A).

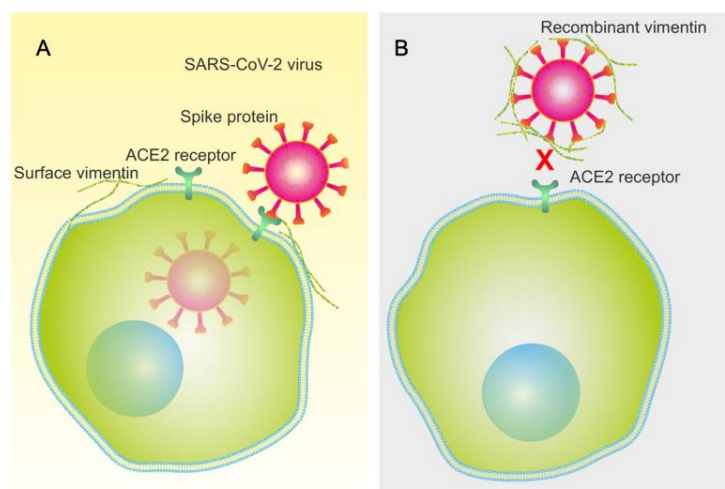


Figure 17. Illustration of the influence of extracellular vimentin in SARS-CoV-2 viral particle entry into cells. (A) Vimentin on the cell surface can act as a co-receptor, to promote further viral membrane association and virus entry into the cells. (B) For the viral particles pre-

treated with recombinant vimentin, this instead restricts viral association with the cell membrane, and thus virus entry into the cells.

In a previous study, pre-incubation of viral particles with recombinant vimentin restricted human Papillomavirus 16 (HPV) viral entry into HeLa, HaCaT, and NIKS cells [76]. In the present study, we used the same method, and preincubated SARS-CoV-2 RBD and recombinant vimentin prior to the treatment of the cell monolayers with this mixture. In the MCF-7 cancer cells, the permeability was decreased by SARS-CoV-2 RBD. However, this effect was not seen for the MCF-10a cells. This could be due to lack of ACE2 receptor, that RBD does not have any additional effect on MCF-10a cells [77].

Further studies are required to understand the full mechanisms involved in the phenomena described here. However, we have shown that extracellular vimentin influences a range of cellular functions and might become an important player in the treatment of diseases or the prevention of particular infections. Additionally, extracellular vimentin can exist in different isoforms such as oxidised vimentin, citrullinated vimentin, and carbamylated vimentin which undergo post-translational modifications under certain circumstances (senescence, rheumatoid arthritis) [4,53,54]. Imitation of recombinant vimentin as extracellular vimentin could pose some limitations in the practical setting. Therefore, future studies should investigate the effect of native isoforms of extracellular vimentin on cells.

4.2 Characteristics of extracellular vimentin

The detection of vimentin in the extracellular space then promoted the question as to how it is secreted from inside these TNF- α -activated macrophages. Previously this extracellular vimentin was thought to have been released from necrotic cells, although it has also been suggested that it might be secreted. Previous studies have shown exosomes as a source of vimentin, and demonstrated that these can transport and release vimentin into the extracellular space [78-80]. Exosomes are packaged with membranes in the Golgi apparatus, and in activated macrophages, block of transport through the Golgi apparatus inhibits the release of extracellular vimentin [15]. This has thus strengthened the idea that vimentin is secreted with the help of exosomes. However, it has remained unclear what the characteristics of this secreted vimentin are.

In the present study, we show that vimentin is released from the back of these TNF- α -activated macrophages, and that this polarised release is enhanced by the macrophage activation. Moreover, using confocal, TIRF and SEM, we have confirmed that the structure of the secreted vimentin is not filamentous, as is its intracellular counterpart, but is in form of fragments, as indicated in recent studies [51, 81]. Nevertheless, further confirmation of data from GFP-vimentin HL60 is needed as it may not behave identical to endogenous vimentin.

It is believed that post-translational modifications are a prerequisite for vimentin secretion from macrophages and endothelial cells [41, 62, 82], which would appear necessary to break down the long vimentin filaments to smaller fragments [83]. In the case of activated macrophages, the extracellular vimentin was shown to be phosphorylated [15]. A recent study showed that vimentin is recruited to the cell membrane via an alteration in the filamentous form to an oligomeric form that consists of 4-12 monomers [84]. This multimeric form of vimentin showed a higher binding affinity to lipid bilayers compared to that of filamentous vimentin. However, the mechanism by which the intracellular vimentin is secreted into the extracellular space is not well characterised. Here, by combining data from the literature and the findings from the present study, we can predict a secretion mechanism as we illustrated in Figure 18. As seen from the present study, extracellular cell-surface vimentin is polarised at the back of TNF- α -activated macrophages, and the images from TIRF shows that small fragments of vimentin either from exosomes or filaments are released close to a large agglomerate of vimentin on the cell surface. Therefore, we propose that at the membrane surface of these TNF- α -activated macrophages, vimentin filaments disassemble into small fragments, to form agglomerates, which can then be released into cell medium or into blood serum (Fig. 18B).

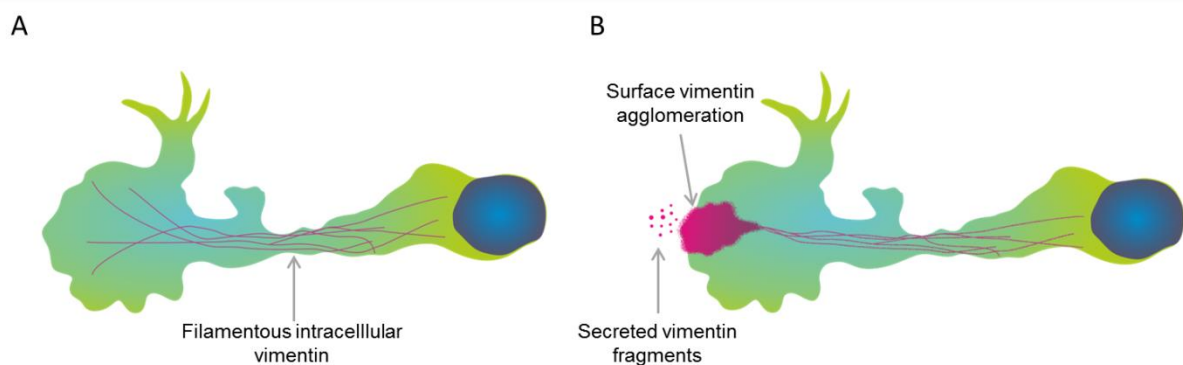


Figure 18. Proposed model of vimentin secretion. (A) A macrophage with intracellular vimentin in the filamentous form. (B) Dissociation of filamentous vimentin at the cell membrane in the activated macrophage might lead to agglomeration at the surface of the macrophage. Then, the vimentin can be released into the extracellular space in the form of small fragments.

Vimentin expression in the extracellular space of cells has been attributed to circumstances such as cell activation, senescence, injury and stress [15, 16, 32]. In most of these scenarios, the secretion of vimentin is related to immune activity [64]. For example, the vimentin secreted by activated macrophages has been suggested to be involved in immune functions via generation of oxidative metabolites and elimination of bacteria [15]. Another example is shown in patients with rheumatic arthritis, where neutrophils secrete citrullinated vimentin during the release of neutrophil extracellular traps that are produced to immobilise pathogens and promote immune responses [19, 26]. Further, in the mycobacterium tuberculosis, vimentin binds to the natural killer cell surface receptor NKp46 and contributes to lysis of

infected cells [36]. Finally, extracellular vimentin blocks pro-inflammatory secretion by activated dendritic cells, which promotes inhibition of adaptive immune responses. This mechanism prevents tissue damage and promotes bacteria elimination [37].

On the basis of this evidence that extracellular vimentin partially regulates inflammatory processes, we investigated the role of extracellular vimentin on macrophage function. Using migration assays, we show that elevated levels of extracellular cell-surface vimentin enhance the migration speed of macrophages. Here, it was not relevant if the extracellular vimentin was added as recombinant vimentin or if it was from secretion of activated macrophages. This increase in macrophage migration by addition of recombinant vimentin complements our recent study where we showed similar effects in MCF-7 cells [17].

Earlier studies have demonstrated that increases in phagocytic activity by macrophages involves extracellular vimentin. However, in these previous studies, the vimentin was expressed on the surface of apoptotic neutrophils and T cells and acted as a signalling agent to attract macrophages and further facilitate the elimination process [20, 21, 85, 86]. On the surface of phagocytes, vimentin interacts with O-GlcNAc-modified proteins expressed on apoptotic cells, which generates an 'eat me' signal for elimination by macrophages [86]. To date, surface vimentin has been believed to be a mediator that helps to attract macrophages towards the cells that need to be phagocytosed. However, one study that investigated extracellular vimentin directly expressed on activated macrophages demonstrated enhanced bacteria elimination [15]. In the present study, we further explored the effects of extracellular vimentin expressed on the surface of macrophages in terms of macrophage function. We show that recombinant vimentin treatment of HL-60 differentiated macrophages has a similar effect as TNF- α -activated macrophages in terms of enhanced phagocytic activity. Interestingly, in a recent study it was shown that extracellular addition of vimentin lead to TNF- α secretion in macrophages [63]. Consequently, this could be a possible mechanism behind the enhanced migration and phagocytic activity in macrophages.

Taken together, we demonstrate that vimentin is expressed in a polarised form on the surface of activated macrophages, and that it is released in a fragmented form. We also show that extracellular vimentin influences the functionality of macrophages by enhancing their migration and phagocytosis.

Altogether, these data suggests that extracellular vimentin is used to regulate macrophages in the immune system through effective elimination of bacterial pathogens.

5 CONCLUSION AND FUTURE WORK

The fact that investigation of extracellular vimentin is incredibly unconventional and raises lots of interest in the IF community. Ever since Mor-Vaknin and colleagues demonstrated the secretion of vimentin from activated macrophages, the curiosity among the scientific community has increased in understanding and discovering the role of extracellular vimentin on par with its intracellular counterpart. Vimentin secretion to extracellular space is mainly attributed to activation, injury, stress, senescence and certain pathological conditions. Furthermore, vimentin secretion is associated with immune activity in most scenarios. Interestingly, the functional aspects of the extracellular vimentin range from being a cancer marker to its involvement in the recent SARS-CoV-2 infection.

The first of this thesis focused on extracellular vimentin's role in cellular functions. This work demonstrated the effect of recombinant, extracellular vimentin on the proliferation, migration and adhesion of a non-tumorigenic cell line and a cancer cell line. Moreover, the findings show that the cancerous cells react stronger to extracellular vimentin than the non-tumorigenic cells in terms of general cellular functions, namely proliferation, adhesion and migration. Therefore, it gives an outlook on understanding fundamental cancer cell behaviour in areas of inflammation.

The current pandemic situation allowed expanding the eventual role of extracellular vimentin in monolayer permeability caused by SARS-CoV-2 RBD in cancer cells with the potential to develop strategies for decreasing infections in future.

The second part of this thesis focused on the characteristics of extracellular vimentin. The findings from this part of the study demonstrated the secretion of vimentin from the back of activated macrophages in the form of small fragments, enhancing phagocytosis and migration of activated macrophages.

Even though it is evident that extracellular vimentin is not just a mislocalised protein but has various functional roles, the secretion mechanism is not yet well established. The future focus will be on finding vimentin's secretion mechanism. The recent reports show that inside the cell, vimentin templates microtubules and gets transported to the cell periphery via microtubules. Therefore by studying the role of microtubules in vimentin secretion, a potential secretion pathway of vimentin can be demonstrated, which would open up a wide range of possibilities in treating various diseases and viral infections.

6 REFERENCES

1. Bershadsky, A.D. and J.M. Vasiliev, *Cytoskeleton*. 2012.
2. Fletcher, D.A. and R.D. Mullins, *Cell mechanics and the cytoskeleton*. *Nature*, 2010. **463**(7280): p. 485-492.
3. *The Cell: A Molecular Approach. 2nd Edition*. 2000: Sinauer Associates, Incorporated.
4. Sept, D., et al., *Annealing Accounts for the Length of Actin Filaments Formed by Spontaneous Polymerisation*. *Biophysical Journal*, 1999. **77**(6): p. 2911-2919.
5. Pollard, T.D. and J.A. Cooper, *Actin, a Central Player in Cell Shape and Movement*. *Science*, 2009. **326**(5957): p. 1208-1212.
6. Hohmann, T. and F. Dehghani, *The Cytoskeleton—A Complex Interacting Meshwork*. *Cells*, 2019. **8**(4): p. 362.
7. Nogales, E., *Structural Insights into Microtubule Function*. *Annual Review of Biochemistry*, 2000. **69**(1): p. 277-302.
8. de Pablo, P.J., et al., *Deformation and Collapse of Microtubules on the Nanometer Scale*. *Physical Review Letters*, 2003. **91**(9): p. 098101.
9. Goodson, H.V. and E.M. Jonasson, *Microtubules and Microtubule-Associated Proteins*. *Cold Spring Harb Perspect Biol*, 2018. **10**(6).
10. Herrmann, H., et al., *Intermediate filaments: from cell architecture to nanomechanics*. *Nature Reviews Molecular Cell Biology*, 2007. **8**(7): p. 562-573.
11. Leduc, C. and S. Etienne-Manneville, *Intermediate filaments in cell migration and invasion: the unusual suspects*. *Current Opinion in Cell Biology*, 2015. **32**: p. 102-112.
12. Fuchs, E. and K. Weber, *INTERMEDIATE FILAMENTS: Structure, Dynamics, Function and Disease*. *Annual Review of Biochemistry*, 1994. **63**(1): p. 345-382.
13. Herrmann, H. and U. Aebi, *Intermediate Filaments: Structure and Assembly*. *Cold Spring Harb Perspect Biol*, 2016. **8**(11).
14. Danielsson, F., et al., *Vimentin Diversity in Health and Disease*. *Cells*, 2018. **7**(10).
15. Mor-Vaknin, N., et al., *Vimentin is secreted by activated macrophages*. *Nat Cell Biol*, 2003. **5**(1): p. 59-63.

16. Frescas, D., et al., *Senescent cells expose and secrete an oxidised form of membrane-bound vimentin as revealed by a natural polyreactive antibody*. Proceedings of the National Academy of Sciences, 2017. **114**(9): p. E1668-E1677.
17. Thalla, D.G., et al., *Role of Extracellular Vimentin in Cancer-Cell Functionality and Its Influence on Cell Monolayer Permeability Changes Induced by SARS-CoV-2 Receptor Binding Domain*. International Journal of Molecular Sciences, 2021. **22**(14): p. 7469.
18. Greco, T.M., et al., *Quantitative Mass Spectrometry-based Proteomics Reveals the Dynamic Range of Primary Mouse Astrocyte Protein Secretion*. Journal of Proteome Research, 2010. **9**(5): p. 2764-2774.
19. Kaplan, M.J., *Role of neutrophils in systemic autoimmune diseases*. Arthritis Research & Therapy, 2013. **15**(5): p. 219.
20. Boilard, E., et al., *Identification of an autoantigen on the surface of apoptotic human T cells as a new protein interacting with inflammatory group IIA phospholipase A 2*. Blood, 2003. **102**(8): p. 2901-2909.
21. Moisan, E. and D. Girard, *Cell surface expression of intermediate filament proteins vimentin and lamin B1 in human neutrophil spontaneous apoptosis*. Journal of Leukocyte Biology, 2006. **79**(3): p. 489-498.
22. Thiagarajan, P.S., et al., *Vimentin is an endogenous ligand for the pattern recognition receptor Dectin-1*. Cardiovascular Research, 2013. **99**(3): p. 494-504.
23. Li, F.J., et al., *Autoimmunity to Vimentin Is Associated with Outcomes of Patients with Idiopathic Pulmonary Fibrosis*. The Journal of Immunology, 2017. **199**(5): p. 1596-1605.
24. Alcover, A., et al., *Antibodies to vimentin intermediate filaments in sera from patients with systemic lupus erythematosus*. Arthritis & Rheumatism, 1984. **27**(8): p. 922-928.
25. Gong, D.H., et al., *Secretory vimentin is associated with coronary artery disease in patients and induces atherogenesis in ApoE^{-/-} mice*. International Journal of Cardiology, 2019. **283**: p. 9-16.
26. Carmona-Rivera, C., et al., *Neutrophil extracellular traps are a source of citrullinated autoantigens and stimulate inflammatory responses in rheumatoid arthritis (P4061)*. The Journal of Immunology, 2013. **190**(1 Supplement): p. 127.2-127.2.
27. Carter, V. and W.M. Howell, *Vimentin antibody production in transplant patients and immunomodulatory effects of vimentin in-vitro*. Human Immunology, 2013. **74**(11): p. 1463-1469.

28. Azimzadeh, A.M., et al., *Humoral Immunity to Vimentin Is Associated with Cardiac Allograft Injury in Nonhuman Primates*. American Journal of Transplantation, 2005. **5**(10): p. 2349-2359.
29. Carter, V., et al., *Vimentin Antibodies: A Non-HLA Antibody as a Potential Risk Factor in Renal Transplantation*. Transplantation Proceedings, 2005. **37**(2): p. 654-657.
30. Bukhari, S., et al., *Affinity proteomics led identification of vimentin as a potential biomarker in colon cancers: Insights from serological screening and computational modelling*. Molecular BioSystems, 2015. **11**(1): p. 159-169.
31. Sun, S., et al., *Proteomics of Hepatocellular Carcinoma: Serum Vimentin As a Surrogate Marker for Small Tumors (≤ 2 cm)*. Journal of Proteome Research, 2010. **9**(4): p. 1923-1930.
32. Walker, J.L., et al., *In wound repair vimentin mediates the transition of mesenchymal leader cells to a myofibroblast phenotype*. Molecular Biology of the Cell, 2018. **29**(13): p. 1555-1570.
33. Shigyo, M. and C. Tohda, *Extracellular vimentin is a novel axonal growth facilitator for functional recovery in spinal cord-injured mice*. Scientific Reports, 2016. **6**(1): p. 28293.
34. Shigyo, M., et al., *Extracellular vimentin interacts with insulin-like growth factor 1 receptor to promote axonal growth*. Scientific reports, 2015. **5**: p. 12055-12055.
35. Lam, F.W., et al., *Recombinant Human Vimentin Binds to P-Selectin and Blocks Neutrophil Capture and Rolling on Platelets and Endothelium*. J Immunol, 2018. **200**(5): p. 1718-1726.
36. Garg, A., et al., *Vimentin Expressed on Mycobacterium tuberculosis-Infected Human Monocytes Is Involved in Binding to the NKp46 Receptor*. The Journal of Immunology, 2006. **177**(9): p. 6192-6198.
37. Yu, M.B., et al., *Extracellular vimentin modulates human dendritic cell activation*. Molecular Immunology, 2018. **104**: p. 37-46.
38. Da, Q., et al., *Platelet adhesion involves a novel interaction between vimentin and von Willebrand factor under high shear stress*. Blood, 2014. **123**(17): p. 2715-21.
39. Fasipe, T.A., et al., *Extracellular Vimentin/VWF (von Willebrand Factor) Interaction Contributes to VWF String Formation and Stroke Pathology*. Stroke, 2018. **49**(10): p. 2536-2540.
40. Satelli, A. and S. Li, *Vimentin in cancer and its potential as a molecular target for cancer therapy*. (1420-9071 (Electronic)).

41. Noh, H., et al., *Discovery of cell surface vimentin targeting mAb for direct disruption of GBM tumor initiating cells*. *Oncotarget*, 2016. **7**(44).
42. Satelli, A., et al., *Universal Marker and Detection Tool for Human Sarcoma Circulating Tumor Cells*. *Cancer Research*, 2014. **74**(6): p. 1645-1650.
43. Satelli, A., et al., *Epithelial–Mesenchymal Transitioned Circulating Tumor Cells Capture for Detecting Tumor Progression*. *Clinical Cancer Research*, 2015. **21**(4): p. 899-906.
44. Mitra, A., et al., *Cell-surface Vimentin: A mislocalised protein for isolating csVimentin+CD133– novel stem-like hepatocellular carcinoma cells expressing EMT markers*. *International Journal of Cancer*, 2015. **137**(2): p. 491-496.
45. Ghosh, P., et al., *Invasion of the Brain by Listeria monocytogenes Is Mediated by InlF and Host Cell Vimentin*. *mBio*, 2018. **9**(1): p. e00160-18.
46. Bastounis, E.E., Y.T. Yeh, and J.A. Theriot, *Matrix stiffness modulates infection of endothelial cells by Listeria monocytogenes via expression of cell surface vimentin*. *Mol Biol Cell*, 2018. **29**(13): p. 1571-1589.
47. Yang, J., et al., *Superficial vimentin mediates DENV-2 infection of vascular endothelial cells*. *Scientific Reports*, 2016. **6**(1): p. 38372.
48. Bryant, A.E., et al., *Group A Streptococcal Myonecrosis: Increased Vimentin Expression after Skeletal-Muscle Injury Mediates the Binding of Streptococcus pyogenes*. *The Journal of Infectious Diseases*, 2006. **193**(12): p. 1685-1692.
49. Li, W., et al., *Angiotensin-converting enzyme 2 is a functional receptor for the SARS coronavirus*. *Nature*, 2003. **426**(6965): p. 450-454.
50. Yu, Y.T.-C., et al., *Surface vimentin is critical for the cell entry of SARS-CoV*. *Journal of Biomedical Science*, 2016. **23**(1): p. 14.
51. Suprewicz, Ł., et al., *Extracellular Vimentin as a Target Against SARS-CoV-2 Host Cell Invasion*. *Small*. **n/a**(n/a): p. 2105640.
52. Adams, T.E., et al., *Structure and function of the type 1 insulin-like growth factor receptor*. *Cellular and Molecular Life Sciences CMLS*, 2000. **57**(7): p. 1050-1093.
53. Smith, T.J., *Insulin-like growth factor-I regulation of immune function: a potential therapeutic target in autoimmune diseases?* *Pharmacol Rev*, 2010. **62**(2): p. 199-236.
54. Ma, Z., et al., *Silencing of the type 1 insulin-like growth factor receptor increases the sensitivity to apoptosis and inhibits invasion in human lung adenocarcinoma A549 cells*. *Cell Mol Biol Lett*, 2007. **12**(4): p. 556-72.

55. Mezi, S., et al., *involvement of the Src-cortactin pathway in migration induced by IGF-1 and EGF in human breast cancer cells*. *Int J Oncol*, 2012. **41**(6): p. 2128-38.
56. Guillaume-Gentil, O., et al., *Force-controlled manipulation of single cells: from AFM to FluidFM*. (1879-3096 (Electronic)).
57. Buchert, M., K. Turksen, and F. Hollande, *Methods to Examine Tight Junction Physiology in Cancer Stem Cells: TEER, Paracellular Permeability, and Dilution Potential Measurements*. *Stem Cell Reviews and Reports*, 2012. **8**(3): p. 1030-1034.
58. McCaffrey, L.M. and I.G. Macara, *Epithelial organisation, cell polarity and tumorigenesis*. *Trends in Cell Biology*, 2011. **21**(12): p. 727-735.
59. Gray, R.S., K.J. Cheung, and A.J. Ewald, *Cellular mechanisms regulating epithelial morphogenesis and cancer invasion*. *Current Opinion in Cell Biology*, 2010. **22**(5): p. 640-650.
60. Buzhdygan, T.P., et al., *The SARS-CoV-2 spike protein alters barrier function in 2D static and 3D microfluidic in-vitro models of the human blood-brain barrier*. *Neurobiology of disease*, 2020. **146**: p. 105131-105131.
61. Squinto, S.P., et al., *Induction of Macrophage-Like Differentiation of HL-60 Leukemia Cells by Tumor Necrosis Factor- α : Potential Role of fos Expression*. *Molecular Endocrinology*, 1989. **3**(2): p. 409-419.
62. Patteson, A.E., et al., *Mechanical and Non-Mechanical Functions of Filamentous and Non-Filamentous Vimentin*. *BioEssays*, 2020. **42**(11): p. 2000078.
63. Kim, S., et al., *Oxidised LDL induces vimentin secretion by macrophages and contributes to atherosclerotic inflammation*. *Journal of Molecular Medicine*, 2020. **98**(7): p. 973-983.
64. Ramos, I., et al., *Vimentin as a Multifaceted Player and Potential Therapeutic Target in Viral Infections*. *International journal of molecular sciences*, 2020. **21**(13): p. 4675.
65. Liu, Z., et al., *Beneficial effects of gfap/vimentin reactive astrocytes for axonal remodeling and motor behavioral recovery in mice after stroke*. *Glia*, 2014. **62**(12): p. 2022-2033.
66. Friedl, P. and D. Gilmour, *Collective cell migration in morphogenesis, regeneration and cancer*. *Nature Reviews Molecular Cell Biology*, 2009. **10**(7): p. 445-457.
67. Satelli, A., et al., *Potential Function of Exogenous Vimentin on the Activation of Wnt Signaling Pathway in Cancer Cells*. *Journal of Cancer*, 2016. **7**(13): p. 1824-1832.
68. Komura, K., H. Ise, and T. Akaike, *Dynamic behaviors of vimentin induced by interaction with GlcNAc molecules*. *Glycobiology*, 2012. **22**(12): p. 1741-1759.

69. Hamidi, H. and J. Ivaska, *Every step of the way: integrins in cancer progression and metastasis*. Nature Reviews Cancer, 2018. **18**(9): p. 533-548.
70. Maziveyi, M. and S.K. Alahari, *Cell matrix adhesions in cancer: The proteins that form the glue*. Oncotarget, 2017. **8**(29): p. 48471-48487.
71. Hankinson, S.E., et al., *Circulating concentrations of insulin-like growth factor I and risk of breast cancer*. The Lancet, 1998. **351**(9113): p. 1393-1396.
72. Schernhammer, E.S., et al., *Circulating Levels of Insulin-like Growth Factors, their Binding Proteins, and Breast Cancer Risk*. Cancer Epidemiology Biomarkers & Prevention, 2005. **14**(3): p. 699-704.
73. Davison, Z., et al., *Insulin-like growth factor-dependent proliferation and survival of triple-negative breast cancer cells: implications for therapy*. Neoplasia (New York, N.Y.), 2011. **13**(6): p. 504-515.
74. Dupont, J. and D. Le Roith, *Insulin-like growth factor 1 and oestradiol promote cell proliferation of MCF-7 breast cancer cells: new insights into their synergistic effects*. Molecular pathology : MP, 2001. **54**(3): p. 149-154.
75. Suprewicz, Ł., et al., *Vimentin binds to SARS-CoV-2 spike protein and antibodies targeting extracellular vimentin block in vitro uptake of SARS-CoV-2 virus-like particles*. bioRxiv : the preprint server for biology, 2021: p. 2021.01.08.425793.
76. Schäfer, G., et al., *Vimentin Modulates Infectious Internalisation of Human Papillomavirus 16 Pseudovirions*. Journal of Virology, 2017. **91**(16): p. e00307-17.
77. Leoncikias, V., et al., *Generation of 2,000 breast cancer metabolic landscapes reveals a poor prognosis group with active serotonin production*. Scientific Reports, 2016. **6**(1): p. 19771.
78. Chen, Z., et al., *Cytoskeleton-centric protein transportation by exosomes transforms tumor-favorable macrophages*. (1949-2553 (Electronic)).
79. Adolf, A., et al., *Release of astroglial vimentin by extracellular vesicles: Modulation of binding and internalisation of C3 transferase in astrocytes and neurons*. (1098-1136 (Electronic)).
80. Parvanian, S., et al., *Exosomal vimentin from adipocyte progenitors accelerates wound healing*. Cytoskeleton, 2020. **77**(10): p. 399-413.
81. Lalioti, V., et al., *Immunolocalization studies of vimentin and ACE2 on the surface of cells exposed to SARS-CoV-2 Spike proteins*. bioRxiv, 2021: p. 2021.05.04.442648.

82. Liu, M., et al., *Prognostic significance of PD-L1 expression on cell-surface vimentin-positive circulating tumor cells in gastric cancer patients*. *Molecular Oncology*, 2020. **14**(4): p. 865-881.
83. Mónico, A., et al., *Vimentin disruption by lipoxidation and electrophiles: Role of the cysteine residue and filament dynamics*. *Redox Biology*, 2019. **23**: p. 101098.
84. Hwang, B. and H. Ise, *Multimeric conformation of type III intermediate filaments but not the filamentous conformation exhibits high affinity to lipid bilayers*. *Genes to Cells*, 2020. **25**(6): p. 413-426.
85. Starr, A.E., et al., *Biochemical Characterisation and N-terminomics Analysis of Leukolysin, the Membrane-type 6 Matrix Metalloprotease (MMP25): CHEMOKINE AND VIMENTIN CLEAVAGES ENHANCE CELL MIGRATION AND MACROPHAGE PHAGOCYTIC ACTIVITIES**. *Journal of Biological Chemistry*, 2012. **287**(16): p. 13382-13395.
86. Ise, H., et al., *Engulfment and clearance of apoptotic cells based on a GlcNAc-binding lectin-like property of surface vimentin*. *Glycobiology*, 2012. **22**(6): p. 788-805.

7 SCIENTIFIC PUBLICATIONS

7.1 Publication 1: Extracellular vimentin is expressed at the rear of activated macrophage-like cells: Potential role in enhancement of migration and phagocytosis

Divyendu Goud Thalla¹ , Ashish Chand Rajwar¹ , Annalena Maria Laurent¹ , Johanna Elisabeth Becher² , Lucina Kainka¹ and Franziska Lautenschläger^{1,3}

¹ Experimental Physics, Saarland University, Saarbrücken, Germany,

² Centre for Bioinformatics, Saarland University, Saarbrücken, Germany,

³ Centre for Biophysics, Saarland University, Saarbrücken, Germany

Front. Cell Dev. Biol. 10:891281

doi: 10.3389/fcell.2022.891281

Published: 18 July 2022.

DT was involved in conceptualisation of the project; supervision; data analysis and visualisation; and writing original draft. AR performed polarisation and secretion experiments; data analysis and visualisation; contributed in writing. AL performed the migration and phagocytosis experiments; data analysis and visualisation. JB performed 1D pattern experiments; data analysis and visualisation. LK performed scanning electron microscopy experiments; visualisation. FL was involved in the conceptualisation of the project, contributed in writing/review and editing the manuscript; supervision; project administration; and funding acquisition. All authors have read and agreed to the published version of the manuscript.



OPEN ACCESS

EDITED BY
Dolores Pérez-Sala,
Spanish National Research Council
(CSIC), Spain

REVIEWED BY
Inmaculada Navarro-Lérida,
Autonomous University of Madrid, Spain
Chungho Kim,
Korea University, South Korea
José Luis Rodríguez-Fernández,
Spanish National Research Council
(CSIC), Spain

*CORRESPONDENCE
Franziska Lautenschläger,
f.lautenschlaeger@physik.uni-
saarland.de

SPECIALTY SECTION
This article was submitted to Cell
Growth and Division,
a section of the journal
Frontiers in Cell and Developmental
Biology

RECEIVED 07 March 2022
ACCEPTED 27 June 2022
PUBLISHED 18 July 2022

CITATION
Thalla DG, Rajwar AC, Laurent AM,
Becher JE, Kainka L and
Lautenschläger F (2022), Extracellular
vimentin is expressed at the rear of
activated macrophage-like cells:
Potential role in enhancement of
migration and phagocytosis.
Front. Cell Dev. Biol. 10:891281.
doi: 10.3389/fcell.2022.891281

COPYRIGHT
© 2022 Thalla, Rajwar, Laurent, Becher,
Kainka and Lautenschläger. This is an
open-access article distributed under
the terms of the [Creative Commons
Attribution License \(CC BY\)](https://creativecommons.org/licenses/by/4.0/). The use,
distribution or reproduction in other
forums is permitted, provided the
original author(s) and the copyright
owner(s) are credited and that the
original publication in this journal is
cited, in accordance with accepted
academic practice. No use, distribution
or reproduction is permitted which does
not comply with these terms.

Extracellular vimentin is expressed at the rear of activated macrophage-like cells: Potential role in enhancement of migration and phagocytosis

Divyendu Goud Thalla¹, Ashish Chand Rajwar¹,
Annalena Maria Laurent¹, Johanna Elisabeth Becher²,
Lucina Kainka¹ and Franziska Lautenschläger^{1,3*}

¹Experimental Physics, Saarland University, Saarbrücken, Germany, ²Centre for Bioinformatics, Saarland University, Saarbrücken, Germany, ³Centre for Biophysics, Saarland University, Saarbrücken, Germany

Macrophages have a vital role in the immune system through elimination of cell debris and microorganisms by phagocytosis. The activation of macrophages by tumour necrosis factor- α induces expression of extracellular cell-surface vimentin and promotes release of this vimentin into the extracellular environment. Vimentin is a cytoskeletal protein that is primarily located in the cytoplasm of cells. However, under circumstances like injury, stress, senescence and activation, vimentin can be expressed on the extracellular cell surface, or it can be released into the extracellular space. The characteristics of this extracellular vimentin, and its implications for the functional role of macrophages and the mechanism of secretion remain unclear. Here, we demonstrate that vimentin is released mainly from the back of macrophage-like cells. This polarisation is strongly enhanced upon macrophage activation. One-dimensional patterned lines showed that extracellular cell-surface vimentin is localised primarily at the back of activated macrophage-like cells. Through two-dimensional migration and phagocytosis assays, we show that this extracellular vimentin enhances migration and phagocytosis of macrophage-like cells. We further show that this extracellular vimentin forms agglomerates on the cell surface, in contrast to its intracellular filamentous form, and that it is released into the extracellular space in the form of small fragments. Taken together, we provide new insights into the release of extracellular cell-surface vimentin and its implications for macrophage functionality.

KEYWORDS

extracellular vimentin, macrophages, activation, migration, polarisation, phagocytosis, vimentin secretion

Introduction

Macrophages are immune cells that have multiple roles in physiological processes, which range from removal of cellular waste and tissue regeneration and remodelling, to protection against pathogen invasion (Krzyszczuk et al., 2018; Herzog et al., 2019; Zhang et al., 2021). Due to their heterogeneous functions, macrophages have a crucial role in the immune system (Viola et al., 2019).

An earlier study revealed that activation of macrophages by tumour necrosis factor (TNF)- α leads to extracellular cell-surface expression and release of vimentin into the surrounding medium (Mor-Vaknin et al., 2003). Similarly, in atherosclerosis, monocyte chemoattractant protein-1 (CCL2) and oxidised low-density lipoproteins stimulate secretion of vimentin from macrophages (Kim et al., 2020). Vimentin is a type III intermediate filament that is primarily located inside cells of mesenchymal origin. However, vimentin can also be expressed on the outside of cells under conditions such as inflammation, stress and senescence (Mor-Vaknin et al., 2003; Frescas et al., 2017; Patteson et al., 2020). Previous studies have shown that astrocytes, neutrophils, monocytes, apoptotic lymphocytes and endothelial cells can also secrete vimentin (Boilard et al., 2003; Mor-Vaknin et al., 2003; Moisan and Girard, 2006; Greco et al., 2010; Kaplan, 2013; Patteson et al., 2020). Within the cell, vimentin is involved in cellular functions such as adhesion, migration and signalling (Ivaska et al., 2007), while recent studies have indicated its functions as a dynamic extracellular protein in cancers (Satelli and Li, 2011; Satelli et al., 2014; Satelli et al., 2015), viral infections (Yang et al., 2016; Ghosh et al., 2018; Bryant et al., 2006; Schäfer et al., 2017; Suprewicz et al., 2022) and general cellular functions (Thalla et al., 2021). Despite the many functional roles now defined for extracellular vimentin, the characteristics and the circumstances of its secretion remain unclear.

Vimentin that is secreted by activated macrophages is also involved in bacterial elimination (Mor-Vaknin et al., 2003) and the immune response (Ramos et al., 2020). Therefore, we questioned the role of secreted vimentin in macrophage activity, and particularly in phagocytosis. It is already known that activation of macrophages enhances phagocytic activity and improves pathogen clearance (Leopold Wager and Wormley, 2014; Jaggi et al., 2020). It is also known that activation of macrophages by TNF- α results in enhanced phagocytosis of the fungal pathogen *Cryptococcus neoformans* (Collins and Bancroft, 1992), with the same is seen for glial macrophages in response to TNF- α in glial-neuronal cell co-cultures (Neniskyte et al., 2014). However, the role of extracellular vimentin for macrophage activity and functionality is not known.

In this study, we investigated the location and form of this extracellular vimentin. We further examined the influence of extracellular vimentin on macrophage functionality. Using fluorescence microscopy techniques and one-dimensional (1D) patterned lines, we show that vimentin is not equally distributed

on the surface of activated macrophages, but is located at the 'back' of the cells. We also show that vimentin is released into the extracellular environment in the form of small fragments. Using 2D migration and phagocytosis assays, we further show that addition of recombinant vimentin to macrophages has a similar effect on phagocytic activity and migration as for activated macrophages.

This study thus characterises extracellular vimentin and describes its influence on macrophage functionality. On the basis of these data, we propose a secretion pathway for vimentin. Collectively, these findings are crucial to understand how the immune system is regulated, and they offer new ways to interfere with it.

Materials and methods

Cell culture

HL60 cells were cultured in cell culture flasks (Grenier) in RPMI 1640 medium (Gibco) supplemented with 10% foetal bovine serum (Fischer Scientific), 1% 1:1 penicillin-streptomycin (Fischer Scientific) and 1% Glutamax (Gibco). The cells were passaged at a concentration of 10^6 cells/mL. HL60 cells were differentiated into a macrophage lineage by treatment with 10 nM TPA (Sigma) for 24 h (referred to as macrophages). Post-differentiation, the cells were treated with 5 ng/ml TNF- α (Gibco) for up to 6 days, to induce macrophage activation. Media containing TNF- α was changed every second day for the 3 and 6 days activation.

For confirmation of extracellular vimentin expression, HL60 cells that expressed GFP-tagged vimentin (GFP-Vimentin HL60 cells) were used. These were gifted by Dr. Monika Zwerger, DFG, Germany. These GFP-HL60 cells were cultured as indicated above, with the addition of 0.1 μ g/ml puromycin (Gibco) to the growth medium.

Immunostaining

Immunostaining of extracellular vimentin was carried out using the Alexa 647 fluorophore conjugated to the anti-vimentin V9 antibody (Santa Cruz Biotechnology). The cells were prepared by washing with phosphate-buffered saline (PBS) once to remove traces of the growth medium, and were fixed with 4% paraformaldehyde (Science Service) for 10 min. The samples were then blocked for 1 h with 3% bovine serum albumin (BSA) in phosphate-buffered saline. Finally, the cells were incubated with 1:200 V9 anti-vimentin antibody for 1 h, and then viewed under a fluorescence microscope.

The cell membrane was stained using a WGA CF 488A (Biotium) or Alexa Fluor 549 conjugated wheatgerm agglutinin (WGA) conjugate (W11262, Invitrogen). Cell membrane

staining using WGA was performed in conjunction with the V9 anti-vimentin antibody, with WGA staining by incubation with 1:200 anti-WGA antibody for 10 min, followed by fixing of the cells.

For M1 marker, activated macrophages were incubated with 1:100 anti CD68 antibody Alexa 488 (Santa Cruz Biotechnology) for 1 h.

Live-cell imaging was performed using the CSV anti-cell-surface vimentin antibody (Abnova). For this purpose, the cells were incubated with 1:100 CSV for 1 h prior to microscopy.

For permeabilised and non permeabilised comparison, cells were treated with or without triton x-100 0.2% (v/v) for 10 min prior to blocking with 3% (w/v) BSA and cells were incubated with 1:200 beta actin antibody (Proteintech) for 1 h. After washing with PBS, cells were incubated with 1:500 anti-rabbit 488 secondary antibody. Then samples were incubated with 1:200 V9 anti-vimentin antibody for 1 h.

Quantification of extracellular vimentin

For confirmation and characterisation of the pattern of extracellular vimentin expression on macrophage activation, activation of GFP-vimentin HL60 cells was used. The macrophages were plated on a micro porous transwell membrane (0.4 μm , Corning). The upper and lower compartments were filled with growth medium supplemented with or without TNF- α . Differentiated, inactivated macrophages were used as the control. The medium was collected from the bottom wells after 1 day and 3 days of activation with TNF- α . The collected medium plated into 96-well plates, and the fluorescence intensities were determined using a plate reader (Tecan M200 Pro), with measurement at 488 nm.

1D pattern

To produce 1D patterns we prepared PDMS microchips with channels of 5 μm width and attached them to glass bottom dishes using plasma activation. At the next step, the channels were filled with fibronectin (25 $\mu\text{g}/\text{ml}$, Sigma). The PDMS part of the chips were then pulled off and the glass bottom dishes were washed twice with PBS. Afterwards, cells were placed on these patterns (4,000 cells/ μL , working volume 500 μL) and stored in the incubator for 1 h. The patterns were washed once with PBS before cells were fixed and stained for vimentin with the V9 antibody.

Imaging

Fluorescence images were acquired using inverted microscopes. For polarization experiments, the images were acquired using a Ti-Eclipse (Nikon) equipped with Yokagawa spinning disk. For 1D

pattern experiments and phagocytosis experiments, the images were acquired using an Epi-fluorescence microscope (Ti-Eclipse, Nikon). For GFP-Vimentin HL60 cells, confocal images were acquired using a LSM900 with Airyscan 2 (Zeiss). The TIRF images were acquired using a Ti-Eclipse with TIRF (Nikon).

Scanning electron microscopy

For scanning electron microscopy cells were placed on gridded coverslips and treated for activation and differentiation as described before. Cells were fixed in solution containing 2% (v/v) glutaraldehyde (Merck) and 2% (v/v) PFA (Science Service) diluted in 0.2 M sodium cacodylate buffer (Merck) for 120 min.

The samples were incubated three times with 0.1 g sodium borohydride (Merck) in 10 ml PBS for 10 min before they were stained for vimentin as described before. The images were acquired using a spinning disc as described before. After imaging the cell were again incubated in the fixation solution overnight. Next, the samples were incubated in 0.1% tannic acid (Merck). Cell drying was performed by successively replacing water with ethanol (>99.8%, Fisher Scientific) and ethanol with hexamethyldisilazane (98%, Carl Roth and >99%, Sigma Aldrich). Eventually, the samples were sputtered with 4–6 nm platinum. Images were acquired at 5 kV under high vacuum using FEI Quanta 400 electron microscope. Secondary electrons were detected using an Everhart-Thornley detector.

Migration assay

To investigate the 2D migration of macrophages after activation and stimulation with 100 ng/ml recombinant vimentin (Prospec), fluorescent images of cell nuclei, which were stained using 250 ng/ml Hoechst for 20 min, and bright-field images were recorded over 30 min with a frame rate of 1 min. The cells were kept at 37°C and 5% CO₂ during the experiment. Cell trajectories were analysed using the ImageJ plugin Trackmate. For blocking the effect of vimentin in activated macrophages, live cell stain of cell surface vimentin antibody (Abnova) was added for 2 h prior to acquisition of migration data. For each cell, the mean migration speed was calculated as the mean value of the instantaneous speeds in between two successive recorded positions.

Phagocytosis assay

To investigate the phagocytic activity of macrophages under stimulation with extracellular recombinant vimentin, fluorescently-labelled latex beads were used in phagocytosis assays. The assay protocol was developed following the

manufacturer instructions (Phagocytosis Assay kits; IgG FITC; Item No. 500290; Cayman Chemicals). For vimentin treatment, differentiated cells were treated with human recombinant vimentin 100 ng/ml (Prospec) for 24 h and activated macrophages were preincubated with V9 anti-vimentin antibody (Santa Cruz) for 2 h prior to phagocytosis experiment.

For quantification of phagocytosis, the microscopy images obtained were analysed using the ImageJ software (Fiji). The analysis consisted of two steps: first, the cell shape was determined by manually outlining the cell on the bright-field image using the Polygon selections tool. The cell 'mask' obtained was then saved in the ROI Manager and layered over the fluorescent image. The mean fluorescent intensity of the beads within the cell area can be measured. Additionally, the background fluorescence in an area without cells was then measured for each image. With this data, the "phagocytic index" was calculated for each condition, as $PI = I_{\text{beads}}/I_{\text{background}}$. The average measurement of bead fluorescence corresponded to the number of fluorescently labelled beads that had been phagocytized by the macrophages, and was thus used to quantify their phagocytic activity.

Results

Activated macrophages express cell-surface vimentin in a polarised manner

First, we asked whether vimentin is expressed isotopically on the surface of cells. For this, we differentiated HL-60 cells into macrophages by treating them with 12-O-tetradecanoylphorbol-13-acetate (TPA). After 24 h, these macrophages were activated with TNF- α . Interestingly, TNF- α also induces HL-60 macrophage differentiation (Squinto et al., 1989). However, we used TPA to differentiate our cells.

With permeabilisation of the cell membrane during immunofluorescence staining omitted, this ensured that the images acquired using the fluorescently labelled V9 anti-vimentin antibody only showed vimentin on the surface of the cells.

Upon treatment of the HL-60 cells with TPA for 24 h, they were seen to differentiate into macrophages (Figure 1A). TNF- α treatment of these macrophages triggered the appearance of cell-surface vimentin in a polarised manner, as seen using the V9 anti-vimentin antibody; i.e., the vimentin expressed was not equally distributed over the cell surface. The vimentin expressed on the extracellular surface of these macrophages was instead polarised, as it was predominantly seen over particular areas of the cell surface (Figure 1B). The proportion of the cells that expressed vimentin in this polarised manner was determined by cell counting. There was a >2-fold increase in the polarisation of extracellular cell-surface vimentin in these TNF- α -activated macrophages compared to the non-activated macrophages. During TNF- α activation for up to 6 days, greater proportions macrophages with polarised surface vimentin were seen after 1 day and 2 days (Figure 1C). These data

thus show that extracellular cell-surface vimentin is expressed in a polarised manner on these TNF- α -activated macrophages.

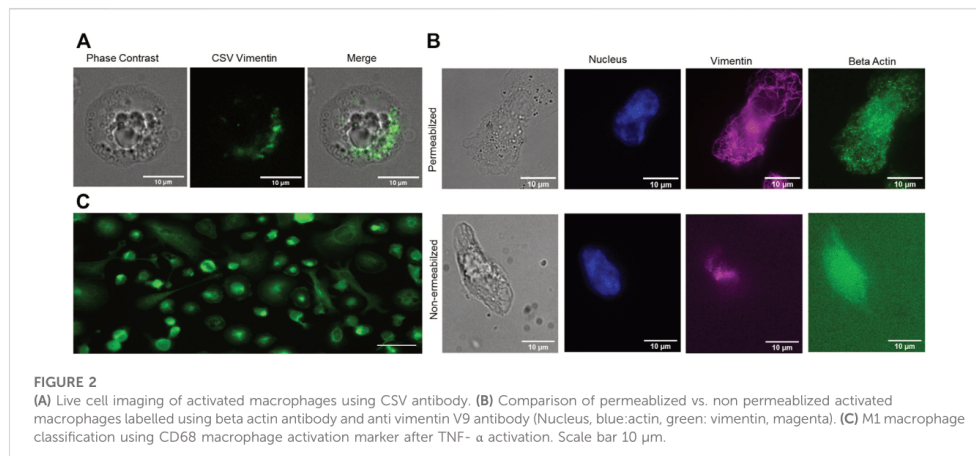
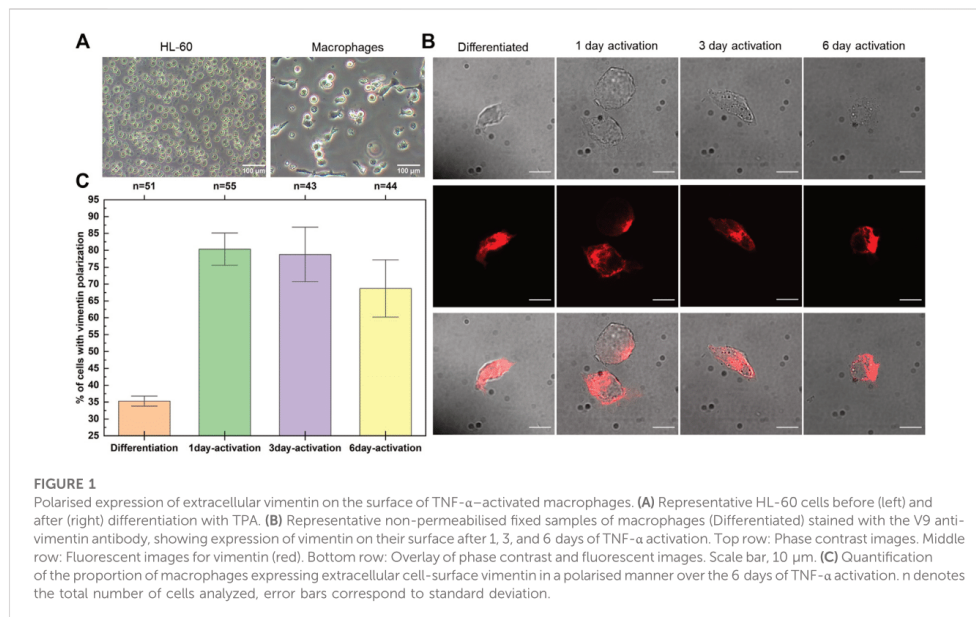
We further confirm the extracellular localization of vimentin by using CSV antibody which specifically binds to the extracellular vimentin in live activated macrophages (Figure 2A). This was complemented with comparing the permeabilized and non permeabilized cells where beta actin was labelled along with vimentin in activated macrophages. Nevertheless, some fluorescent signal can be observed around the nucleus which could be from the antibody that has been endocytosed. In Figure 2B, it can be clearly seen that fluorescence signal from permeabilized activated macrophages is more prominent. However, only unspesific signal can be observed in non-permeabilized activated macrophages. We also classify the macrophages into M1 macrophages upon activation by TNF- α by using CD68 activation marker (Figure 2C).

Extracellular cell-surface vimentin is predominantly expressed at the back of activated macrophages and secreted in the form small fragments

Although the vimentin was polarised on the surface of these TNF- α -activated macrophages, as the "front" and "back" of these cells were not easily differentiable in these 2D fixed samples, its exact positioning was unknown (Figure 3A). To solve this problem, patterned migration lines on glass coverslips were used, whereby the front and back of the cells can be distinguished by recording time-lapse movies. By following the macrophage migration on patterned lines coated with fibronectin, a simplified cell shape can be defined that allows visualisation of the position on the extracellular cell surface of the vimentin upon TNF- α activation (Figure 3B).

Here, the nucleus was always at the front end of these macrophages during migration. The position of the nucleus was then used as the reference to define the front of the fixed cells. Using this method, the surface vimentin was seen to be polarised at the back of the activated macrophages, allowing us to conclude that vimentin was secreted from the back of these TNF- α -activated macrophages. In contrast, prior to TNF- α activation, the differentiated macrophages were seen to secrete vimentin at a site close to the nucleus (Figure 3C). As, 1 and 3 days activation showed comparable vimentin polarization (Figure 1C), here we used 3 days activation in 1D pattern experiment (Figure 3C).

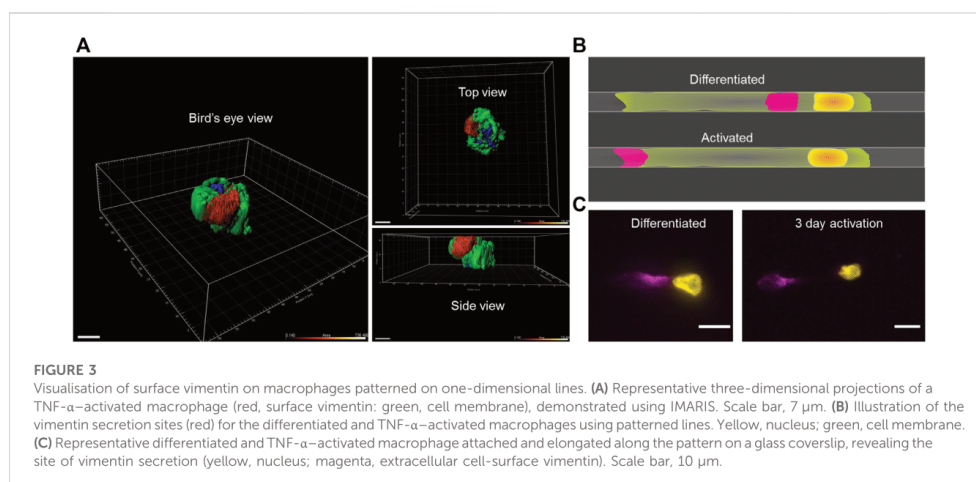
To further resolve the structure of the polarized vimentin on the cell surface, we used confocal microscopy for imaging. For this, genetically transformed HL-60 cells with vimentin tagged with green fluorescent protein (GFP-vimentin HL60 cells) were differentiated and activated. Here, images of elongated macrophages were acquired in order to evaluate the structure as well as the position of the surface vimentin. We observed small fragments of vimentin at the secretion sites of both differentiated



and TNF- α -activated macrophages (Figure 4A). In order to confirm the small fragments are on the outside of the cell, images of differentiated and TNF- α -activated macrophages were acquired using scanning electron microscopy (SEM) (Figure 4B). Further, we confirmed the presence of vimentin on the dot like structure by visualizing the same cell in both confocal and SEM by using coverslip with grid (Figure 4C).

Quantification of vimentin secretion upon activation

It is known that as well as being expressed on the extracellular cell surface, vimentin can then be released into the extracellular surroundings of the cell (Danielsson et al., 2018). We thus asked whether, and in what way, the vimentin secreted by these TNF-



α -activated macrophages is functional. Here, we imaged the contact region between the activated macrophages and the glass bottom of the dish to visualise the vimentin released into the medium from the extracellular surface of the activated macrophages, using total internal reflection fluorescence (TIRF) microscopy. Fixed non-permeabilised 3-days-activated macrophages were fluorescently labelled using the V9 antibody. This revealed vimentin agglomerates in the vicinity of the activated macrophages (Figure 5A). These vimentin agglomerates appeared to be in a non-filamentous and fragmented form.

To quantify the vimentin released from these activated macrophages, 0.4- μ m transwell insert assays were used with genetically transformed HL-60 cells in which vimentin was tagged with green fluorescent protein (GFP-vimentin HL60 cells). These GFP-vimentin HL60 cells were differentiated using TPA and placed inside the upper chambers of transwell inserts. They were then activated with TNF- α , and left for 1 day and 3 days. The vimentin released into the cell medium passed through the pores of the membrane and was collected in the bottom chamber along with the culture medium. The medium in the bottom chamber was transferred to 96-well plates, and the fluorescence intensity was measured using a plate reader. These data showed that the amount of vimentin released into the medium depended on the time of TNF- α activation of these macrophages (Figure 5B).

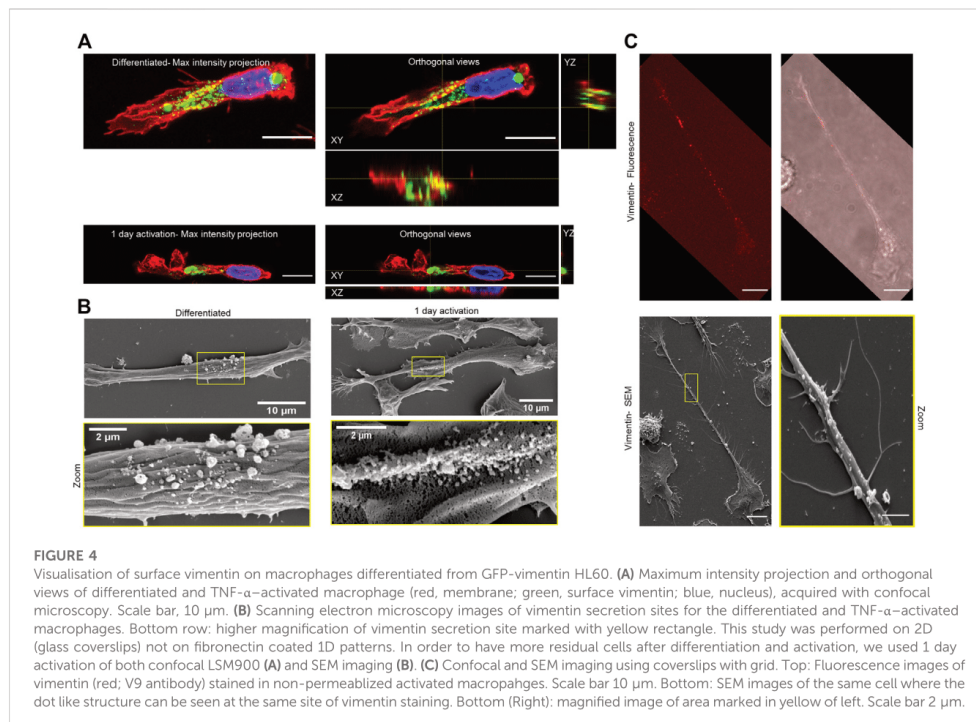
Extracellular vimentin enhances migration and phagocytosis of macrophages

Macrophages are known to have a vital role in the immune system through phagocytosis of cellular debris and

elimination of bacterial pathogens. We thus next investigated this extracellular cell-surface vimentin on the functionality of macrophages, in terms of their migration and phagocytosis.

The migration speeds of the macrophages were measured using a 2D migration assay (Figure 6A). As the media from the TNF- α -activated macrophages that contained secreted vimentin is expected to have some residual TNF- α , recombinant vimentin was used here. Addition of recombinant vimentin to the differentiated macrophages significantly increased their migration speed. Further, the migration speed of the TNF- α -activated macrophages was significantly reduced when they were pre-incubated with the CSV antibody (Figure 6B).

To investigate the phagocytic activity of macrophages under the influence of extracellular vimentin, phagocytosis assays using fluorescently-labeled latex beads were carried out to measure the phagocytic process *in vitro*. With phagocytosis analysed according to the phagocytotic index defined by the intracellular fluorescence intensities following phagocytosis of fluorescent beads (Figure 6C), this was seen to be significantly increased in the TNF- α -activated macrophages compared to the differentiated macrophages (Figure 6D). Further, this effect was mimicked by addition of 100 ng/ml recombinant vimentin to the differentiated macrophages, while it was blocked by the V9 anti-vimentin antibody in the TNF- α -activated macrophages (Figure 6D). As for the migration effect, this enhanced phagocytosis might be due to the high expression levels of vimentin in the TNF- α -activated macrophages. Thus, from these data, we can conclude that extracellular addition of recombinant vimentin enhances both the migration and phagocytosis of these macrophages.



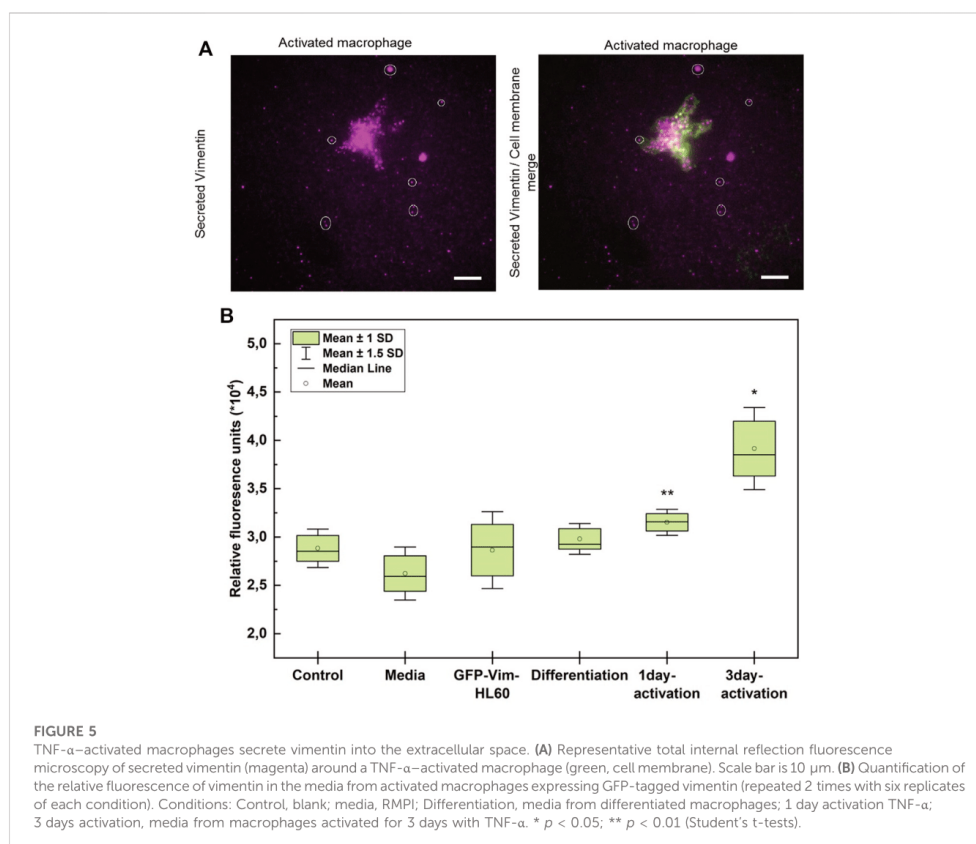
Discussion

The detection of vimentin in the extracellular space then promoted the question as to how it is secreted from inside these TNF- α -activated macrophages. Previously this extracellular vimentin was thought to have been released from necrotic cells, although it has also been suggested that it might be secreted. Previous studies have shown exosomes as a source of vimentin, and demonstrated that these can transport and release vimentin into the extracellular space (Chen et al., 2016; Adolf et al., 2018; Parvanian et al., 2020). Exosomes are packaged with membranes in the Golgi apparatus, and in activated macrophages, block of transport through the Golgi apparatus inhibits the release of extracellular vimentin (Mor-Vaknin et al., 2003). This has thus strengthened the idea that vimentin is secreted with the help of exosomes. However, it has remained unclear what the characteristics of this secreted vimentin are.

In the present study, we show that vimentin is released from the back of these TNF- α -activated macrophages, and that this polarised release is enhanced by the macrophage activation.

Moreover, using confocal, TIRF and SEM, we have confirmed that the structure of the secreted vimentin is not filamentous, as is its intracellular counterpart, but is in form of fragments, as indicated in recent studies (Suprewicz et al., Lalioti et al., 2021). Nevertheless, further confirmation of data from GFP-vimentin HL60 is needed as it may not behave identical to endogenous vimentin.

It is believed that post-translational modifications are a prerequisite for vimentin secretion from macrophages and endothelial cells (Noh et al., 2016; Liu et al., 2020; Patteson et al., 2020), which would appear necessary to break down the long vimentin filaments to smaller fragments (Mónico et al., 2019). In the case activated macrophages, the extracellular vimentin was shown to be phosphorylated (Mor-Vaknin et al., 2003). A recent study showed that vimentin is recruited to the cell membrane via an alteration in the filamentous form to an oligomeric form that consists of 4–12 monomers (Hwang and Ise, 2020). This multimeric form of vimentin showed a higher binding affinity to lipid bilayers compared to that of filamentous vimentin. However, the mechanism by which the intracellular vimentin is secreted into the extracellular space is not well characterised. Here, by combining data from the literature and

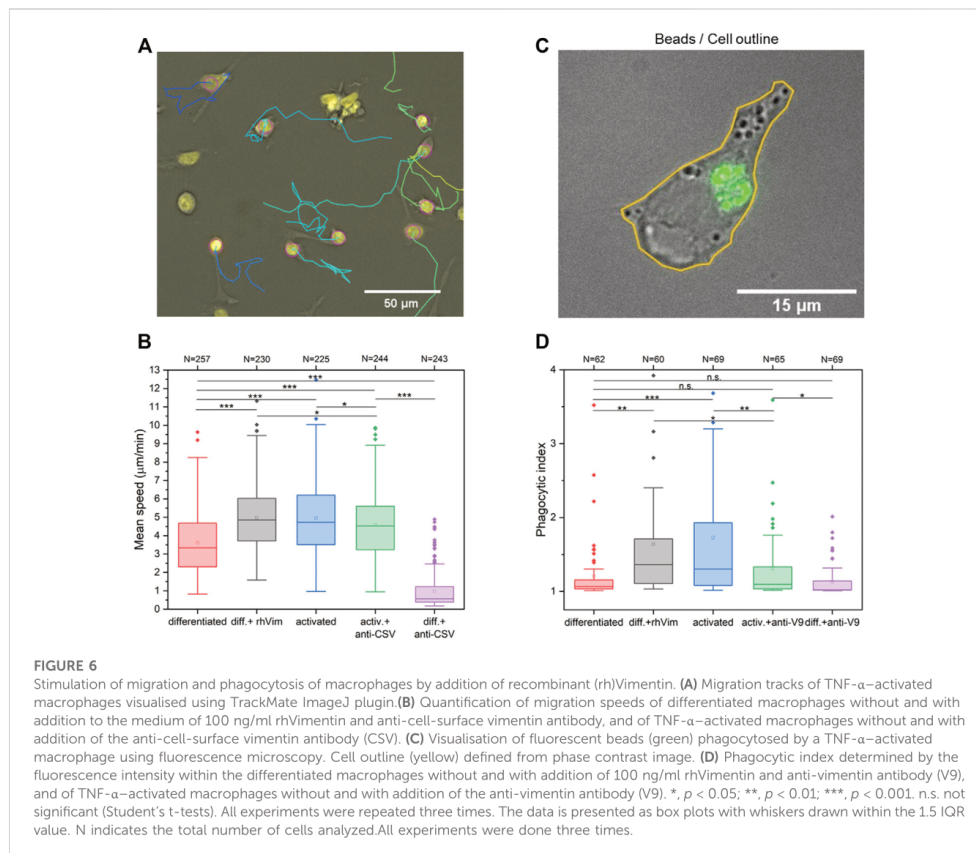


the findings from the present study, we can predict a secretion mechanism as we illustrated in Figure 6. As seen from the present study, extracellular cell-surface vimentin is polarised at the back of TNF- α -activated macrophages, and the images from TIRF shows that small fragments of vimentin either from exosomes or filaments are released close to a large agglomerate of vimentin on the cell surface. Therefore, we propose that at the membrane surface of these TNF- α -activated macrophages, vimentin filaments disassemble into small fragments, to form agglomerates, which can then be released into cell medium or into blood serum (Figure 7B).

Vimentin expression in the extracellular space of cells has been attributed to circumstances such as cell activation, senescence, injury and stress (Mor-Vaknin et al., 2003; Frescas et al., 2017; Walker et al., 2018). In most of these scenarios, the secretion of vimentin is related to immune activity (Ramos et al., 2020). For example, the vimentin secreted by activated macrophages has been suggested to be involved

in immune functions via generation of oxidative metabolites and elimination of bacteria (Mor-Vaknin et al., 2003). Another example is shown in patients with rheumatic arthritis, where neutrophils secrete citrullinated vimentin during the release of neutrophil extracellular traps that are produced to immobilise pathogens and promote immune responses (Carmona-Rivera et al., 2013; Kaplan, 2013). Further, in the *Mycobacterium tuberculosis*, vimentin binds to the natural killer cell surface receptor NKp46 and contributes to lysis of infected cells (Garg et al., 2006). Finally, extracellular vimentin blocks pro-inflammatory secretion by activated dendritic cells, which promotes inhibition of adaptive immune responses. This mechanism prevents tissue damage and promotes bacteria elimination (Yu et al., 2018).

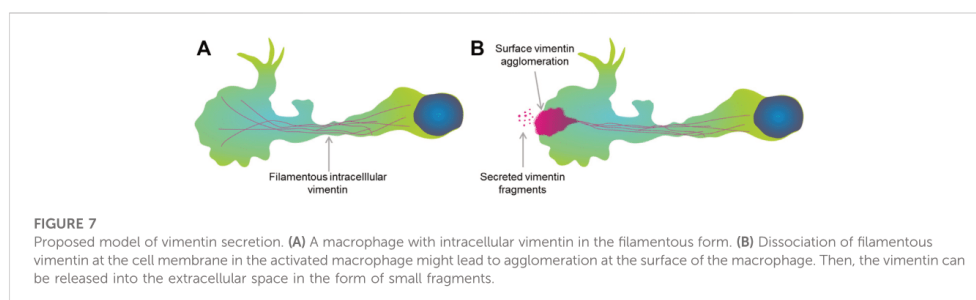
On the basis of this evidence that extracellular vimentin partially regulates inflammatory processes, we investigated the role of extracellular vimentin on macrophage function. Using migration assays, we show that elevated levels of extracellular



cell-surface vimentin enhance the migration speed of macrophages. Here, it was not relevant if the extracellular vimentin was added as recombinant vimentin or if it was from secretion of activated macrophages. This increase in macrophage migration by addition of recombinant vimentin complements our recent study where we showed similar effects in MCF-7 cells (Thalla et al., 2021).

Earlier studies have demonstrated that increases in phagocytic activity by macrophages involves extracellular vimentin. However, in these previous studies, the vimentin was expressed on the surface of apoptotic neutrophils and T cells and acted as a signalling agent to attract macrophages and further facilitate the elimination process (Boilard et al., 2003; Moisan and Girard, 2006; Ise et al., 2012; Starr et al., 2012). On the surface of phagocytes, vimentin interacts with O-Glc-Nac-modified proteins expressed on apoptotic cells, which generates an “eat me”

signal for elimination by macrophages (Ise et al., 2012). To date, surface vimentin has been believed to be a mediator that helps to attract macrophages towards the cells that need to be phagocytosed. However, one study that investigated extracellular vimentin directly expressed on activated macrophages demonstrated enhanced bacteria elimination (Mor-Vaknin et al., 2003). In the present study, we further explored the effects of extracellular vimentin expressed on the surface of macrophages in terms of macrophage function. We show that recombinant vimentin treatment of HL-60 differentiated macrophages has a similar effect as TNF- α -activated macrophages in terms of enhanced phagocytic activity. Interestingly, in a recent study it was shown that extracellular addition of vimentin lead to TNF- α secretion in macrophages (Kim et al., 2020). Consequently, this could be a possible mechanism behind the enhanced migration and phagocytic activity in macrophages.



Taken together, we demonstrate that vimentin is expressed in a polarised form on the surface of activated macrophages, and that it is released in a fragmented form. We also show that extracellular vimentin influences the functionality of macrophages by enhancing their migration and phagocytosis.

Altogether, these data suggests that extracellular vimentin is used to regulate macrophages in the immune system through effective elimination of bacterial pathogens.

Data availability statement

The raw data supporting the conclusions of this article will be made available by the authors, without undue reservation.

Author contributions

DT was involved in conceptualization of the project; supervision; data analysis and visualization; and writing original draft. AR performed polarization and secretion experiments; data analysis and visualization; contributed in writing. AL performed the migration and phagocytosis experiments; data analysis and visualization. JB performed 1D pattern experiments; data analysis and visualization. LK performed scanning electron microscopy experiments; visualization. FL was involved in the conceptualisation of the project, contributed in writing/review and editing the manuscript; supervision; project administration; and funding acquisition. All authors have read and agreed to the published version of the manuscript.

References

- Adolf, A., Rohrbeck, A., Münster-Wandowski, A., Johansson, M., Kuhn, H. G., Kopp, M. A., et al. (2018). Release of astroglial vimentin by extracellular vesicles: Modulation of binding and internalization of C3 transferase in astrocytes and neurons. *Glia* 67, 703–717. doi:10.1002/glia.23566
- Boilard, E., Bourgoin, S. G., Bernatchez, C., and Surette, M. E. (2003). Identification of an autoantigen on the surface of apoptotic human T cells as a

Funding

This research was funded with the support of the DFG (SFB 1027, project A10).

Conflict of interest

The authors declare that the research was conducted in the absence of any commercial or financial relationships that could be construed as a potential conflict of interest.

Publisher's note

All claims expressed in this article are solely those of the authors and do not necessarily represent those of their affiliated organizations, or those of the publisher, the editors and the reviewers. Any product that may be evaluated in this article, or claim that may be made by its manufacturer, is not guaranteed or endorsed by the publisher.

Acknowledgments

We are thankful to Monika Zwerger for transfecting the GFP-HL60 cells. Additionally, we would like to thank Alexandra K. Kierner for her active participation in discussions and suggestions.

new protein interacting with inflammatory group IIA phospholipase A2. *Blood* 102, 2901–2909. doi:10.1182/blood-2002-12-3702

Bryant, A. E., Bayer, C. R., Huntington, J. D., and Stevens, D. L. (2006). Group A streptococcal myonecrosis: Increased vimentin expression after skeletal-muscle injury mediates the binding of *Streptococcus pyogenes*. *J. Infect. Dis.* 193, 1685–1692. doi:10.1086/504261

- Chen, Z., Yang, L., Cui, Y., Zhou, Y., Yin, X., Guo, J., et al. (2016). Cytoskeleton-centric protein transportation by exosomes transforms tumor-favorable macrophages. *Oncotarget* 7, 767387–767402. doi:10.18632/oncotarget.11794
- Collins, H. L., and Bancroft, G. J. (1992). Cytokine enhancement of complement-dependent phagocytosis by macrophages: Synergy of tumor necrosis factor- α and granulocyte-macrophage colony-stimulating factor for phagocytosis of *Cryptococcus neoformans*. *Eur. J. Immunol.* 22, 1447–1454. doi:10.1002/eji.1830220617
- Danielsson, F., Peterson, M. K., Caldeira Araújo, H., Lautenschläger, F., and Gad, A. K. B. (2018). Vimentin diversity in health and disease. *Cells* 7. doi:10.3390/cells7100147
- Frescas, D., Roux, C. M., Ayygun-Sunar, S., Gleiberman, A. S., Krasnov, P., Kurnasov, O. V., et al. (2017). Senescent cells expose and secrete an oxidized form of membrane-bound vimentin as revealed by a natural polyreactive antibody. *Proc. Natl. Acad. Sci.* 114, E1668–E1677. doi:10.1073/pnas.1614661114
- Garg, A., Barnes, P. F., Porgador, A., Roy, S., Wu, S., Nanda, J. S., et al. (2006). Vimentin expressed on *Mycobacterium tuberculosis*-infected human macrophages is involved in binding to the NKp46 receptor. *J. Immunol.* 177, 6192–6198. doi:10.4049/jimmunol.177.9.6192
- Ghosh, P., Halvorsen, E. M., Ammendolia, D. A., Mor-Vaknin, N., O'riordan, M. X. D., Brumell, J. H., et al. (2018). Invasion of the brain by *Listeria monocytogenes* is mediated by INF and host cell vimentin. *mBio* 9, e00160–18. doi:10.1128/mBio.00160-18
- Greco, T. M., Seeholzer, S. H., Mak, A., Spruce, L., and Ischiropoulos, H. (2010). Quantitative mass spectrometry-based proteomics reveals the dynamic range of primary mouse astrocyte protein secretion. *J. Proteome Res.* 9, 2764–2774. doi:10.1021/pr100134n
- Herzog, C., Pons Garcia, L., Keatinge, M., Greenald, D., Moritz, C., Peri, F., et al. (2019). Rapid clearance of cellular debris by microglia limits secondary neuronal cell death after brain injury in vivo. *Development* 146, dev174698. doi:10.1242/dev.174698
- Hwang, B., and Ise, H. (2020). Multimeric conformation of type III intermediate filaments but not the filamentous conformation exhibits high affinity to lipid bilayers. *Genes Cells* 25, 413–426. doi:10.1111/gtc.12768
- Ise, H., Goto, M., Komura, K., and Akaiki, T. (2012). Engulfment and clearance of apoptotic cells based on a GlcNAc-binding lectin-like property of surface vimentin. *Glycobiology* 22, 788–805. doi:10.1093/glycob/cws052
- Ivaska, J., Pallari, H. M., Nevo, J., and Eriksson, J. E. (2007). Novel functions of vimentin in cell adhesion, migration, and signaling. *Exp. Cell Res.* 313, 2050–2062. doi:10.1016/j.yexcr.2007.03.040
- Jaggi, U., Yang, M., Matundan, H. H., Hirose, S., Shah, P. K., Sharifi, B. G., et al. (2020). Increased phagocytosis in the presence of enhanced M2-like macrophage responses correlates with increased primary and latent HSV-1 infection. *PLoS Pathog.* 16, e1008971. doi:10.1371/journal.ppat.1008971
- Kaplan, M. J. (2013). Role of neutrophils in systemic autoimmune diseases. *Arthritis Res. Ther.* 15, 219. doi:10.1186/ar4325
- Khandpur, C., Carmona-Rivera, R., Vivekanandan-Giri, A., Gizinski, A., Yalavarthi, S., Knight, J., et al. (2013). Neutrophil extracellular traps are a source of citrullinated autoantigens and stimulate inflammatory responses in rheumatoid arthritis (P4061). *J. Immunol.* 190, 127.2. doi:10.1126/scitranslmed.3005580
- Kim, S., Cho, W., Kim, I., Lee, S.-H., Oh, G. T., and Park, Y. M. (2020). Oxidized LDL induces vimentin secretion by macrophages and contributes to atherosclerotic inflammation. *J. Mol. Med.* 98, 973–983. doi:10.1007/s00109-020-01923-w
- Krzyszczak, P., Schloss, R., Palmer, A., and Berthiaume, F. (2018). The role of macrophages in acute and chronic wound healing and interventions to promote pro-wound healing phenotypes. *Front. Physiology* 9. doi:10.3389/fphys.2018.00419
- Lalioti, V., González-Sanz, S., Lois-Bermejo, I., González-Jiménez, P., Viedma-Poyatos, Á., Merino, A., et al. (2021). Immunolocalization studies of vimentin and ACE2 on the surface of cells exposed to SARS-CoV-2 Spike proteins. *bioRxiv* 2021, 442648. doi:10.1101/2021.05.04.442648
- Leopold Wager, C. M., and Wormley, F. L. (2014). Classical versus alternative macrophage activation: The ying and the yang in host defense against pulmonary fungal infections. *Mucosal Immunol.* 7, 1023–1035. doi:10.1038/mi.2014.65
- Liu, M., Wang, R., Sun, X., Liu, Y., Wang, Z., Yan, J., et al. (2020). Prognostic significance of PD-L1 expression on cell-surface vimentin-positive circulating tumor cells in gastric cancer patients. *Mol. Oncol.* 14, 865–881. doi:10.1002/1878-0261.12643
- Moisan, E., and Girard, D. (2006). Cell surface expression of intermediate filament proteins vimentin and lamin B1 in human neutrophil spontaneous apoptosis. *J. Leukoc. Biol.* 79, 489–498. doi:10.1189/jlb.0405190
- Mónico, A., Duarte, S., Pajares, M. A., and Pérez-Sala, D. (2019). Vimentin disruption by lipoxidation and electrophiles: Role of the cysteine residue and filament dynamics. *Redox Biol.* 23, 101098.
- Mor-Vaknin, N., Punturieri, A., Sitwala, K., and Markovitz, D. M. (2003). Vimentin is secreted by activated macrophages. *Nat. Cell Biol.* 5, 59–63. doi:10.1038/ncb898
- Neniskyte, U., Vilalta, A., and Brown, G. C. (2014). Tumour necrosis factor alpha-induced neuronal loss is mediated by microglial phagocytosis. *FEBS Lett.* 588, 2952–2956. doi:10.1016/j.febslet.2014.05.046
- Noh, H., Yan, J., Hong, S., Kong, L.-Y., Gabrusiewicz, K., Xia, X., et al. (2016). Discovery of cell surface vimentin targeting mAb for direct disruption of GBM tumor initiating cells. *Oncotarget* 7. doi:10.18632/oncotarget.12458
- Parvanian, S., Yan, F., Su, D., Coelho-Rato, L. S., Venu, A. P., Yang, P., et al. (2020). Exosomal vimentin from adipocyte progenitors accelerates wound healing. *Cytoskeleton* 77, 399–413. doi:10.1002/cm.21634
- Patterson, A. E., Vahabikashi, A., Goldman, R. D., and Janney, P. A. (2020). Mechanical and non-mechanical functions of filamentous and non-filamentous vimentin. *BioEssays* 42, 2000078. doi:10.1002/bies.202000078
- Ramos, I., Stamatakis, K., Oeste, C. L., and Pérez-Sala, D. (2020). Vimentin as a multifaceted player and potential therapeutic target in viral infections. *Int. J. Mol. Sci.* 21, 4675. doi:10.3390/ijms21134675
- Satelli, A., and Li, S. (2011). Vimentin in cancer and its potential as a molecular target for cancer therapy. *Cell Mol. Life Sci.* 68, 3033–3046. doi:10.1007/s00018-011-0735-1
- Satelli, A., Mitra, A., Brownlee, Z., Xia, X., Bellister, S., Overman, M. J., et al. (2015). Epithelial-mesenchymal transitioned circulating tumor cells capture for detecting tumor progression. *Clin. Cancer Res.* 21, 899–906. doi:10.1158/1078-0432.ccr-14-0894
- Satelli, A., Mitra, A., Cutrera, J. J., Devarie, M., Xia, X., Ingram, D. R., et al. (2014). Universal marker and detection tool for human sarcoma circulating tumor cells. *Cancer Res.* 74, 1645–1650. doi:10.1158/0008-5472.can-13-1739
- Schäfer, G., Graham, L. M., Lang, D. M., Blumenthal, M. J., Bergant Marušić, M., and Katz, A. A. (2017). Vimentin modulates infectious internalization of human papillomavirus 16 pseudovirions. *J. Virology* 91, e00307–17. doi:10.1128/JVI.00307-17
- Squinto, S. P., Doucet, J. P., Block, A. L., Morrow, S. L., and Davenport, W. D., Jr. (1989). Induction of macrophage-like differentiation of HL-60 leukemia cells by tumor necrosis factor- α : Potential role of fos expression. *Mol. Endocrinol.* 3, 409–419. doi:10.1210/mend-3-2-409
- Starr, A. E., Bellac, C. L., Dufour, A., Goebeler, V., and Overall, C. M. (2012). Biochemical characterization and N-terminomics analysis of leukolysin, the membrane-type 6 matrix metalloprotease (MMP25): Chemokine and vimentin cleavages enhance cell migration and macrophage phagocytic activities. *J. Biol. Chem.* 287, 13382–13395. doi:10.1074/jbc.m111.314179
- Suprewicz, Ł., Swoger, M., Gupta, S., Piktet, E., Byfield, F. J., Iwamoto, D. V., et al. (2022). Extracellular vimentin as a target against SARS-CoV-2 host cell invasion. *Small* 18, e2105640. doi:10.1002/smll.202105640
- Thalla, D. G., Jung, P., Bischoff, M., and Lautenschläger, F. (2021). Role of extracellular vimentin in cancer-cell functionality and its influence on cell monolayer permeability changes induced by SARS-CoV-2 receptor binding domain. *Int. J. Mol. Sci.* 22, 7469. doi:10.3390/ijms22147469
- Viola, A., Munari, F., Sánchez-Rodríguez, R., Scolari, T., and Castegna, A. (2019). The metabolic signature of macrophage responses. *Front. Immunol.* 10. doi:10.3389/fimmu.2019.01462
- Walker, J. L., Bleaken, B. M., Romisher, A. R., Alnwbitt, A. A., and Menko, A. S. (2018). In wound repair vimentin mediates the transition of mesenchymal leader cells to a myofibroblast phenotype. *Mol. Biol. Cell* 29, 1555–1570. doi:10.1091/mbc.e17-06-0364
- Yang, J., Zou, L., Yang, Y., Yuan, J., Hu, Z., Liu, H., et al. (2016). Superficial vimentin mediates DENV-2 infection of vascular endothelial cells. *Sci. Rep.* 6, 38372. doi:10.1038/srep38372
- Yu, M. B., Guerra, J., Firek, A., and Langridge, W. H. R. (2018). Extracellular vimentin modulates human dendritic cell activation. *Mol. Immunol.* 104, 37–46. doi:10.1016/j.molimm.2018.09.017
- Zhang, C., Yang, M., and Ericsson, A. C. (2021). Function of macrophages in disease: Current understanding on molecular mechanisms. *Front. Immunol.* 12. doi:10.3389/fimmu.2021.620510

7.2 Publication 2: Role of Extracellular Vimentin in Cancer-Cell Functionality and Its Influence on Cell Monolayer Permeability Changes Induced by SARS-CoV-2 Receptor Binding Domain

Divyendu Goud Thalla ^{1, 2}, Philipp Jung ³, Markus Bischoff ^{3,4} and Franziska Lautenschläger ^{2,4}

¹Leibniz Institute for New Materials, 66123 Saarbrücken, Germany

²Faculty of Natural Sciences and Technology, Experimental Physics, Saarland University, 66123 Saarbrücken, Germany

³Institute for Medical Microbiology and Hygiene, Saarland University, 66421 Homburg, Germany

⁴Centre for Biophysics, Saarland University, 66123 Saarbrücken, Germany

Int. J. Mol. Sci. 2021, 22(14), 7469;

doi.org/10.3390/ijms22147469

Published: 12 July 2021

D.G.T. performed the experiments except FluidFM; data analysis and visualisation; and writing original draft, P.J. performed FluidFM in Homburg, F.L. contributed in writing/review and editing manuscript; supervision; project administration; and funding acquisition, D.G.T. and F.L. were equally involved in conceptualisation of the project. M.B. was involved in review and editing of manuscript; supervising FluidFM methodology. All authors have read and agreed to the published version of the manuscript.



Article

Role of Extracellular Vimentin in Cancer-Cell Functionality and Its Influence on Cell Monolayer Permeability Changes Induced by SARS-CoV-2 Receptor Binding Domain

Divyendu Goud Thalla ^{1,2}, Philipp Jung ³, Markus Bischoff ^{3,4} and Franziska Lautenschläger ^{2,4,*} 

¹ Leibniz Institute for New Materials, 66123 Saarbrücken, Germany; divyendu.thalla@uni-saarland.de

² Faculty of Natural Sciences and Technology, Experimental Physics, Saarland University, 66123 Saarbrücken, Germany

³ Institute for Medical Microbiology and Hygiene, Saarland University, 66421 Homburg, Germany; Philipp.Jung@uks.eu (P.J.); markus.bischoff@uks.eu (M.B.)

⁴ Centre for Biophysics, Saarland University, 66123 Saarbrücken, Germany

* Correspondence: f.lautenschlaeger@physik.uni-saarland.de



Citation: Thalla, D.G.; Jung, P.; Bischoff, M.; Lautenschläger, F. Role of Extracellular Vimentin in Cancer-Cell Functionality and Its Influence on Cell Monolayer Permeability Changes Induced by SARS-CoV-2 Receptor Binding Domain. *Int. J. Mol. Sci.* **2021**, *22*, 7469. <https://doi.org/10.3390/ijms22147469>

Academic Editor: Jose Maria Gonzalez-Granado

Received: 28 May 2021

Accepted: 8 July 2021

Published: 12 July 2021

Publisher's Note: MDPI stays neutral with regard to jurisdictional claims in published maps and institutional affiliations.



Copyright: © 2021 by the authors. Licensee MDPI, Basel, Switzerland. This article is an open access article distributed under the terms and conditions of the Creative Commons Attribution (CC BY) license (<https://creativecommons.org/licenses/by/4.0/>).

Abstract: The cytoskeletal protein vimentin is secreted under various physiological conditions. Extracellular vimentin exists primarily in two forms: attached to the outer cell surface and secreted into the extracellular space. While surface vimentin is involved in processes such as viral infections and cancer progression, secreted vimentin modulates inflammation through reduction of neutrophil infiltration, promotes bacterial elimination in activated macrophages, and supports axonal growth in astrocytes through activation of the IGF-1 receptor. This receptor is overexpressed in cancer cells, and its activation pathway has significant roles in general cellular functions. In this study, we investigated the functional role of extracellular vimentin in non-tumorigenic (MCF-10a) and cancer (MCF-7) cells through the evaluation of its effects on cell migration, proliferation, adhesion, and monolayer permeability. Upon treatment with extracellular recombinant vimentin, MCF-7 cells showed increased migration, proliferation, and adhesion, compared to MCF-10a cells. Further, MCF-7 monolayers showed reduced permeability, compared to MCF-10a monolayers. It has been shown that the receptor binding domain of SARS-CoV-2 spike protein can alter blood–brain barrier integrity. Surface vimentin also acts as a co-receptor between the SARS-CoV-2 spike protein and the cell-surface angiotensin-converting enzyme 2 receptor. Therefore, we also investigated the permeability of MCF-10a and MCF-7 monolayers upon treatment with extracellular recombinant vimentin, and its modulation of the SARS-CoV-2 receptor binding domain. These findings show that binding of extracellular recombinant vimentin to the cell surface enhances the permeability of both MCF-10a and MCF-7 monolayers. However, with SARS-CoV-2 receptor binding domain addition, this effect is lost with MCF-7 monolayers, as the extracellular vimentin binds directly to the viral domain. This defines an influence of extracellular vimentin in SARS-CoV-2 infections.

Keywords: extracellular vimentin; IGF-1 receptor; cancer; SARS-CoV-2 receptor binding domain

1. Introduction

Vimentin is a cytoskeletal filament of the family of intermediate filaments that has a vital role in cell migration, adhesion, and signaling due to its interactions with various proteins [1]. It forms a filamentous network that extends from the nuclear periphery to the plasma membrane. Vimentin is involved in cell physiology, inflammation, wound healing, and immune responses [2]. Its involvement in these cellular functions is believed to be through its dynamic phosphorylation. Interestingly, as well as being present in the cell cytoplasm, vimentin is found in the extracellular space around various cell types. Vimentin can thus be secreted into the extracellular space under various physiological conditions, such as cell activation, inflammation, senescence, and stress [3,4]. Vimentin is secreted

by various cell types, such as macrophages, astrocytes, neutrophils, monocytes, apoptotic lymphocytes, and endothelial cells [3,5–8]. This extracellular vimentin can either remain bound to the cell surface (i.e., surface vimentin) or it can be secreted in an unbound form in the extracellular matrix (i.e., secreted vimentin).

In epithelium-derived cancers, intracellular vimentin has long been known to be involved in the process known as epithelial-to-mesenchymal transition, which describes a particular moment during the progression of tumor cells to metastases. Interestingly, surface vimentin has also been reported to be involved in this process, because cytoplasmic vimentin is translocated to the cell surface during epithelial-to-mesenchymal transition. This distinct property provides an opportunity to identify and isolate aggressive cancer cells, and thus to target them [9]. Surface vimentin has also been shown to have a role in other cancer cells, such as glioblastoma multiforme cancer stem cells, which are tumor-initiating cells that express vimentin on their surface. By targeting glioblastoma multiforme cells using an antibody against cell-surface vimentin (defined as the CSV antibody; clone 84-1), surface vimentin is internalized, which results in cell apoptosis and inhibition of tumor growth [10].

Surface vimentin also has a role in human circulating tumor cells (CTCs), with CTCs being detected using a CSV antibody. Surface vimentin has also been detected on neuroblastoma, osteosarcoma, and rhabdomyosarcoma cells [11]. In other studies, epithelial-to-mesenchymal transition induced CD45⁺ CTCs in patients with metastatic colorectal cancer, and CD133⁺ CTCs have been isolated from hepatocellular carcinoma using the CSV antibody [12,13]. Isolation of CSV-positive CTCs has resulted in quantification of metastatic cells and evaluation of cancer progression, which helps in clinical decision making.

Surface vimentin has been shown to be involved in the binding to cells and the internalization of numerous bacteria and viruses, such as DENV-2, *Listeria monocytogenes*, *Streptococcus pyogenes*, human Papillomavirus 16 [14–17]. It can also facilitate the entry of SARS-CoV by acting as a co-receptor between the SARS-CoV spike protein and the cell-surface angiotensin-converting enzyme 2 (ACE2) receptor [18]. Indeed, a recent study revealed that the binding of the SARS-CoV-2 spike protein to extracellular vimentin occurs during SARS-CoV-2 infection, and so vimentin was suggested to be a potential target for inhibition of viral particle binding to and entry into cells [19]. Furthermore, for cancer patients, immunosuppression is a major potential side effect, whereby immunosuppression increases the vulnerability of the patients to diseases caused by viral pathogens. Therefore, it is also vital to study the role of surface vimentin in viral and bacterial infections in the context of cancer progression.

To date, all of these studies have shown that detection of the levels of extracellular vimentin represents a diagnostic method and a therapeutic target in patients with sarcoma, and also allows analysis of metastatic precursor subpopulations. However, the functional role of extracellular vimentin in relation to cancer cells has not been studied. Thus, we aimed here to investigate the effects of vimentin on cancer cells in particular. From the literature, it is known that extracellular vimentin is a ligand for the surface-expressed pattern-recognition receptor dectin-1, natural cytotoxicity receptor 1 (NKp46), and insulin-like growth factor-1 receptor (IGF-1R) [20–22]. Of these, IGF-1R is overexpressed in cancer cells, has a crucial role in tissue development, and is activated by the hormone IGF-1. We therefore focused on the role of extracellular vimentin on IGF-1R, to which IGF-1 binds with high affinity [23]. This pathway has a vital role in cell-cycle progression, cell apoptosis, translation of proteins, and pathogenesis of autoimmune diseases [24].

A study on spinal cord injury in mice showed that extracellular vimentin can activate IGF-1R within the same signalling pathway as IGF-1 [22] (Figure 1). We thus hypothesized that extracellular vimentin has functional similarity to IGF-1 and can thus interact with cellular functions such as cell migration, proliferation, adhesion, and monolayer permeability. Here we studied these functions and extracted the relevant quantitative parameters (e.g., proliferation rate, migration speed, adhesion forces, and monolayer permeability) and compared them across non-tumorigenic (MCF-10a) and cancer (MCF-7) cells. This

analysis showed that extracellular vimentin enhances these cellular functions and might thus be used to modulate them.

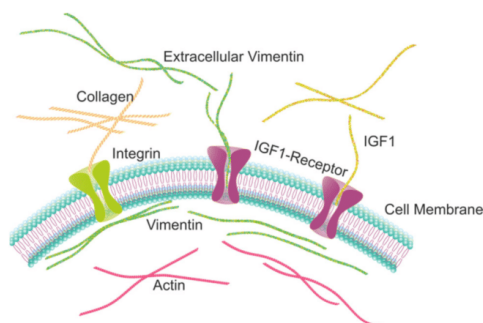


Figure 1. Illustration of the distributions of vimentin (dark green), actin (violet), and collagen (light green) fibers, and their associations with the cell membrane bilayer and the IGF-1 (violet) and integrin (light green) receptors.

At the same time, currently in 2021, we are in the middle of a pandemic, and researchers around the world are looking for ways to interfere with the entry of SARS-CoV-2 into cells. Therefore, in the present study, we also investigated the role of extracellular vimentin in SARS-CoV-2 infection, particularly as viral shedding of coronavirus is greater in patients with cancers compared to those without [25]. A recent study showed the effects of SARS-CoV-2 spike proteins in terms of altered blood–brain barrier properties and integrity [26]. In addition to these effects on the throat and respiratory system, SARS-CoV-2 can have effects on multiple organ vasculatures, which can be lethal under certain circumstances [27].

The data reported here show that surface vimentin enhances the invasive potential caused by the SARS-CoV-2 receptor binding domain (RBD) of the spike protein in monolayers of both non-tumorigenic (MCF-10a) and cancer (MCF-7) cells. If, on the other hand, the RBD of SARS-CoV-2 spike protein binds to secreted extracellular vimentin, this would protect the integrity of the cell monolayers. As there is the need for ways to interfere with the entry of SARS-CoV-2 into human cells, this secreted extracellular vimentin might represent a valuable target for the modulation of SARS-CoV-2 entry into cells.

2. Results

These investigations were carried out using cells derived from human breast epithelium, as the control MCF-10a non-tumorigenic cells and the MCF-7 cancer cells, both of which express IGF-1R. The expression levels of IGF-1R are higher in MCF-7 cells compared to MCF-10a cells [28].

2.1. Extracellular Vimentin Promotes Proliferation in MCF-7 Cells through Activation of IGF-1R

To investigate the proliferation of MCF-10a and MCF-7 cells under the influence of extracellular vimentin, we carried out proliferation assays using 3-[4,5-dimethylthiazole-2-yl]-2,5-diphenyltetrazolium bromide (MTT). The cells were treated with increasing concentrations of recombinant human vimentin (0, 50, 100, 200 ng/mL) for 72 h. The absorbance was then measured using a plate reader, to define the viable cells.

These data for the MCF-7 cells show that the absorbance, and therefore the cell metabolic activity, with addition of recombinant vimentin was greater than for the control cells (Figure 2B). At 100 ng/mL recombinant vimentin, MCF-7 cells showed increased proliferation rates, by $\geq 20\%$. For the MCF-10a cells, those treated with recombinant

vimentin did not show significant change compared to untreated cells at both 48 and 72 h time points (Figure 2B,D).

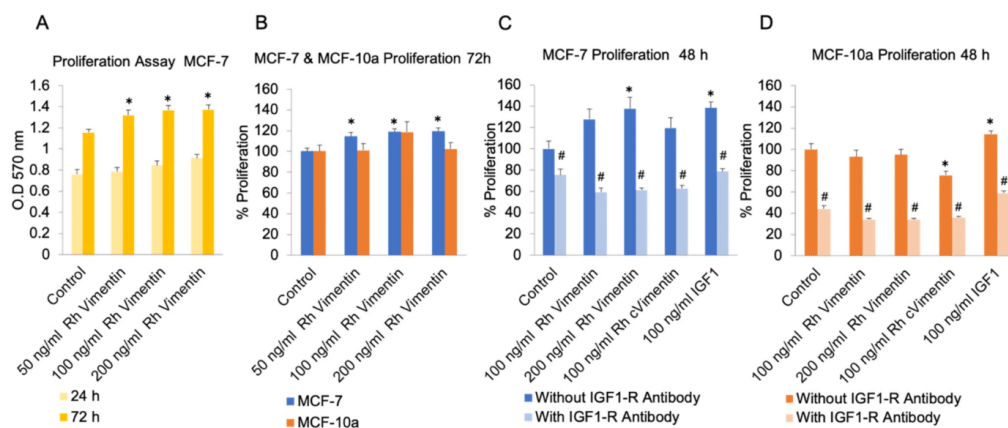


Figure 2. Proliferation of MCF-10a (control) and MCF-7 (cancer) cells under treatment with recombinant (Rh) vimentin. (A) Raw data for absorbance at 570 nm in the MTT assay for MCF-7 cells after 24 and 72 h. (B) Cell proliferation following 72 h treatments of Rh vimentin. (C,D) Proliferation upon blocking of IGF-1R with pretreatment with an anti-IGF-1R antibody along with Rh vimentin; IGF-1; Rh cVimentin (recombinant citrullinated form of vimentin). * $p < 0.05$, compared to control (unpaired t -tests). # $p < 0.05$, compared to corresponding counterparts without IGF-1R antibody (unpaired t -tests). Experiments were performed at least two times in triplicates. Error bars indicate SEM.

It has been suggested in the literature that vimentin binds directly to and activates IGF-1R [22]. To determine whether or not cell proliferation was stimulated by a direct interaction between vimentin and IGF-1R, a 15-min pre-incubation with an anti-IGF-1R antibody (ARG51076; anti-IGF1 Receptor antibody; Arigobio) was used to block IGF-1R in the MCF-10a and MCF-7 cells, with cell proliferation monitored over 48 h (Figure 2C,D). Indeed, blocking IGF-1R inhibited 200 ng/mL vimentin-stimulated cell proliferation in MCF-7 cells. Here, we also treated cells with citrullinated vimentin, which is the form of vimentin that is secreted in patients suffering from rheumatoid arthritis, to see whether the effects seen here are different to those of recombinant vimentin. These data also indicated that addition of extracellular citrullinated vimentin did not improve proliferation in MCF-7 cancer cells through the activation of IGF-1R (Figure 2C). However, proliferation was significantly reduced in MCF-10a cells upon Rh cVimentin treatment (Figure 2D).

2.2. Extracellular Vimentin Promotes Stronger Adherence to the Underlying Substrate for MCF-7 Cells

As mesenchymal cell migration is strongly dependent on cell adhesion, we wanted to quantify the adhesion forces between these cells and their underlying substrate. Therefore, we investigated the force necessary to detach the MCF-10a and MCF-7 cells from the fibronectin-coated glass substrate without and with the vimentin treatments, to quantify the adhesion strengths of the cells to this substrate. This was achieved using fluidic force microscopy (FluidFM). This is a particular single-cell force spectroscopy set-up with hollow cantilevers, which, in addition to the measurement of conventional cell mechanical properties, can be used to hold, immobilize, or move cells by negative pressure (Figure 3A,B) [29]. Unfortunately, the force spectroscopy measurements with the MCF-10a control cells led to cell disruption or disengagement of the attachment between the cells and micropipette, which thus overstrained the experimental set-up. Therefore, only the effects of vimentin on the adhesion forces of the MCF-7 cells were considered here. The untreated MCF-7

cells had a maximum detachment force of 14.7 ± 2.1 nN, while with 200 ng/mL vimentin treatment, this was significantly increased to 21.0 ± 1.5 nN (Figure 3C). This was also reflected in the modest increase (not statistically significant) to the young's modulus of these cells upon vimentin treatment (Figure 3D). We also concluded that the adhesion force of the MCF-10a cells was particularly high and appeared to exceed the adhesion force of MCF-7 cells, although it cannot be quantified using this method.

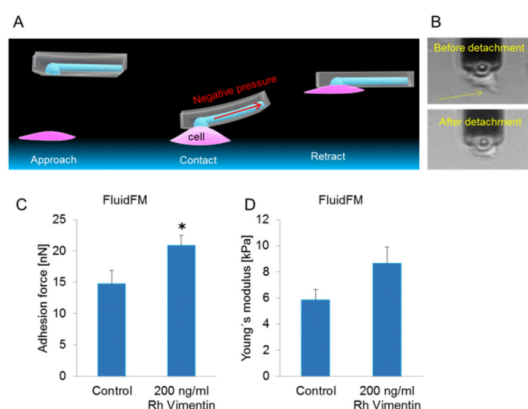


Figure 3. Adhesion force measurements of the MCF-7 (cancer) cells under treatment with recombinant (Rh) vimentin. (A) Illustration of the approach, with cell contact establishment and probe retraction during the FluidFM-based single-cell force spectroscopy. (B) Representative images showing an MCF-7 cell treated with 200 ng/mL recombinant vimentin which was detached by the retraction movement of the FluidFM probe. (C,D) Adhesion force (C) and stiffness (D) measured during the detachment of MCF-7 cells ($n \leq 7$ cells per condition) after 24 h without and with 200 ng/mL vimentin. * $p < 0.05$, compared to control (0) (unpaired t -tests). Error bars indicate SEM.

Therefore, as indicated above, the vimentin-treated MCF-7 cells adhered more strongly to the substrate than the control MCF-7 cells.

2.3. Extracellular Vimentin Induces Migration of MCF-10a and MCF-7 Cells

To further define the role of extracellular vimentin in the functions of these cells, its effects on cell migration were investigated using migration assays. To exclude the possibility that increased cell proliferation after vimentin treatment can obscure a migration result, the cells were initially serum-starved for 24 h. For the migration assays, a circular gap was prepared using soft polydimethylsiloxane (PDMS) pillars of 500 μm diameter on cell culture dishes (Figure 4A). Once the seeded cells had reached confluency, the PDMS pillars were removed, and cell migration was recorded over 24 h using video microscopy.

We analyzed the sizes of the gaps directly after removing the PDMS pillar using the ImageJ software, with calculation of the area (μm^2) of gap closure per hour (Figure 4). Migration rate for MCF-10a cells treated with 100 ng/mL vimentin and 100 ng/mL IGF-1 were approximately 1.8 and 1.5 times higher compared to the untreated cells (Figure 4D). In the MCF-7 cancer cells, the migration rate upon 100 ng/mL vimentin and 100 ng/mL IGF-1 treatments, these reached 2.5 and 3 times higher than control respectively (Figure 4D). Gap closure was therefore faster after the treatment with extracellular vimentin in both the MCF-10a and MCF-7 cells. This suggests that activation of these cells with extracellular vimentin enhances cell migration, which results in faster closure of these wounds. Interestingly, the effects of added recombinant vimentin were again stronger in the MCF-7 cancer cells compared to the MCF-10a cells.

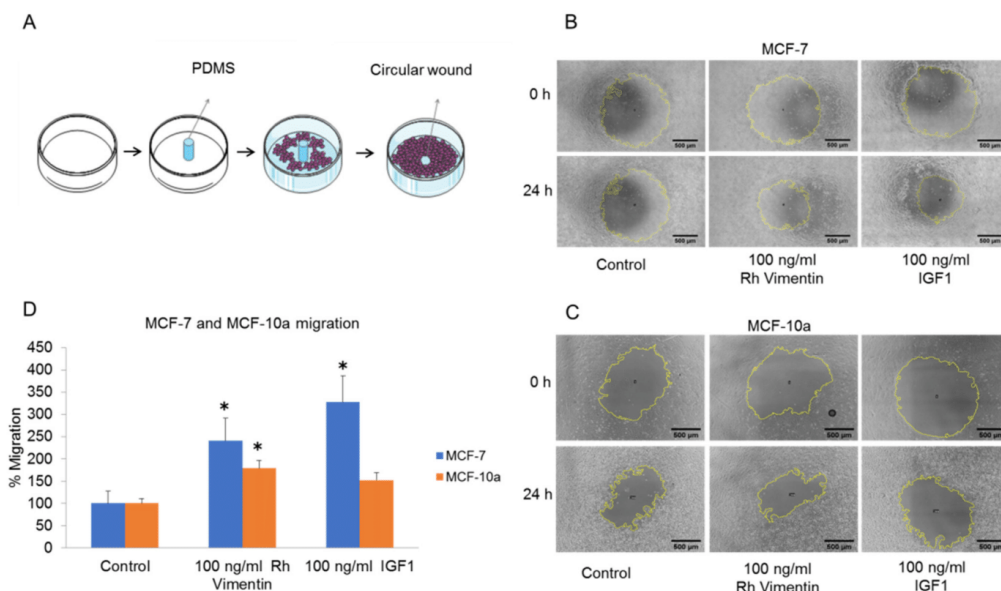


Figure 4. Gap closure assays for the MCF-10a and MCF-7 cells under treatment with recombinant (Rh) vimentin. (A) Schematic representation of the creation of the circular gaps using a PDMS column. (B,C) Representative images of the gap closure of MCF-10a cells (B) and MCF-7 cells (C) without and with treatments with vimentin and IGF-1 (scale bar 500 μm , yellow line indicates the edge of gap closure). (D) Migration rate is calculated by measuring gap closure (area covered by cell monolayer) over the time in terms of $\mu\text{m}^2/\text{h}$ and then it is normalized to control. To exclude effects of cell proliferation on cell migration, the cells were initially starved for 24 h in serum-free medium. * $p < 0.05$, compared to relevant control (unpaired t -tests). Error bars indicate SEM.

In addition to gap closure assay, we also carried out transwell migration assays. The MCF-10a and MCF-7 cells were placed in the upper reservoirs of individual systems and cultured in the presence or absence of Rh vimentin and IGF-1. The number of cells that moved through the porous membranes was then quantified at 48 h post-seeding (Figure 5).

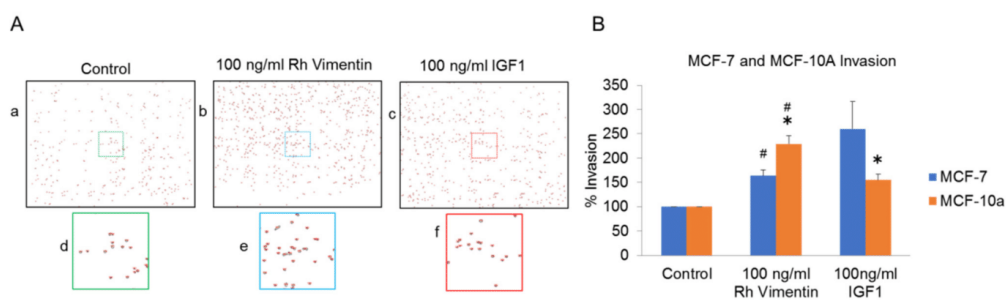


Figure 5. Transwell migration assays for the MCF-10a (control) and MCF-7 (cancer) cells under treatment with recombinant (Rh) vimentin. (A) Representative images used for the quantification of the MCF-10a cells that had migrated through the transwell membranes. (B) Quantification of the migrated cells without and with vimentin and IGF-1. Individual experiment was normalized to control and then mean values of three experiments were calculated. # * $p < 0.05$, compared to group indicating same symbol (unpaired t -tests). Error bars indicate SEM.

Both the MCF-10a and MCF-7 cells showed enhanced migration through the porous membranes upon vimentin treatment, and for their adherence to the well plate, as compared to the untreated control cells (Figure 5). Interestingly, the IGF-1-treated MCF-7 cells showed higher migration rates when compared to the vimentin-treated cells, with the converse seen for the IGF-1-treated MCF-10a cells (Figure 5B). This effect complements our findings for gap closure (Figure 4D).

2.4. Extracellular Vimentin Effects on MCF-10a and MCF-7 Cell Monolayer Permeabilities and Alterations of Cell Monolayer Integrity Caused by the Receptor Binding Domain of SARS-CoV-2 Spike Protein

Alterations to epithelial cell monolayer permeability are an indicator of disease conditions in epithelial tissues, as well as a marker of oncogenesis [30–32]. Such alterations might have a role in tumor invasiveness, and also in viral invasion into various organs. Indeed, it was shown in a recent study that SARS-CoV-2 receptor binding domain can affect the endothelial cell monolayer permeability [26]. Here, we measured the fluorescence intensity of 3 kDa FITC-dextran that passed through MCF-10a and MCF-7 cell monolayers upon addition of 10 nM recombinant vimentin and 10 nM SARS-CoV-2 RBD, using a protocol that is illustrated in Figure 6.

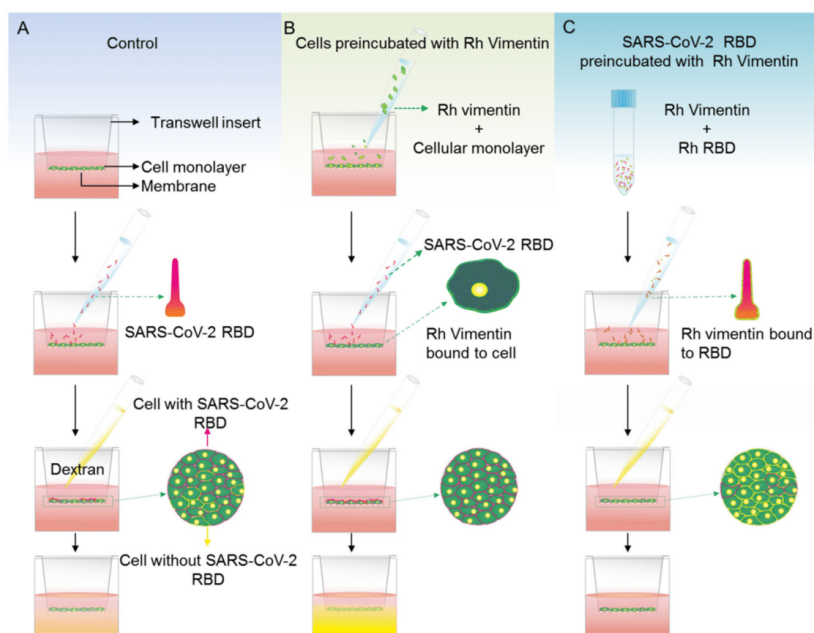


Figure 6. Stepwise procedures for determination of MCF-10a and MCF-7 cell monolayer permeabilities under SARS-CoV-2 RBD treatments using 3 kDa FITC-dextran. (A–C) Cell monolayers were treated for 24 h with SARS-CoV-2 RBD, either alone (A) or after treatment with recombinant (Rh) vimentin for 1 h (B), and with SARS-CoV-2 RBD that had been preincubated with Rh vimentin for 1 h (C).

First, the effects of recombinant vimentin on the permeability of MCF-10a and MCF-7 cell monolayers were determined. MCF-10a control cell monolayers treated with vimentin showed a 45% increase in the monolayer permeability compared to untreated MCF-10a control monolayers. Instead, monolayers of MCF-7 cells treated with recombinant vimentin

showed the inverse trend, as a 35% decrease in monolayer permeability compared to the MCF-7 control monolayers (Figure 7A).

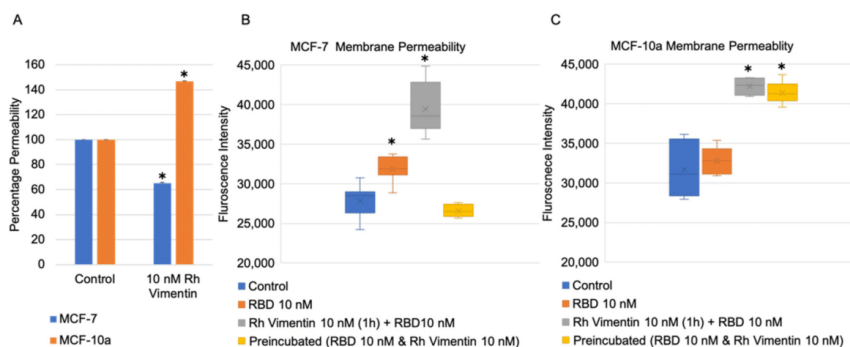


Figure 7. Monolayer permeabilities of MCF-10a and MCF-7 cells using 3 kDa of FITC-dextran treatment for 1 h. (A) Cell monolayers treated with 10 nM of recombinant (Rh) vimentin for 24 h, with data normalized to the controls. (B,C) Treatments of MCF-10a (B) and MCF-7 (C) cell monolayers without (control) and with SARS-CoV-2 RBD for 24 h (RBD), including 10 nM of vimentin monolayer pre-treatment for 1 h followed by SARS-CoV-2 RBD for 24 h; or 10 nM of vimentin and SARS-CoV-2 RBD pre-incubated together for 1 h, followed by SARS-CoV-2 RBD for 24 h. * $p < 0.05$, compared to control (unpaired t -tests).

We then checked whether recombinant vimentin has an influence on MCF-10a and MCF-7 cell monolayer permeability when the monolayers are also exposed to SARS-CoV-2 RBD. Two different conditions for the recombinant vimentin treatment were used here. In the first (Figure 7B,C), the cell monolayers were pretreated with 10 nM of recombinant vimentin for 1 h prior to addition of 10 nM of SARS-CoV-2 RBD. After 24 h, for both MCF-10a and MCF-7 cells, their monolayer permeabilities were increased significantly compared to treatment of the monolayers with 10 nM of SARS-CoV-2 RBD alone. For the second condition, 10 nM of SARS-CoV-2 RBD and 10 nM of vimentin were preincubated together for 1 h, and then added to the cell monolayers. Interestingly, with the SARS-CoV-2 RBD and 10 nM of vimentin preincubation, the monolayer permeability alteration was not affected for the MCF-10a control cells, but it was inhibited for the MCF-7 cancer cells.

To summarize these data in general, we have shown that recombinant vimentin has effects on cell proliferation, adhesion, and migration, and on epithelial cell monolayer permeability in MCF-10a control cells and MCF-7 cancer cells. Vimentin also affects the cell monolayer permeability changes triggered by SARS-CoV-2 RBD.

3. Discussion

For about a decade, the existence of extracellular vimentin has been questioned by the scientific community, and even by researchers working on vimentin. However, recent studies have shown that vimentin can indeed be secreted into the extracellular space under several physiological conditions, such as cell activation, inflammation, senescence, and stress [3,4,33]. Vimentin is secreted by various cell types, such as macrophages, astrocytes, neutrophils, monocytes, apoptotic lymphocytes, and endothelial cells [3,5–8,33]. Mor-Vaknin et al. (2003) reported that activated macrophages secrete vimentin when treated with okadaic acid. Recently, it was shown that oxidized low-density lipoprotein induced vimentin secretion via CD36 in macrophages [34]. Recent studies have also provided evidence that extracellular vimentin is involved in several diseases, in repair mechanisms for spinal cord injury, and in the infection mechanisms of viruses [35]. We also described some of these roles of extracellular vimentin in health and disease in a recent review [2]. The functions of extracellular vimentin are still under debate, however, and these functions appear to depend on the form of this extracellular vimentin (Figure 8).

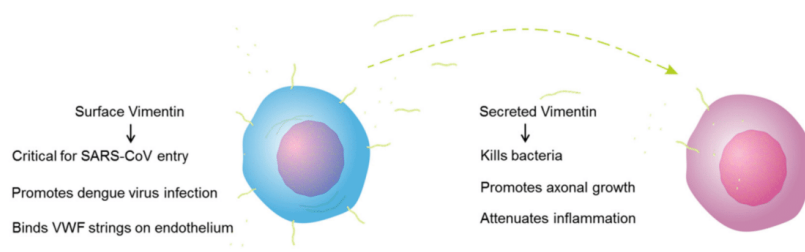


Figure 8. Functional roles of the different forms of extracellular vimentin, as surface vimentin and secreted vimentin. VWF, von Willebrand factor.

Secreted vimentin could have a potential role in wound healing, although to date, the role of vimentin in wound healing has mainly focused on cytoplasmic vimentin. Nevertheless, recent studies have explored the possibility of extracellular vimentin as a potential remedy for tissue repair in many injuries [2]. Post-injury, vimentin released into the extracellular milieu facilitates wound closure by binding to mesenchymal leader cells. This extracellular vimentin promotes mesenchymal to myofibroblast differentiation of leader cells [36]. However, here the interaction of extracellular vimentin with receptors on leader cells that lead to wound healing remains an open question.

Vimentin has also been shown to have a role in wound healing during functional recovery after trauma in the central nervous system, which is a challenge that is still faced in the field of neuroscience [37]. In this context, a newly described compound, denosomin, was shown to provide added benefits in the treatment of mice for spinal cord injury [38]. During the course of these treatments, it was noted that the astrocytes tended to secrete vimentin at the site of the injury. This secreted vimentin promoted axonal growth by activation of IGF-1R, to thus promote improved functional recovery of the spinal cord in mice [22]. However, this previous study was focused mainly on the promotion of axonal growth via the vimentin interaction with IGF-1R, so in the present study we specifically explored the role of the extracellular vimentin and IGF-1R interaction across a range of cellular functions, as cell proliferation, adhesion, and migration; these are all crucial for tumor progression.

In cancers, the collective migration of cells is a critical event for establishment of metastases, and this indicates how cells contribute to cancer invasion [39]. Extracellular vimentin was shown previously to be involved in cancer-cell invasion [40]. In another study, the interaction between surface vimentin and GlcNAc-polymers led to an increase in migration and invasion of MDCK and MCF-7 cells [41]. In the present study, we showed that addition of recombinant vimentin promoted wound closure for both MCF-10a and MCF-7 cells, presumably through increased migratory speed of the cells following activation of the IGF-1R cell-surface receptor. We also showed that recombinant vimentin stimulated a greater increase in cell migration rate in the MCF-7 cancer cells than for the MCF-10a cells. Here, we also compared the effect of vimentin on cell migration with that of IGF-1 itself, as it is well known that IGF-1 induces cell migration in breast epithelial cells [42]. Interestingly, in the MCF-10a cells, the addition of vimentin resulted in greater migratory speed for these cells compared to the addition of IGF-1. We also saw similar effects by using the transwell migration assay here, which was greater with treatment with vimentin, and even higher than for the IGF-1 treatment for the MCF-10a cells.

In invasion by cancer cells, cell adhesion is one of the first steps during metastasis [43]. In addition, cell migration and proliferation are regulated by cell adhesion to the extracellular matrix [44]. Therefore, we additionally investigated cell adhesion upon vimentin treatment in the present study, which showed that vimentin treatment increased the adhesion strength in MCF-7 cancer cells. Interestingly, we also showed that the vimentin-treated MCF-7 cells showed a higher trend towards Young's modulus during these FluidFM measurements. This suggests that the stiffness of the MCF-7 cells was increased by vimentin.

Higher circulating IGF-1 levels are indicative of higher risk of breast cancer in premenopausal women [45,46], and it has been reported that IGF-1 stimulates proliferation of breast cancer cells [47,48]. Although serum vimentin expression has been reported for various cancers, these previous studies did not emphasize the significant role of extracellular vimentin in cell proliferation [49,50]. Therefore, we also tested whether this extracellular (soluble) vimentin had similar effects as IGF-1 on cell proliferation. Interestingly, treatment with vimentin promoted increased proliferation rates in the MCF-7 cancer cells but not in MCF-10a cells. This effect was diminished when IGF-1R was blocked (using an anti-IGF-1R antibody), which further supports our hypothesis that vimentin binding to IGF-1R is involved in general cellular functions.

Conclusively, as the migration rate of the MCF-10a cancer cells was higher in the presence of vimentin than the migration rate of MCF-7 cells in transwell assays under the same conditions, we hypothesized that transwell migration assays in the presence of vimentin can be used for sorting cancer cells. From this study, we concluded that cancer cells tend to be more sensitive to extracellular vimentin, and hence that extracellular vimentin has an effect on general cellular functions. Taking these parameters into consideration during clinical decision making can have a major role in the treatment of patients with cancers in general, and also under specific disease conditions.

Extracellular vimentin has a vital role in various viral and bacterial infections [35]. A recent study that used a pseudo virus showed that surface vimentin is involved in SARS-CoV-2 infection, through its binding by the viral spike protein. Using an antibody against extracellular vimentin, they showed that vimentin can be used as a potential target to inhibit viral particle entry into cells [19]. In the present study, in the cell permeability assays, vimentin decreased the barrier permeability in MCF-7 cancer cells and increased it in MCF-10a cells. These MCF-7 cancer cells overexpress IGF-1R, which might lead to more binding of vimentin to the cell membrane, and a block (i.e., decreased permeability) of the paracellular junctions. The permeability increases in the cell monolayers of both MCF-10a and MCF-7 cells induced by SARS-CoV-2 RBD and was further enhanced when the cells were pretreated with vimentin. This effect might be because extracellular vimentin can act as a co-receptor for the SARS-CoV and SARS-CoV-2 spike proteins [18]. This role for vimentin as a co-receptor will lead to more attachment of the SARS-CoV2 RBD to the cells treated with vimentin, and will also affect the cell monolayer permeability. This might result in enhanced viral particle invasion into tissues and internalization into cells (Figure 9A).

In a previous study, pre-incubation of viral particles with recombinant vimentin restricted human Papillomavirus 16 (HPV) viral entry into Hela, HaCaT, and NIKS cells [17]. In the present study, we used the same method, and preincubated SARS-CoV-2 RBD and recombinant vimentin prior to the treatment of the cell monolayers with this mixture. In the MCF-7 cancer cells, the permeability was decreased by SARS-CoV-2 RBD. However, this effect was not seen for the MCF-10a cells. This could be due to lack of ACE2 receptor, that RBD does not have any additional effect on MCF-10a cells [51].

Further studies are required to understand the full mechanisms involved in the phenomena described here. However, we have shown that extracellular vimentin influences a range of cellular functions and might become an important player in the treatment of diseases or the prevention of particular infections. Additionally, extracellular vimentin can exist in different isoforms such as oxidized vimentin, citrullinated vimentin, and carbamylated vimentin which undergo post-translational modifications under certain circumstances (senescence, rheumatoid arthritis) [4,52,53]. Imitation of recombinant vimentin as extracellular vimentin could pose some limitations in the practical setting. Therefore, future studies should investigate the effect of native isoforms of extracellular vimentin on cells.

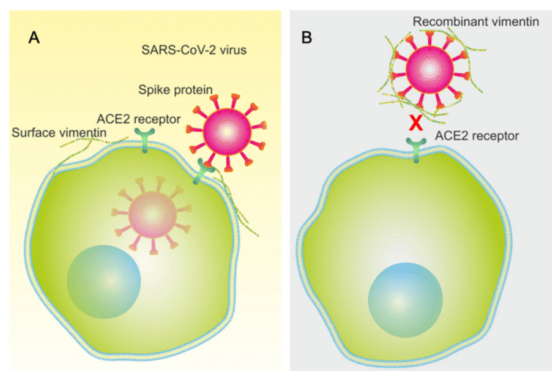


Figure 9. Illustration of the influence of extracellular vimentin in SARS-CoV-2 viral particle entry into cells. **(A)** Vimentin on the cell surface can act as a co-receptor, to promote further viral membrane association and virus entry into the cells. **(B)** For the viral particles pre-treated with recombinant vimentin, this instead restricts viral association with the cell membrane, and thus virus entry into the cells.

4. Materials and Methods

4.1. Cell Culture

The MCF-10A spontaneously immortalized breast epithelial (non-tumorigenic) cells were a kind gift from Marc Stemmler (FAU-Erlangen, Germany), and were cultured in Dulbecco's modified Eagle's medium/F12 supplemented (Gibco, Bleiswijk, The Netherlands) with 5% horse serum (Fisher Scientific, Schwerte, Germany), 5% penicillin/streptomycin (Gibco, NY, USA), 20 ng/mL of epidermal growth factor (PeproTech, Hamburg, Germany), 0.5 µg/mL of hydrocortisone (Sigma Aldrich, MO, USA), 100 ng/mL of cholera toxin, (Sigma Aldrich, MO, USA), 10 µg/mL of insulin (Sigma Aldrich, MO, USA), and 10 mM of HEPES (Gibco, Bleiswijk, The Netherlands). The MCF-7 malignant breast epithelial (cancer) cells were cultured in Dulbecco's modified Eagle's medium/F12 supplemented with 10% fetal bovine serum (Fisher Scientific, Schwerte, Germany), 5% penicillin/streptomycin (Gibco, NY, USA), and 5% Glutamax (Gibco, Paisley, UK).

4.2. Proliferation Assay

The MTT assay was used to monitor cell proliferation. Upon treating cells with MTT, the viable cells reduce the MTT reagent to formazan, with the formation of purple crystals. These crystals were dissolved by incubation of the samples in dimethylsulfoxide. The numbers of viable cells were proportional to the absorbance.

The MCF-10A and MCF-7 cells were plated into 96-well plates at 10,000 cells/well and were left to attach for 24 h. The medium was then replaced with serum-free medium, for starvation of the cells for 12 h. The cells were treated with various concentrations of recombinant vimentin (R&D systems, Minneapolis, MN, USA), citrullinated vimentin (Cayman Chemical, Ann Arbor, MI, USA), and/or recombinant IGF-1 (Invitrogen, Waltham, MA, USA) in serum-free medium for 24 h, as indicated. After aspiration of the medium, the cells were incubated in fresh medium with fetal bovine serum for 24 and 72 h. The cells were then washed with phosphate-buffered saline (PBS) and treated with 0.5 mg/mL MTT (Sigma Aldrich, St. Louis, MO, USA) for 3 h. Then 100 µL of dimethylsulfoxide was added to each well to dissolve the purple formazan crystals that had formed. After 15 min, the absorbance was measured at 570 nm in a plate reader (Infinite M200 Pro; Tecan, Crailsheim, Germany). For blocking the IGF-1 receptor, the cells were pre-incubated with 1.5 µg/mL anti-IGF-1R antibody (ARG51076; Arigo bio, Hsinchu, Taiwan) for 15 min and then incubated with recombinant vimentin, citrullinated vimentin, and IGF-1 for 48 h.

4.3. Migration Assay

Soft PDMS chips were made by mixing a curing agent and PDMS base (1:30). After curing in an oven at 75 °C for 1 h, pillars of 500 µm diameter were cut using a PDMS punch. These PDMS pillars were attached to each well in an eight-well chambered coverslip (Ibidi µ-slide, Gräfelting, Germany). Then the MCF-10a and MCF-7 cells were seeded into each (50,000 cells/well) and incubated until confluent monolayers had formed. The cells were starved without serum for 24 h, and then the medium was replaced with fresh serum-free medium containing various concentrations of recombinant vimentin and IGF-1, as required. After 24 h, the medium was replaced with fresh medium (with fetal bovine serum). The PDMS pillars were then removed, which left a circular wound in each well, and the wound closure was monitored and recorded under an inverted microscope (Ti-Eclipse; Nikon, Düsseldorf, Germany) up to 24 h. During the imaging, the temperature in the chamber (Okolab, Ambridge, PA, USA) was maintained at 37 °C, and also using 5% CO₂.

4.4. Transwell Migration Assay

Transwell inserts (pore size, 8 µm; Corning, Corning, NY, USA) were used for the MCF-10A and MCF-7 cell migration experiments. Inserts were placed in 12-well plates and 200 µL of cell solution was loaded into the upper chamber for 24 h, to attach to the membrane. The cells attached to the membrane were then starved without serum for 12 h. The medium in the upper chamber was replaced with fresh medium containing 100 ng/mL IGF-1 and 100 ng/mL recombinant vimentin. Then, 500 µL medium with serum was loaded into the bottom chamber. The transwell chambers were incubated for 48 h at 37 °C, to allow migration of the cells from the upper chamber into the lower chamber. Furthermore, the loading side of the upper chamber was cleaned using a cotton swab, to remove the cells that did not invade. Fresh medium containing 250 ng/mL Hoechst (Sigma Aldrich, MO, USA) was added to the bottom chamber, and then the upper chamber was placed into it for 20 min to stain the nuclei of the cells that had invaded the lower side of the membrane. Before imaging of the cells, the medium containing Hoechst was replaced with fresh medium.

4.5. Single-Cell Force Spectroscopy

Single-cell force spectroscopy was performed on an atomic force microscope (Flex-Bio) in FluidFM mode (Nanosurf GmbH, Liestal, Switzerland) and with FluidFM hollow micropipettes (Cytosurge, Glattburg, Switzerland), with a spring constant of 0.3 N/m and an opening diameter of 4 µm. The experiments were carried out with a relative force trigger of 8 nN and a z-range of 30 µm. Prior to the experiments, glass-bottomed dishes were coated with 25 µg/mL fibronectin (Sigma Aldrich, MO, USA) for 1 h. Subsequently, the cells (1×10^6 cells/dish) were seeded into the glass-bottomed dish and allowed to attach for 24 h. Next, the cells were treated with 200 ng/mL recombinant vimentin and/or 100 ng/mL IGF-1 for 24 h. The cells were approached with the FluidFM micropipette, grabbed on the apical top, held by negative pressure (−500 mbar), and detached from the coated glass substrate by the retraction movement of the micropipette. Experimental data were only obtainable for the MCF-7 cells, as this procedure led to cell disruption or disengagement of the attachment between the cells and the spectroscopy probe. Thus, the forces were recorded only for the MCF-7 cells, as force–distance curves. Successful cell detachment was monitored by light microscopy (Zeiss AG, Oberkochen, Germany). The force–distance curve analysis was carried out with the SPIP software, version 6.6.2 (Image Metrology, Hørsholm, Denmark).

4.6. Permeability Assay

Transwell inserts (pore size, 0.4 µm; Corning, ME, USA) were used for the permeability assays for both the MCF-10A and MCF-7 cells. The inserts were placed into 12-well plates, and 200 µL of cells was loaded into the upper chamber (5000 cells/well). The cells were left to attach and form monolayers. The cell monolayers were then treated with 10 nM of

recombinant vimentin. For the SARS-CoV-2 RBD analysis, the samples were treated under four primary conditions: (i) control cells as only cell monolayers; (ii) cell monolayers treated with 10 nM of SARS-CoV-2 RBD (R&D systems, MN, USA) for 24 h; (iii) cell monolayers treated with 10 nM of recombinant vimentin for 1 h and then with the addition of 10 nM of SARS-CoV-2 RBD for 24 h; and (iv) 10 nM of Rh vimentin and 10 nM of SARS-CoV-2 RBD were preincubated together for 1 h, and then added to cell monolayers for 24 h. After the appropriate treatments, 1 mg/mL of 3 kDa FITC-dextran (Sigma Aldrich, MO, USA) was added to the chambers and incubated for 1 h. The fluorescence intensities for the basolateral medium were then determined using a plate reader (Infinite M200 Pro; Tecan, Crailsheim, Germany).

Author Contributions: D.G.T. performed the experiments except FluidFM; data analysis and visualization; and writing original draft, P.J. performed FluidFM in Homburg, F.L. contributed in writing/review and editing manuscript; supervision; project administration; and funding acquisition, D.G.T. and F.L. were equally involved in conceptualization of the project. M.B. was involved in review and editing of manuscript; supervising FluidFM methodology. All authors have read and agreed to the published version of the manuscript.

Funding: This research was funded by DFG (SFB 1027, project A10, project B2).

Institutional Review Board Statement: Not applicable.

Informed Consent Statement: Not applicable.

Data Availability Statement: Not applicable.

Acknowledgments: We are thankful to Marc Stemmler for providing MCF-10a cells. We would like to acknowledge Magdalena Kaus-Drobek for discussing preparation of citrullinated vimentin. We would like to thank Luiza Stankevics, Emmanuel Terriac, and Annica Karin Britt Gad for their active involvement in project discussions and suggestions.

Conflicts of Interest: The authors declare no conflict of interest.

Abbreviations

ACE2	Angiotensin-converting enzyme 2
BSA	Bovine serum albumin
CSV	Cell-surface vimentin
CTCs	Circulating tumor cells
FluidFM	Fluidic force microscopy
IGF-1	Insulin-like growth factor-1
IGF-1R	Insulin-like growth factor-1 receptor
MCF-7 cells	Human breast cancer epithelial cell line
MCF-10a	Non-tumorigenic epithelial cell line
MTT	3-[4,5-dimethylthiazole-2-yl]-2,5-diphenyltetrazolium bromide
PBS	Phosphate-buffered saline
PDMS	Polydimethylsiloxane
RBD	Receptor binding domain
SARS-CoV	Severe acute respiratory syndrome coronavirus

References

- Ivaska, J.; Pallari, H.-M.; Nevo, J.; Eriksson, J.E. Novel functions of vimentin in cell adhesion, migration, and signaling. *Exp. Cell Res.* **2007**, *313*, 2050–2062. [[CrossRef](#)] [[PubMed](#)]
- Danielsson, F.; Peterson, M.K.; Caldeira Araújo, H.; Lautenschläger, F.; Gad, A.K.B. Vimentin diversity in health and disease. *Cells* **2018**, *7*, 147. [[CrossRef](#)]
- Mor-Vaknin, N.; Punturieri, A.; Sitwala, K.; Markovitz, D.M. Vimentin is secreted by activated macrophages. *Nat. Cell Biol.* **2003**, *5*, 59–63. [[CrossRef](#)]
- Frescas, D.; Roux, C.M.; Aygun-Sunar, S.; Gleiberman, A.S.; Krasnov, P.; Kurnasov, O.V.; Strom, E.; Virtuoso, L.P.; Wrobel, M.; Osterman, A.L.; et al. Senescent cells expose and secrete an oxidized form of membrane-bound vimentin as revealed by a natural polyreactive antibody. *Proc. Natl. Acad. Sci. USA* **2017**, *114*, E1668–E1677. [[CrossRef](#)] [[PubMed](#)]

5. Greco, T.; Seeholzer, S.H.; Mak, A.; Spruce, L.; Ischiropoulos, H. Quantitative Mass Spectrometry-based Proteomics Reveals the Dynamic Range of Primary Mouse Astrocyte Protein Secretion. *J. Proteome Res.* **2010**, *9*, 2764–2774. [[CrossRef](#)]
6. Kaplan, M.J. Role of neutrophils in systemic autoimmune diseases. *Arthritis Res. Ther.* **2013**, *15*, 1–9. [[CrossRef](#)]
7. Boilard, E.; Bourgoin, S.G.; Bernatchez, C.; Surette, M.E. Identification of an autoantigen on the surface of apoptotic human T cells as a new protein interacting with inflammatory group IIA phospholipase A2. *Blood* **2003**, *102*, 2901–2909. [[CrossRef](#)] [[PubMed](#)]
8. Moisan, E.; Girard, D. Cell surface expression of intermediate filament proteins vimentin and lamin B1 in human neutrophil spontaneous apoptosis. *J. Leukoc. Biol.* **2005**, *79*, 489–498. [[CrossRef](#)]
9. Satelli, A.; Li, S. Vimentin in cancer and its potential as a molecular target for cancer therapy. *Cell. Mol. Life Sci.* **2011**, *68*, 3033–3046. [[CrossRef](#)] [[PubMed](#)]
10. Noh, H.; Hyangsoon, N.; Hong, S.; Kong, L.-Y.; Gabrusiewicz, K.; Xia, X.; Heimberger, A.B.; Ling-Yuan, K. Discovery of cell surface vimentin targeting mAb for direct disruption of GBM tumor initiating cells. *Oncotarget* **2016**, *7*, 72021–72032. [[CrossRef](#)]
11. Satelli, A.; Mitra, A.; Cutrera, J.J.; Devarie, M.; Xia, X.; Ingram, D.R.; Dibra, D.; Somaiah, N.; Torres, K.E.; Ravi, V.; et al. Universal Marker and Detection Tool for Human Sarcoma Circulating Tumor Cells. *Cancer Res.* **2014**, *74*, 1645–1650. [[CrossRef](#)] [[PubMed](#)]
12. Satelli, A.; Mitra, A.; Brownlee, Z.; Xia, X.; Bellister, S.; Overman, M.J.; Kopetz, S.; Ellis, L.M.; Meng, Q.H.; Li, S. Epithelial-Mesenchymal Transitioned Circulating Tumor Cells Capture for Detecting Tumor Progression. *Clin. Cancer Res.* **2015**, *21*, 899–906. [[CrossRef](#)] [[PubMed](#)]
13. Mitra, A.; Satelli, A.; Xia, X.; Cutrera, J.; Mishra, L.; Li, S. Cell-surface Vimentin: A mislocalized protein for isolating csVimentin+CD133—novel stem-like hepatocellular carcinoma cells expressing EMT markers. *Int. J. Cancer* **2015**, *137*, 491–496. [[CrossRef](#)]
14. Yang, J.; Zou, L.; Yang, Y.; Yuan, J.; Hu, Z.; Liu, H.; Peng, H.; Shang, W.; Zhang, X.; Zhu, J.; et al. Superficial vimentin mediates DENV-2 infection of vascular endothelial cells. *Sci. Rep.* **2016**, *6*, 38372. [[CrossRef](#)]
15. Ghosh, P.; Halvorsen, E.M.; Ammendolia, D.A.; Mor-Vaknin, N.; O’Riordan, M.; Brumell, J.H.; Markovitz, D.M.; Higgins, D.E. Invasion of the Brain by *Listeria monocytogenes* Is Mediated by InlF and Host Cell Vimentin. *mBio* **2018**, *9*, e00160-18. [[CrossRef](#)]
16. Bryant, A.E.; Bayer, C.R.; Huntington, J.D.; Stevens, D.L. Group A Streptococcal Myonecrosis: Increased Vimentin Expression after Skeletal-Muscle Injury Mediates the Binding of *Streptococcus pyogenes*. *J. Infect. Dis.* **2006**, *193*, 1685–1692. [[CrossRef](#)] [[PubMed](#)]
17. Schäfer, G.; Graham, L.M.; Lang, D.M.; Blumenthal, M.; Marušič, M.B.; Katz, A.A. Vimentin Modulates Infectious Internalization of Human Papillomavirus 16 Pseudovirions. *J. Virol.* **2017**, *91*, 00307–00317. [[CrossRef](#)] [[PubMed](#)]
18. Yu, Y.T.C.; Chien, S.C.; Chen, I.Y.; Lai, C.T.; Tsay, Y.G.; Chang, S.C.; Chang, M.F. Surface vimentin is critical for the cell entry of SARS-CoV. *J. Biomed. Sci.* **2016**, *23*, 1–10. [[CrossRef](#)] [[PubMed](#)]
19. Suprewicz, L.; Swoger, M.; Gupta, S.; Piktel, E.; Byfield, F.J.; Iwamoto, D.V.; Germann, D.A.; Reszeć, J.; Marcińczyk, N.; Janmey, P.; et al. Vimentin binds to SARS-CoV-2 spike protein and antibodies targeting extracellular vimentin block in vitro uptake of SARS-CoV-2 virus-like particles. *bioRxiv* **2021**. [[CrossRef](#)]
20. Thiagarajan, P.S.; Yakubenko, V.P.; Elson, D.H.; Yadav, S.P.; Willard, B.; Tan, C.D.; Rodriguez, E.R.; Febbraio, M.; Cathcart, M.K. Vimentin is an endogenous ligand for the pattern recognition receptor Dectin-1. *Cardiovasc. Res.* **2013**, *99*, 494–504. [[CrossRef](#)]
21. Garg, A.; Barnes, P.F.; Porgador, A.; Roy, S.; Wu, S.; Nanda, J.S.; Griffith, D.E.; Girard, W.M.; Rawal, N.; Shetty, S.; et al. Vimentin Expressed on Mycobacterium tuberculosis-Infected Human Monocytes Is Involved in Binding to the NKP46 Receptor. *J. Immunol.* **2006**, *177*, 6192–6198. [[CrossRef](#)]
22. Shigyo, M.; Kuboyama, T.; Sawai, Y.; Tada-Umezaki, M.; Tohda, C. Extracellular vimentin interacts with insulin-like growth factor 1 receptor to promote axonal growth. *Sci. Rep.* **2015**, *5*, 12055. [[CrossRef](#)] [[PubMed](#)]
23. Adams, T.E.; Epa, V.C.; Garrett, T.P.J.; Ward, C.W. Structure and function of the type 1 insulin-like growth factor receptor. *Cell. Mol. Life Sci.* **2000**, *57*, 1050–1093. [[CrossRef](#)]
24. Smith, T.J. Insulin-like growth factor-I regulation of immune function: A potential therapeutic target in autoimmune diseases? *Pharmacol. Rev.* **2010**, *62*, 199–236. [[CrossRef](#)] [[PubMed](#)]
25. Milano, F.; Campbell, A.P.; Guthrie, K.A.; Kuypers, J.; Englund, J.A.; Corey, L.; Boeckh, M. Human rhinovirus and coronavirus detection among allogeneic hematopoietic stem cell transplantation recipients. *Blood* **2010**, *115*, 2088–2094. [[CrossRef](#)]
26. Buzhdygan, T.P.; DeOre, B.J.; Baldwin-Leclair, A.; Bullock, T.A.; McGary, H.M.; Khan, J.A.; Razmpour, R.; Hale, J.F.; Galie, P.A.; Potula, R.; et al. The SARS-CoV-2 spike protein alters barrier function in 2D static and 3D microfluidic in-vitro models of the human blood-brain barrier. *Neurobiol. Dis.* **2020**, *146*, 105131. [[CrossRef](#)] [[PubMed](#)]
27. Bradley, B.T.; Maioli, H.; Johnston, R.; Chaudhry, I.; Fink, S.L.; Xu, H.; Najafian, B.; Deutsch, G.; Lacy, J.M.; Williams, T.; et al. Histopathology and ultrastructural findings of fatal COVID-19 infections in Washington State: A case series. *Lancet* **2020**, *396*, 320–332. [[CrossRef](#)]
28. Solomon-Zemler, R.; Sarfstein, R.; Werner, H. Nuclear insulin-like growth factor-1 receptor (IGF1R) displays proliferative and regulatory activities in non-malignant cells. *PLoS ONE* **2017**, *12*, e0185164. [[CrossRef](#)]
29. Guillaume-Gentil, O.; Potthoff, E.; Ossola, D.; Franz, C.; Zambelli, T.; Vorholt, J.A. Force-controlled manipulation of single cells: From AFM to FluidFM. *Trends Biotechnol.* **2014**, *32*, 381–388. [[CrossRef](#)]
30. Buchert, M.; Turksen, K.; Hollande, F. Methods to Examine Tight Junction Physiology in Cancer Stem Cells: TEER, Paracellular Permeability, and Dilution Potential Measurements. *Stem Cell Rev. Rep.* **2012**, *8*, 1030–1034. [[CrossRef](#)]

31. McCaffrey, L.M.; Macara, I.G. Epithelial organization, cell polarity and tumorigenesis. *Trends Cell Biol.* **2011**, *21*, 727–735. [[CrossRef](#)]
32. Gray, R.; Cheung, K.J.; Ewald, A.J. Cellular mechanisms regulating epithelial morphogenesis and cancer invasion. *Curr. Opin. Cell Biol.* **2010**, *22*, 640–650. [[CrossRef](#)] [[PubMed](#)]
33. Patteson, A.E.; Vahabikashi, A.; Goldman, R.D.; Janmey, P.A. Mechanical and Non-Mechanical Functions of Filamentous and Non-Filamentous Vimentin. *BioEssays* **2020**, *42*, 2000078. [[CrossRef](#)]
34. Kim, S.; Cho, W.; Kim, I.; Lee, S.-H.; Oh, G.T.; Park, Y.M. Oxidized LDL induces vimentin secretion by macrophages and contributes to atherosclerotic inflammation. *J. Mol. Med.* **2020**, *98*, 973–983. [[CrossRef](#)]
35. Ramos, I.; Stamatakis, K.; Oeste, C.L.; Pérez-Sala, D. Vimentin as a Multifaceted Player and Potential Therapeutic Target in Viral Infections. *Int. J. Mol. Sci.* **2020**, *21*, 4675. [[CrossRef](#)] [[PubMed](#)]
36. Walker, J.L.; Bleaken, B.M.; Romisher, A.R.; Alnwibit, A.A.; Menko, A.S. In wound repair vimentin mediates the transition of mesenchymal leader cells to a myofibroblast phenotype. *Mol. Biol. Cell* **2018**, *29*, 1555–1570. [[CrossRef](#)] [[PubMed](#)]
37. Liu, Z.; Li, Y.; Cui, Y.; Roberts, C.; Lu, M.; Wilhelmsson, U.; Pekny, M.; Chopp, M. Beneficial effects of gfap/vimentin reactive astrocytes for axonal remodeling and motor behavioral recovery in mice after stroke. *Glia* **2014**, *62*, 2022–2033. [[CrossRef](#)]
38. Shigyo, M.; Tohda, C. Extracellular vimentin is a novel axonal growth facilitator for functional recovery in spinal cord-injured mice. *Sci. Rep.* **2016**, *6*, 28293. [[CrossRef](#)] [[PubMed](#)]
39. Friedl, P.; Gilmour, D. Collective cell migration in morphogenesis, regeneration and cancer. *Nat. Rev. Mol. Cell Biol.* **2009**, *10*, 445–457. [[CrossRef](#)]
40. Satelli, A.; Hu, J.; Xia, X.; Li, S. Potential Function of Exogenous Vimentin on the Activation of Wnt Signaling Pathway in Cancer Cells. *J. Cancer* **2016**, *7*, 1824–1832. [[CrossRef](#)]
41. Komura, K.; Ise, H.; Akaike, T. Dynamic behaviors of vimentin induced by interaction with GlcNAc molecules. *Glycobiology* **2012**, *22*, 1741–1759. [[CrossRef](#)] [[PubMed](#)]
42. Mezi, S.; Todi, L.; Orsi, E.; Angeloni, A.; Mancini, P. Involvement of the Src-cortactin pathway in migration induced by IGF-1 and EGF in human breast cancer cells. *Int. J. Oncol.* **2012**, *41*, 2128–2138. [[CrossRef](#)] [[PubMed](#)]
43. Hamidi, H.; Ivaska, J. Every step of the way: Integrins in cancer progression and metastasis. *Nat. Rev. Cancer* **2018**, *18*, 533–548. [[CrossRef](#)]
44. Maziveyi, M.; Alahari, S.K. Cell matrix adhesions in cancer: The proteins that form the glue. *Oncotarget* **2017**, *8*, 48471–48487. [[CrossRef](#)]
45. Hankinson, S.E.; Willett, W.C.; Colditz, G.A.; Hunter, D.J.; Michaud, D.S.; Deroo, B.; Rosner, B.; Speizer, F.E.; Pollak, M. Circulating concentrations of insulin-like growth factor I and risk of breast cancer. *Lancet* **1998**, *351*, 1393–1396. [[CrossRef](#)]
46. Schernhammer, E.S.; Holly, J.M.; Pollak, M.N.; Hankinson, S.E. Circulating Levels of Insulin-like Growth Factors, their Binding Proteins, and Breast Cancer Risk. *Cancer Epidemiol. Biomark. Prev.* **2005**, *14*, 699–704. [[CrossRef](#)] [[PubMed](#)]
47. Davison, Z.; de Blacquièrre, G.E.; Westley, B.R.; May, F.E. Insulin-like growth factor-dependent proliferation and survival of triple-negative breast cancer cells: Implications for therapy. *Neoplasia* **2011**, *13*, 504–515. [[CrossRef](#)] [[PubMed](#)]
48. Dupont, J.; Le Roith, D. Insulin-like growth factor 1 and oestradiol promote cell proliferation of MCF-7 breast cancer cells: New insights into their synergistic effects. *Mol. Pathol.* **2001**, *54*, 149–154. [[CrossRef](#)]
49. Sun, S.; Poon, R.T.P.; Lee, N.P.; Yeung, C.; Chan, K.L.; Ng, I.O.-L.; Day, P.J.R.; Luk, J.M. Proteomics of Hepatocellular Carcinoma: Serum Vimentin As a Surrogate Marker for Small Tumors (≤ 2 cm). *J. Proteome Res.* **2010**, *9*, 1923–1930. [[CrossRef](#)]
50. Bukhari, S.; Mokhdomi, T.A.; Chikan, N.; Amin, A.; Qazi, H.; Wani, S.H.; Wafai, A.H.; Tyub, S.; Mustafa, F.; Mir, M.S.; et al. Affinity proteomics led identification of vimentin as a potential biomarker in colon cancers: Insights from serological screening and computational modelling. *Mol. Biosyst.* **2014**, *11*, 159–169. [[CrossRef](#)]
51. Leoncikas, V.; Wu, H.; Ward, L.T.; Kierzek, A.; Plant, N.J. Generation of 2000 breast cancer metabolic landscapes reveals a poor prognosis group with active serotonin production. *Sci. Rep.* **2016**, *6*, 19771. [[CrossRef](#)] [[PubMed](#)]
52. Van Steendam, K.; Tilleman, K.; De Ceuleneer, M.; De Keyser, F.; Elewaut, D.; Deforce, D. Citrullinated vimentin as an important antigen in immune complexes from synovial fluid of rheumatoid arthritis patients with antibodies against citrullinated proteins. *Arthritis Res. Ther.* **2010**, *12*, R132. [[CrossRef](#)] [[PubMed](#)]
53. Ospelt, C.; Bang, H.; Feist, E.; Camici, G.; Keller, S.; Detert, J.; Krämer, A.; Gay, S.; Ghanam, K.; Burmester, G.R. Carbamylation of vimentin is inducible by smoking and represents an independent autoantigen in rheumatoid arthritis. *Ann. Rheum. Dis.* **2017**, *76*, 1176–1183. [[CrossRef](#)] [[PubMed](#)]

7.3 Publication 3: Actin stabilisation in cell migration

Carsten Baltes ¹ , Divyendu Goud Thalla¹ , Uli Kazmaier ² and Franziska Lautenschläger ^{1,3}

¹Experimental Physics, Saarland University, Saarbrücken, Germany

²Organic Chemistry, Saarland University, Saarbrücken, Germany

³Centre for Biophysics, Saarland University, Saarbrücken, Germany

Front. Cell Dev. Biol. 10:931880

<https://doi.org/10.3389/fcell.2022.931880>

Published: 11 August 2022

CB, FL, and DG contributed to conception and design of the study. CB performed the experiments and the analysis of data. UK provided the compound. All authors contributed to manuscript revision, read, and approved the submitted version.



OPEN ACCESS

EDITED BY
Claudia Tanja Mierke,
Leipzig University, Germany

REVIEWED BY
Silvia C. Finnemann,
Fordham University, United States
Dave Gau,
University of Pittsburgh, United States

*CORRESPONDENCE
Franziska Lautenschläger,
f.lautenschlaeger@physik.uni-saarland.

SPECIALTY SECTION
This article was submitted to Cell
Adhesion and Migration,
a section of the journal
Frontiers in Cell and Developmental
Biology

RECEIVED 29 April 2022
ACCEPTED 08 July 2022
PUBLISHED 11 August 2022

CITATION
Baltes C, Thalla DG, Kazmaier U and
Lautenschläger F (2022), Actin
stabilization in cell migration.
Front. Cell Dev. Biol. 10:931880.
doi: 10.3389/fcell.2022.931880

COPYRIGHT
© 2022 Baltes, Thalla, Kazmaier U and
Lautenschläger. This is an open-access
article distributed under the terms of the
[Creative Commons Attribution License
\(CC BY\)](https://creativecommons.org/licenses/by/4.0/). The use, distribution or
reproduction in other forums is
permitted, provided the original
author(s) and the copyright owner(s) are
credited and that the original
publication in this journal is cited, in
accordance with accepted academic
practice. No use, distribution or
reproduction is permitted which does
not comply with these terms.

Actin stabilization in cell migration

Carsten Baltes¹, Divyendu Goud Thalla¹, Uli Kazmaier² and Franziska Lautenschläger^{1,3*}

¹Experimental Physics, Saarland University, Saarbrücken, Germany, ²Organic Chemistry, Saarland University, Saarbrücken, Germany, ³Centre for Biophysics, Saarland University, Saarbrücken, Germany

Actin is a cytoskeletal filament involved in numerous biological tasks, such as providing cells a shape or generating and transmitting forces. Particularly important for these tasks is the ability of actin to grow and shrink. To study the role of actin in living cells this dynamic needs to be targeted. In the past, such alterations were performed by destabilizing actin. In contrast, we used the natural compound miuraenamides in living retinal pigmented epithelial (RPE-1) cells to stabilize actin filaments and show that it decreases actin filament dynamics and elongates filament length. Cells treated with miuraenamide A increased their adhesive area and express more focal adhesion sites. These alterations result in a lower migration speed as well as a shift of nuclear position. We therefore postulate that miuraenamides are a promising new tool to stabilize actin polymerization and study cellular behavior such as migration.

KEYWORDS

actin, migration, miuraenamide, nucleus, adhesion

Introduction

Actin is one of the most preserved proteins in eukaryotic cells and is therefore involved in many cellular functions like cell division, migration, signaling and adhesion (Thomas and John, 2009). This variety of tasks illustrates its importance within living cells. Therefore, researchers are interested in understanding its role and its relevance by altering its properties and investigating the corresponding cellular behavior. To alter actin properties, actin binding compounds like phalloidin, latrunculin and jasplakinolide have been used (Figure 1). While actin depolymerizing compounds such as latrunculin have been part on many studies on the actin network, studying the effects of stabilized filaments remains challenging. The two most prominent compounds to stabilize actin filaments were phalloidin and jasplakinolide, both carrying major disadvantages: Phalloidin is not able to pass the cell membrane (Risinger and Du, 2020) which limits its use to fixed cells and the effect of jasplakinolide heavily relies on the used concentration and time scales (Ou et al., 2002). To bypass these disadvantages, we decided to use the alternative natural compound miuraenamide A (MiuA), which was isolated in 2006 from slightly halophilic marine myxobacterium (Iizuka et al., 2006). The structural relationship to jasplakinolide forced us to develop a total synthesis of MiuA (Wang et al., 2019) as well as other derivatives (Moser et al., 2017; Gegenfurtner et al., 2018) for structure-activity studies. By the synthetic protocols developed, miuraenamides are accessible on the gram scale for

biological studies, e. g., regarding their possible binding mode (Wang et al., 2019), their effect on cell migration under chemotaxis (Moser et al., 2017) and their regulatory effects on gene expression (Gegenfurtner et al., 2018). Modifications to the structure of MiuA have also been shown to reverse the stabilizing properties of MiuA into a destabilizing compound (Wang et al., 2021), increasing its versatility.

In this study, we show the quantitative effects which MiuA has on the dynamics of actin filaments, as well as on the length of actin filaments in living cells. We additionally observed that treated cells occupied a larger area when allowed to freely spread and that their number of focal adhesions increased. We further found that MiuA treatment led to repositioning of the nucleus towards the cell center during migration and that cell migration speed decreased.

Material and methods

UV-patterning

We used two different types of patterns: “crossbow” patterns, that forced single cells to transform into a polarized shape and straight lines with a thickness of 10 μm to observe migration in 1D. For the production of the micropatterns, PEG-coated glass cover slips were placed on a photomask and illuminated with UV light according to the protocol of Azioune et al. (2010). We activated the photomask for 5 min before placing any glass objects on it and afterward put it back in for another 6 min. A fibronectin (concentration 25 $\mu\text{g}/\text{ml}$) solution (purchased from Thermo Fisher) was used to fill the holes among the PEG layer to create adhesive islands. For this procedure, the UV treated glass cover slips were placed upside down on a fibronectin droplet and kept either at room temperature for 1 h or placed in a sealed box inside a refrigerator (+ 4°C) overnight.

Cell culture

RPE-1 cells transfected with LifeAct mCherry [as described by Maiuri et al. (2015)] and mouse embryonic fibroblasts (MEFs) were cultured at 37.5°C and 5% CO₂ in Dulbecco’s Modified Eagle Medium Nutrient Mix F12 with 10% FBS, 1% GlutaMax and 1% Streptomycin + Penicillin (ThermoFisher). The RPE-1 cells were kindly given by the lab of Matthieu Piel, Institut Curie, Paris. The MEFs were kindly given by Dr. Jennifer Kasper, Leibniz Institut für neue Materialien, Saarbrücken.

Miuraenamide A treatment

Miuraenamide A used in this study was obtained by total synthesis as reported previously (Karmann et al., 2015). It was

given to cells 1 h prior to life cell imaging or fixation with PFA. Concentrations of MiuA were chosen to be 20 nM in each experiment. For this, MiuA has been added to the cell culture medium (DMEM/F12) which was given to cells and incubated for the duration of the experiments.

Fixation of cells

Cell medium was removed, and cells were washed with PBS before adding a 4% PFA solution for 10 min. After that PFA was removed and samples were washed in PBS for 5 more minutes 3 times. Samples were then mounted with Fluoromount G + DAPI (Thermo Fisher) on a microscope slide, sealed with nail polish and stored at +4°C, protected from light.

Paxillin staining

For visualization of focal adhesions, we took samples (RPE-1 LifeAct-mCherry) after the fixation with 4% PFA and dissolved the cell membrane. For this we used a 0.1% solution of TritonX-100 and put cells in it for 10 min. After three times washing with PBS we added a 3% BSA solution to them to block on specific binding for at least 1 h. A 1:1000 solution of paxillin antibodies (ThermoFisher, catalog nb. PA-34910) and 3%BSA was then added to the cells for another hour prior to washing with PBS and mounting the samples with Fluoromount G + Dapi on a microscope slide.

Fluorescence microscopy

Fixed cells were imaged with a ZEISS Axio observer using a $\times 63$ magnification oil objective. Life cell imaging was performed with a Nikon Eclipse Ti microscope using a $\times 10$ magnification objective. Inside the microscope incubation chamber the temperature was set to 37°C and the CO₂ concentration was set to 5%. The whole setup was allowed to stabilize at this temperature and CO₂ concentration 1 h prior to the start of the experiments. Cell migration was observed by treating RPE-1 LifeAct mCherry cells with 250 ng/ml of Hoechst for 30 min before beginning the experiments and then taking pictures of them every 5 min.

Actin staining for FRAP measurements and FRAP measurements

Dynamics of the actin network were measured by fluorescence recovery after photobleaching (FRAP) using a Zeiss LSM880 microscope. RPE-1 wild type cells were treated with BacMam2.0 (Thermo Fisher) at least 2 days before the experiment.

The amount of BacMam used was set to 60 μL per 100,000 cells. Samples were placed in a glass bottom dish and were allowed to spread for at least 3 h before starting the FRAP measurements. Light with a wavelength of 405 nm was used to achieve the bleaching effects on single actin filaments. The parameters for the experiment were acquired using the protocol by Fritzsche and Charras (2015). Fluorescence intensity in areas of bleaching events was measured by the microscope software itself. A second and third ROI were set to measure the overall bleaching effect on the cell and the background signal. Final graphical presentation and statistical tests were performed using a home written Python3 script.

MTT-assay

5,000 RPE-1 cells were placed inside several wells of a 96 well plate and the following five different conditions were chosen for testing:

- 1 μL DMSO per 1 ml medium, as (negative) control MiuA (20 nM, 40 nM and 60 nM)
- 10 $\mu\text{g}/\text{mg}$ mitomycin, as (positive) control

Cells were allowed to proliferate for 48 h under their respective conditions before the medium was removed and the cells were rinsed with PBS. MTT solvent at a concentration of 0.5 $\mu\text{g}/\text{ml}$ (in cell culture medium) was added to the cells, before placing them in an incubator (37°C, 5% CO_2) for 1 h. After the MTT solution was removed and the purple crystals that formed were dissolved in 100 μL of DMSO. To achieve a homogeneous dissolution, we placed the 96-well plate on a beacon shaker for at least 30 min. The light absorption, correlating with the number of cells inside each plate was then measured using a Tecan infinite 200 Pro, which automatically measures the absorbance coefficient in each well and provides xlsx files with the collected data. The machine was set to “multi-measurement” mode, meaning that nine distinct spots inside each well were measured and an average value for the absorbance coefficient was formed for each of them. The wavelength was set to 570 nm.

Image analysis

All images were analyzed with Fiji (ImageJ) (Schindelin et al., 2012). Length of actin filaments was measured by hand using Fiji’s “line” tool. Time-lapse images of migrating cells were analyzed using the plug in “TrackMate” (Tinevez et al., 2017; Ershov et al., 2021). Nuclear distances were defined as the length between the back of the cell and the center of the nucleus divided by the total length of the cell. The number and size of focal adhesions were determined by paxillin staining. Paxillin signal was put under a threshold and then analyzed with Fiji’s build-in function “Analyze particles”, giving us the number and sizes of

focal adhesions in those cells. All data were saved as csv. files and used for further analysis. Kymographs were performed using Fiji’s “Kymograph” tool.

Statistical testing

Student’s t test were conducted on all experimental data and Pearson R values were calculated using a home build Python3 script. *p*-values were calculated and assigned as follows:

- $p > 0.05$: no significance (n.s.)
- $p < 0.05$: *
- $p < 0.01$: **
- $p < 0.001$: ***

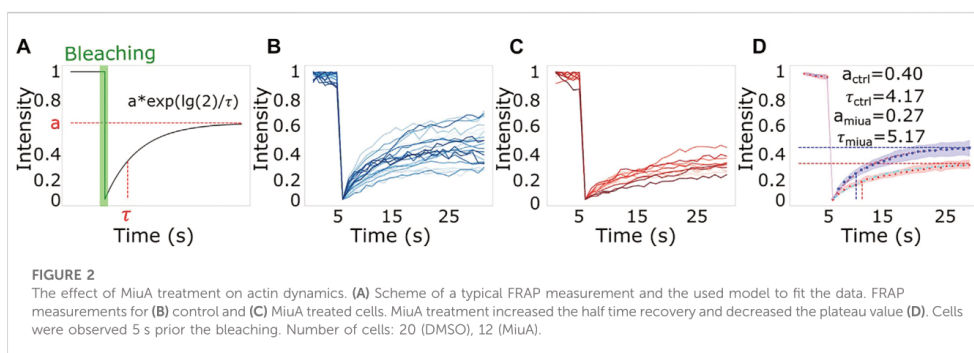
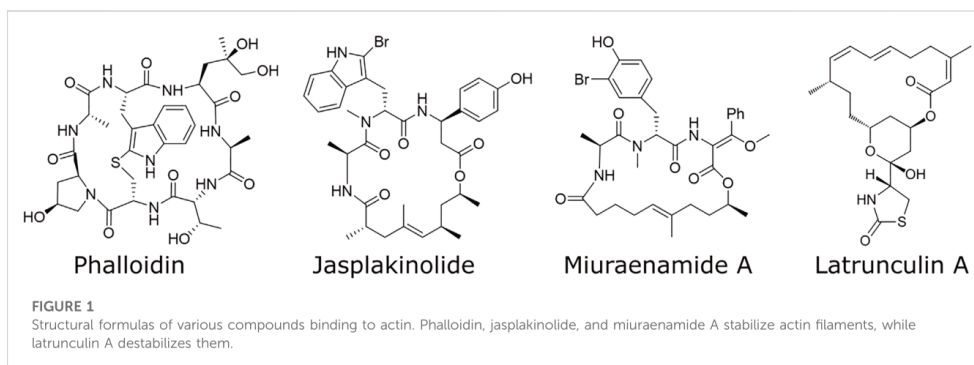
Results

MTT assay

To confirm that a concentration of 20 nM MiuA is suitable for our experiments, we conducted a MTT assay on RPE-1 cells (Supplementary Figure S1). There we could see that cells treated with 20 nM of MiuA proliferated similar to the control group, while those treated with 40 nM MiuA showed the same behavior as the positive control group, treated with mitomycin C. When we increased the concentration further to 60 nM MiuA, we observed that the number of cells was even lower than that in our positive control group. Taking this into account, we decided to use 20 nM MiuA for all our experiments in this study.

Actin dynamics

To determine whether treatment with MiuA affected on the dynamics of actin filaments, we performed fluorescent recovery after photobleaching (FRAP) measurements. For this purpose, we bleached actin fibers in RPE-1 cells transfected with BacMan2.0 and measured the time evolution of the fluorescence intensity. We used BacMam staining as it stains G-actin and thus allows us to observe the network dynamics. Using a model for the recovery of the fluorescence intensity proposed by Fritzsche and Charras, (2015) we found that both the plateau level and the recovery time were altered in cells treated with MiuA. An alteration of the plateau level indicates a lower fraction of restored fluorescence and an alteration of the recovery time indicates a changing rate of exchanging actin monomers. Since upon treatment with MiuA, the plateau level decreased and the half-time recovery time increased (Figure 2), we concluded that MiuA treatment slows actin dynamics.

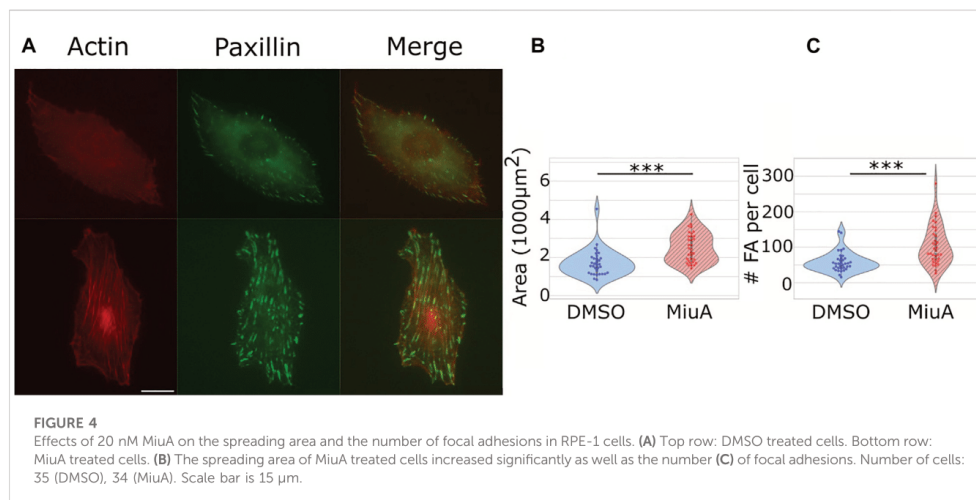
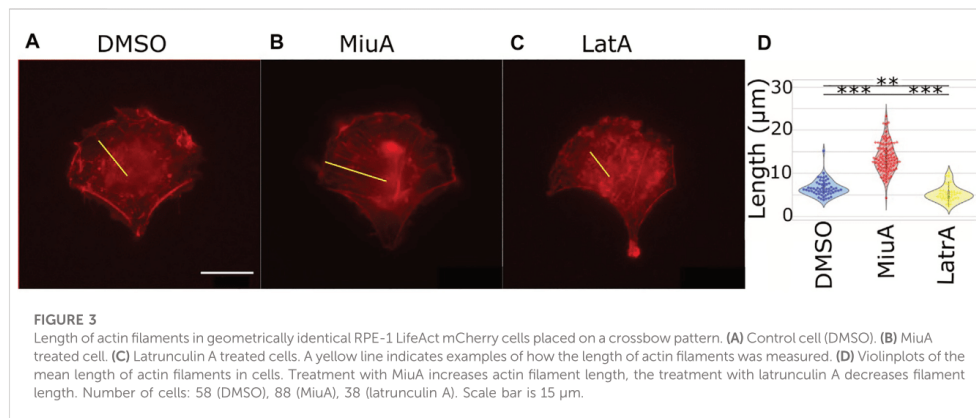


Length of actin filaments

Because actin filament dynamics might influence the length of actin filaments, we next wanted to compare actin filament length depending on MiuA. Therefore, we first aimed to obtain geometrically identical cells so that we could compare similar structures (Théry, 2010). We placed RPE-1 cells that express LifeAct mCherry as a fluorescent dye on crossbow micropatterns (Figure 3). Once cells had a similar shape, compared the length of actin filaments in cells treated with 20 nM MiuA with the length of actin filaments in untreated cells. This concentration was chosen from the literature and was used throughout the study (Moser et al., 2017). Additionally, we used latrunculin A to destabilize the actin network as a negative control group. We manually analyzed the actin filament length using ImageJ. MiuA treatment resulted in a mean length of 13.57 μm compared to 6.26 μm in untreated cells and 4.89 μm in cells exposed to latrunculin A. Taken together, we can conclude that the length of actin filaments in MiuA treated cells increased significantly.

Number of focal adhesions and spreading area

We placed cells on micropatterns to compare cells which all had the same shape in order to compare the length of similar actin filaments. However, micropatterns are a rather artificial approach, which is helpful for understanding particular parameters, but is difficult to relate to the *in vivo* situation. Therefore, we next compared the adhesion of cells on 2D fibronectin coated glass surfaces. We quantified the number of focal adhesions in RPE-1 cells treated with MiuA: We stained for paxillin (Figure 4A), a protein involved in the formation of focal adhesions and counted the focal adhesions using ImageJ. Interestingly, the mean number of focal adhesions in MiuA treated cells increased from 57.829 in control cells to 103.235 in MiuA treated cells, resulting in an overall increase by a factor of 1.7 (Figure 4C). Following the number of focal adhesions, we also measured the spreading area of fully adhered cells. Consistent with the increased number of focal adhesions, MiuA treated cells occupied a significantly larger area

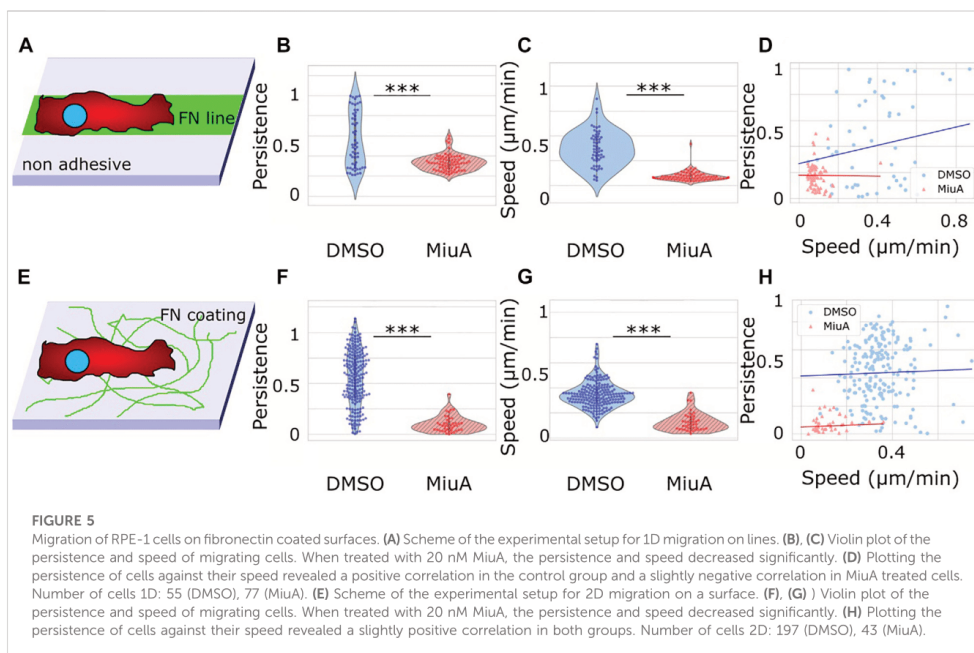


than control cells. The spreading area increased by a factor of 1.5 from 1,693.06 μm^2 in untreated cells to 2,605.78 μm^2 in MiuA treated cells (Figure 4B).

Migration behavior and position of nuclei

To understand how elongated actin filaments, a higher number of focal adhesions and larger spreading areas affect the migration behavior of RPE-1 cells, we placed cells on fibronectin lines of 10 μm width as well as on a fibronectin coated glass surface and recorded their migration behavior (Figure 5). RPE-1 cells were chosen for

their mesenchymal migration properties and their use in other migration studies (Maiuri et al., 2015; Terriac et al., 2019). We tracked cellular movements by staining the nuclei with Hoechst and taking pictures every 5 min. We analyzed the resulting trajectories using the ImageJ plug in TrackMate. Upon treatment with MiuA, cellular movement in 1D decreased significantly from 0.372 $\mu\text{m}/\text{min}$ in the control case to 0.09 $\mu\text{m}/\text{min}$ in the MiuA treated cells (Figure 5C) as well as the persistence of cellular movement, which decreased from 0.442 in untreated cells to 0.168 in cells exposed to MiuA (Figure 5B). Kymographs of those cells also showed a reduction in membrane activity during migration (Supplementary Figure S2). The same effect occurred in cells



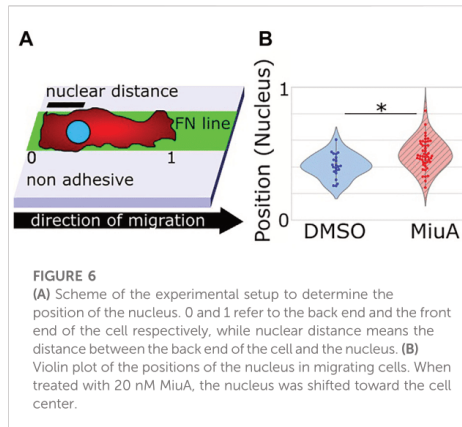
migrating on a fibronectin coated glass surface. Their speed and persistence decreased after treatment with MiuA from 0.346 $\mu\text{m}/\text{min}$ to 0.124 $\mu\text{m}/\text{min}$ and from 0.444 to 0.079, respectively (Figures 5F,G). We also calculated the Pearson R correlation value between the speed and the persistence of migrating cells (Figures 5D,H), revealing an R value of 0.35 for untreated cells and -0.01 for MiuA treated cells in 1D. In the 2D case the R value stayed the same for both conditions at 0.06.

We also performed a 2D migration experiment using MEFs and observed the same effects (Supplementary Figure S3). The mean speed and persistence of MEF cells dropped from 0.259 $\mu\text{m}/\text{min}$ and 0.311 to 0.125 $\mu\text{m}/\text{min}$ and 0.153 respectively.

Additionally, we measured the position of the nuclei in RPE-1 cells during migration on fibronectin lines. We imaged the nuclei by Hoechst staining and analyzed the position within the cell using ImageJ. Interestingly, the position of the nuclei of cells treated with MiuA significantly shifted toward the cell center (Figure 6B).

Discussion

Actin, which is omnipresent in eukaryotic cells, has various in living systems (Thomas and John, 2009). Therefore, altering aspects of actin always affects many aspects of the entire system, increasing the challenge of understanding single actions



of actin in cells such as the role of actin filament length in cell migration, proliferation etc. One way to study actin is by compounds which stabilize or destabilize actin by altering the polymerization rates. Although both types of such compounds are well known since the end of the 20th century, research has mainly focused on actin destabilizing compounds like latrunculin A or

cytochalasin D (Risinger and Du, 2020). Nevertheless, it is not sufficient to only destabilize actin, but means of stabilizing actin are needed. However, stabilizing actin filaments remains challenging, as the two most prominent compounds, phalloidin and jasplakinolide, have serious disadvantages. Phalloidin cannot pass through cell membrane, rendering it impossible to use this compound in living cells. The second compound, jasplakinolide, stabilizes actin filaments in living cells. However, this stabilizing effect relies on the concentration and the duration of treatment (Ou et al., 2002). Therefore, handling jasplakinolide is challenging and often not reproducible. In our study we used a synthetic sample of the natural compound miuraenamamide A, a secondary metabolite of a halophilic myxobacterium isolated from soil samples of the Japanese coast (Iizuka et al., 2006). This marine actin stabilizer (Ojika et al., 2008) can, similar to jasplakinolide, pass through the cell membrane and is therefore suitable for observing living cells. Due to its structural similarity to other cyclopeptideptides, MiuA also targets actin filaments (Iizuka et al., 2006; Ojika et al., 2008; Sumiya et al., 2011; Karmann et al., 2015; Ojima et al., 2016). We therefore used MiuA to test the effect of actin stabilization on the dynamic behavior of actin inside living cells. The overall dynamics of actin filaments were decreased by treatment with MiuA. We showed that the half time recovery of actin filaments in MiuA treated cells increased in FRAP measurements meaning that the dynamics of the filaments decreased. These data are supported by the results of Florian A. Gegenfurtner and colleagues showing that the diffusion of actin monomers in the cytoplasm of MiuA treated cells is reduced when compared to the control group (Gegenfurtner et al., 2018). Following the change in actin dynamics due to MiuA, we wanted to see how the architecture of actin filaments in living cells might be affected. In 2019, Shuaijun Wang and colleagues showed that actin filaments *in vitro* exposed to MiuA increased their elongation rate and overall length, as well as the number of filaments (Wang et al., 2019). This finding matches our observations in living RPE-1 cells, where treatment with MiuA induces longer actin filaments. Because these data were taken on micropatterns, we then moved to RPE-1 cells on 2D and compared their adhesion capacity regarding number of focal adhesions and spreading area. Christina Moser et al. observed no significant change in the spreading area of HUVECs treated with MiuA after 90 min of spreading time (Moser et al., 2017). This finding is in contrast to our study, where we found that RPE-1 cells exposed to MiuA occupy a larger area than the control group. One explanation for such differences might be the different time scales used in our experiments. As we seeded the cells on fibronectin coated glass surfaces, we allowed the cells to fully adhere for at least 4 h. We then treated them with MiuA for 1 h prior to fixing the cells with 4% PFA. The longer adhesion time might explain the significant difference in the spreading area of MiuA treated cells compared to the work of Moser et al. We also counted the number of focal adhesions per cell and found a significantly increased number. Nevertheless, the interplay

between the spreading area and the number of focal adhesions remains open for further studies. Adhesion and actin are directly linked to migration. One study using MiuA investigated 2D chemotaxis in HUVECs treated with MiuA and showed no change in migration speed (Moser et al., 2017; Wang et al., 2019). However, in our study, RPE-1 and MEF cells treated with MiuA showed a significant decrease in mean speed compared to the control group. This difference between both studies might be because we investigated 1D and 2D migration on fibronectin without chemotaxis. Regarding other possibilities of altering the migration of cells, Ali et al. (2021) showed that jasplakinolide affects the phosphorylation of alpha-1-syntrophin, which in turn leads to a decrease in motility. As MiuA and jasplakinolide have a similar molecular structure (Karmann et al., 2015), MiuA might also be capable of interfering with the alpha-1-syntrophin pathway. We also reproduced the correlation between speed and persistence that have been shown by Maiuri et al. (2015). Thus fast cells in 1D migrate in a more persistent manner. The treatment with MiuA, as well as the migration on 2D surfaces in general resulted in low migration speed paired with R values close to zero, meaning we could draw no conclusion about the correlation between these two values. As actin plays an active role in the positioning of the nucleus during cell migration (Thomas and John, 2009; Gardel et al., 2010; Calero-Cuenca et al., 2018), we measured the position of the nuclei in the migrating cells while being on fibronectin lines and under treatment with MiuA. Because disassembly of actin filaments is a crucial step during mesenchymal migration (Louise, 1999) and the organization of the actin network is linked to the position of cell organelles (Gardel et al., 2010) we hypothesized that the position of the nucleus during migration might also be affected by a change in the actin network. Indeed, we measured a repositioning of the nucleus toward the cell center under MiuA treatment. Our data are supported by the finding that the treatment of fibroblasts with jasplakinolide resulted in an increase in both cell body movement and in lamellipodia (Louise, 1999). As MiuA and jasplakinolide show similar effects on the actin cytoskeleton and their molecular structures are related (Karmann et al., 2015), we assume that MiuA might also affect the mechanism responsible for positioning the nucleus. However, further investigations are needed as the mechanism itself and its link to the cytoskeleton were not revealed by our study.

In this work we show that miuraenamamide A is a powerful tool to affect the dynamics and architecture of the actin cytoskeleton. Following this finding, we showed that actin filaments play a crucial role in the positioning of nuclei in migrating cells, as treatment with MiuA induced not only longer filaments but also shifted the nucleus toward the cell center. Furthermore, we could see that longer filaments lead to cells occupying a larger area and increasing their number of focal adhesions. In the future, we and others will be able to use this tool to further understand the role of actin in living cells.

Data availability statement

The raw data supporting the conclusions of this article will be made available by the authors, without undue reservation.

Author contributions

CB, FL, and DG contributed to conception and design of the study. CB performed the experiments and the analysis of data. UK provided the compound. All authors contributed to manuscript revision, read, and approved the submitted version.

Acknowledgments

We gratefully thank Dr. Jennifer Herrmann and Prof. Dr. Rolf Müller for useful follow up discussions. We further thank the DFG for financial support (CRC 1027).

References

- Ali, R., Mir, H. A., Hamid, R., Shah, R. A., Khanday, F. A., Bhat, S. S., et al. (2021). Jasplakinolide attenuates cell migration by impeding alpha-1-syntrophin protein phosphorylation in breast cancer cells. *Protein J.* 40 (2), 234–244. doi:10.1007/s10950-021-09963-y
- Azioune, A., Carpi, N., Tseng, Q., Théry, M., and Piel, M. (2010). "Chapter 8 - protein micropatterns: A direct printing protocol using deep UVs." *Methods Cell Biol.* 97, 133–146. doi:10.1016/S0091-679X(10)97008-8
- Calero-Cuenca, F. J., Janota, C. S., and Gomes, E. R. (2018). Dealing with the nucleus during cell migration. *Curr. Opin. Cell Biol.* 50, 35–41. doi:10.1016/j.cob.2018.01.014
- Ershov, D., Phan, M.-S., Pylvänäinen, J. W., Rigaud, S. U., Le Blanc, L., Charles-Orszag, A., et al. (2021). Bringing TrackMate into the era of machine-learning and deep-learning. *bioRxiv* 2021. doi:10.1101/2021.09.03.458852
- Fritzsche, M., and Charras, G. (2015). Dissecting protein reaction dynamics in living cells by fluorescence recovery after photobleaching. *Nat. Protoc.* 10 (5), 660–680. doi:10.1038/nprot.2015.042
- Gardel, M. L., Schneider, I. C., Aratyn-Schaus, Y., and Waterman, C. M. (2010). Mechanical integration of actin and adhesion dynamics in cell migration. *Annu. Rev. Cell Dev. Biol.* 26 (1), 315–333. doi:10.1146/annurev.cellbio.011209.122036
- Gegenfurtner, F. A., Zisis, T., Al Danaf, N., Schrimpf, W., Kliesmete, Z., Ziegenhain, C., et al. (2018). Transcriptional effects of actin-binding compounds: The cytoplasm sets the tone. *Cell. Mol. Life Sci.* 75 (24), 4539–4555. doi:10.1007/s00018-018-2919-4
- Iizuka, T., Fudou, R., Jojima, Y., Ogawa, S., Yamanaka, S., Inukai, Y., et al. (2006). Miuraenamides A and B, novel antimicrobial cyclic depsipeptides from a new slightly halophilic myxobacterium: Taxonomy, production, and biological properties. *J. Antibiot.* 59 (7), 385–391. doi:10.1038/ja.2006.55
- Karmann, L., Schultz, K., Herrmann, J., Müller, R., and Kazmaier, U. (2015). Total syntheses and biological evaluation of miuraenamides. *Angew. Chem. Int. Ed. Engl.* 54 (15), 4502–4507. doi:10.1002/anie.201411212
- Louise, P. C. (1999). Role of actin-filament disassembly in lamellipodium protrusion in motile cells revealed using the drug jasplakinolide. *Curr. Biol.* 9 (19), 1095–1105. doi:10.1016/S0960-9822(99)80478-3
- Maiuri, P., Rupprecht, J.-F., Wieser, S., Rupprecht, V., Bénichou, O., Carpi, N., et al. (2015). Actin flows mediate a universal coupling between cell speed and cell persistence. *Cell* 161 (2), 374–386. doi:10.1016/j.cell.2015.01.056
- Moser, C., Rüdiger, D., Förster, F., von Blume, J., Yu, P., Kuster, B., et al. (2017). Persistent inhibition of pore-based cell migration by sub-toxic doses of

Conflict of interest

The authors declare that the research was conducted in the absence of any commercial or financial relationships that could be construed as a potential conflict of interest.

Publisher's note

All claims expressed in this article are solely those of the authors and do not necessarily represent those of their affiliated organizations, or those of the publisher, the editors and the reviewers. Any product that may be evaluated in this article, or claim that may be made by its manufacturer, is not guaranteed or endorsed by the publisher.

Supplementary material

The Supplementary Material for this article can be found online at: <https://www.frontiersin.org/articles/10.3389/fcell.2022.931880/full#supplementary-material>

miuraenamides, an actin filament stabilizer. *Sci. Rep.* 7 (1), 16407. doi:10.1038/s41598-017-16759-7

Ojika, M., Inukai, Y., Kito, Y., Hirata, M., Iizuka, T., Fudou, R., et al. (2008). Miuraenamides: Antimicrobial cyclic depsipeptides isolated from a rare and slightly halophilic myxobacterium. *Chem. Asian J.* 3 (1), 126–133. doi:10.1002/asia.200700233

Ojima, D., Yasui, A., Tohyama, K., Tokuzumi, K., Torihara, E., Ito, K., et al. (2016). Total synthesis of miuraenamides A and D. *J. Org. Chem.* 81 (20), 9886–9894. doi:10.1021/acs.joc.6b02061

Ou, G. S., Chen, Z. L., and Yuan, M. (2002). Jasplakinolide reversibly disrupts actin filaments in suspension-cultured tobacco BY-2 cells. *Protoplasma* 219 (3), 168–175. doi:10.1007/s007090200018

Risinger, A. L., and Du, L. (2020). Targeting and extending the eukaryotic druggable genome with natural products: Cytoskeletal targets of natural products. *Nat. Prod. Rep.* 37 (5), 634–652. doi:10.1039/c9np00053d

Schindelin, J., Arganda-Carreras, I., Frise, E., Kaynig, V., Longair, M., Pietzsch, T., et al. (2012). Fiji: An open-source platform for biological-image analysis. *Nat. Methods* 9 (7), 676–682. doi:10.1038/nmeth.2019

Sumiya, E., Shimogawa, H., Sasaki, H., Tsutsumi, M., Yoshita, K., Ojika, M., et al. (2011). Cell-morphology profiling of a natural product library identifies bisbromoamide and miuraenamides A as actin filament stabilizers. *ACS Chem. Biol.* 6 (5), 425–431. doi:10.1021/cb1003459

Terriac, E., Schütz, S., and Lautenschläger, F. (2019). Vimentin intermediate filament rings deform the nucleus during the first steps of adhesion. *Front. Cell Dev. Biol.* 7, 106. doi:10.3389/fcell.2019.00106

Théry, M. (2010). Micropatterning as a tool to decipher cell morphogenesis and functions. *J. Cell Sci.* 123 (24), 4201–4213. doi:10.1242/jcs.075150

Thomas, D. P., and John, A. C. (2009). Actin, a central player in cell shape and movement. *Science* 326 (5957), 1208–1212. doi:10.1126/science.1175862

Tinevez, J.-Y., Perry, N., Schindelin, J., Hoopes, G. M., Reynolds, G. D., Laplantine, E., et al. (2017). TrackMate: An open and extensible platform for single-particle tracking. *Methods* 115, 80–90. doi:10.1016/j.ymeth.2016.09.016

Wang, S., Crevenna, A. H., Ugur, I., Marion, A., Antes, I., Kazmaier, U., et al. (2019). Actin stabilizing compounds show specific biological effects due to their binding mode. *Sci. Rep.* 9 (1), 9731. doi:10.1038/s41598-019-46282-w

Wang, S., Meixner, M., Yu, L., Zhuo, L., Karmann, L., Kazmaier, U., et al. (2021). Turning the actin nucleating compound miuraenamides into nucleation inhibitors. *ACS Omega* 6 (34), 22165–22172. doi:10.1021/acsomega.1c02838

7.4 Publication 4: A novel universal algorithm for filament network tracing and cytoskeleton analysis

Daniel A. D. Flormann^{1,2}, Moritz Schu¹, Emmanuel Terriac², Divyendu Thalla^{1,2},
Lucina Kainka^{1,2}, Marcus Koch², Annica K. B. Gad^{3,4}, Franziska Lautenschläger^{1,2}

¹Department of Physics, Saarland, University, Saarbruecken, Germany

² INM - Leibniz Institute for New Materials, Saarbruecken, Germany

³Department of Oncology and Metabolism, The Medical School, Weston Park Cancer, Centre, Sheffield, UK

⁴Centro de Química da Madeira, Universidade da Madeira, Funchal, Portugal

The FASEB Journal. 2021;35:e21582

<https://doi.org/10.1096/fj.202100048R>

Published: 09 April 2021

D.A.D. Flormann, M. Schu, and E. Terriac designed the study. D.A.D. Flormann and F. Lautenschläger supervised the work. M. Schu developed the algorithm. D.A.D. Flormann and M. Schu tested the algorithm. D.A.D. Flormann and M. Koch prepared the samples and provided the electron microscopy images, which were obtained at the Leibniz Institute for New Materials (INM), Saarbruecken, Germany. A.K.B. Gad prepared samples and provided the STORM images, which were obtained at The Wolfson Light Microscopy Facility, University of Sheffield, UK. D. Thalla prepared samples and provided fluorescent STED images of vimentin, which were obtained at the Leibniz Institute for New Materials (INM), Saarbruecken, Germany. L. Kainka prepared samples and provided confocal images of microtubules, which were obtained at the Leibniz Institute for New Materials (INM), Saarbruecken, Germany. D.A.D. Flormann prepared samples and provided Expansion microscopy images of microtubules and vimentin, which were obtained at the Leibniz Institute for New Materials (INM), Saarbruecken, Germany. D.A.D. Flormann, A.K.B. Gad, and F. Lautenschläger wrote and revised the manuscript.

A novel universal algorithm for filament network tracing and cytoskeleton analysis

Daniel A. D. Flormann^{1,2} | Moritz Schu¹ | Emmanuel Terriac² | Divyendu Thalla^{1,2} |
Lucina Kainka^{1,2} | Marcus Koch² | Annica K. B. Gad^{3,4} | Franziska Lautenschläger^{1,2}

¹Department of Physics, Saarland University, Saarbruecken, Germany

²INM - Leibniz Institute for New Materials, Saarbruecken, Germany

³Department of Oncology and Metabolism, The Medical School, Weston Park Cancer Centre, Sheffield, UK

⁴Centro de Química da Madeira, Universidade da Madeira, Funchal, Portugal

Correspondence

Daniel A. D. Flormann, Department of Physics, Saarland University, Campus D2.2, 66123 Saarbruecken, Germany.
Email: Daniel.Flormann@web.de

Funding information

Leibniz Institute for New Materials (INM); Saarland University; DFG, Grant/Award Number: CRC 1027; Fundação para a Ciência e a Tecnologia (FCT); Portuguese Government, Grant/Award Number: PEst-OE/QUI/UI0674/2013; Agência Regional para o Desenvolvimento da Investigação Tecnologia e Inovação (ARDITI); Centro de Química da Madeira, Grant/Award Number: M1420-01-0145-FEDER-000005; Universität des Saarlandes (US)

Abstract

The rapid development of advanced microscopy techniques over recent decades has significantly increased the quality of imaging and our understanding of subcellular structures, such as the organization of the filaments of the cytoskeleton using fluorescence and electron microscopy. However, these recent improvements in imaging techniques have not been matched by similar development of techniques for computational analysis of the images of filament networks that can now be obtained. Hence, for a wide range of applications, reliable computational analysis of such two-dimensional methods remains challenging. Here, we present a new algorithm for tracing of filament networks. This software can extract many important parameters from grayscale images of filament networks, including the mesh hole size, and filament length and connectivity (also known as Coordination Number). In addition, the method allows sub-networks to be distinguished in two-dimensional images using intensity thresholding. We show that the algorithm can be used to analyze images of cytoskeleton networks obtained using different advanced microscopy methods. We have thus developed a new improved method for computational analysis of two-dimensional images of filamentous networks that has wide applications for existing imaging techniques. The algorithm is available as open-source software.

KEYWORDS

actin, cytoskeleton, image analysis, intermediate filaments, microtubules

1 | INTRODUCTION

In recent decades, investigation of the filaments of the cytoskeleton, such as actin, vimentin, and microtubules, has become increasingly important for our understanding of cellular functions.¹⁻⁴ For example, the spatial organization of

the cytoskeletal network has an important role in cell migration,^{5,6} cancer metastasis,^{7,8} and cellular mechanics.^{1,9-12} The methods used to detect and image these structures vary from low-resolution fluorescence imaging, through high-resolution fluorescence imaging, to electron microscopy.^{3,6,13-16} The resolution of conventional light microscopy allows imaging

Abbreviations: FiNTA, filament network tracing algorithm; FM, fluorescence microscopy; SEM, scanning electron microscopy; STED, stimulated emission depletion; STORM, stochastic optical reconstruction microscopy.

Daniel A. D. Flormann and Moritz Schu contributed equally to this study.

[Correction added on June 11, 2022, after first online publication: Projekt DEAL funding statement has been added.]

This is an open access article under the terms of the Creative Commons Attribution-NonCommercial-NoDerivs License, which permits use and distribution in any medium, provided the original work is properly cited, the use is non-commercial and no modifications or adaptations are made.

© 2021 The Authors. *The FASEB Journal* published by Wiley Periodicals LLC on behalf of Federation of American Societies for Experimental Biology.

down to 200 nm, and super-resolution microscopy can now detect features with a resolution down to around 20 nm. However, for the full structural networks, the resolution down to the atomic scale of electron microscopy is required.

The structures in these images can then be analyzed computationally, and the most commonly used method to investigate networks of grayscale imaging techniques are based on segmentation or pixel-based center lines, such as with ImageJ plugins; for example, DiameterJ and NeuronJ.^{17,18} These methods are user friendly and have well-defined and convenient output parameters. However, as the user has to define either the ‘best segmented image’ prior to the analysis or draw the starting and end points of each filament by hand, these methods rely upon the subjective analysis of the user. This thus reduces the reliability and reproducibility of these methods. More reliable analysis can be provided by vectorial-based algorithms that allow batch processing of grayscale network images.^{2,19} However, a limitation of this method is that the output parameters are commonly dedicated to a specific interest, and can therefore be limited.

To facilitate our ongoing analyses of scanning electron microscopy images of actin microfilament networks in cells, we have developed an algorithm that can analyze a wide range of filamentous networks that are imaged using different techniques, such as fluorescence microscopy, electron microscopy, and commercial photography techniques. We have named this algorithm the filament network-tracing algorithm (FiNTA). To the best of our knowledge, the FiNTA analyses more parameters than other computational tools designed for network analysis. These parameters include the filament length, the connectivity (also known as the coordination number, and the persistence length in combination with the angle distribution). Thus, this algorithm can be used to analyze any kind of network in grayscale two-dimensional (2D) images.

2 | MATERIALS AND METHODS

2.1 | Vectorial filament network-tracing algorithm

The FiNTA is based on vectorial tracing of grayscale images. The tracing data generated by FiNTA consist of connected nodes which travel along the filaments. Since neither the node positions nor their connection lengths need to be constrained to the discrete positions of pixels, we call FiNTA “vectorial.” Therefore, although binary images can be analyzed, there is no need to create binary images or pixel-based center lines prior to an analysis. To recognize the filaments in grayscale images, the FiNTA first identifies the directions of the filaments using image convolution with the Hessian matrix of the Gaussian kernels; thus, by validation of every pixel in terms of their intensities.²⁰ This is followed by the generation and connection

of nodes along the filaments, which results in the tracing lines (Figure 1A). Since this procedure differs from segmentation or pixel-based center lines, we compared the tracing results of FiNTA with DiameterJ and NeuronJ, respectively (Figure S1). It is possible to manually adjust the sensitivity of the method to any grayscale image by changing the input parameters, as described in Supporting Information (Table S1). For a more detailed description of the working principles and the mechanisms behind the algorithm, please see Supporting Information. The FiNTA identifies the filaments in a suitable time range; depending on the network complexity, the time range can be from seconds to minutes. It then automatically extracts the important network parameters. The algorithm is available on: <https://github.com/SRaent/FiNTA>.

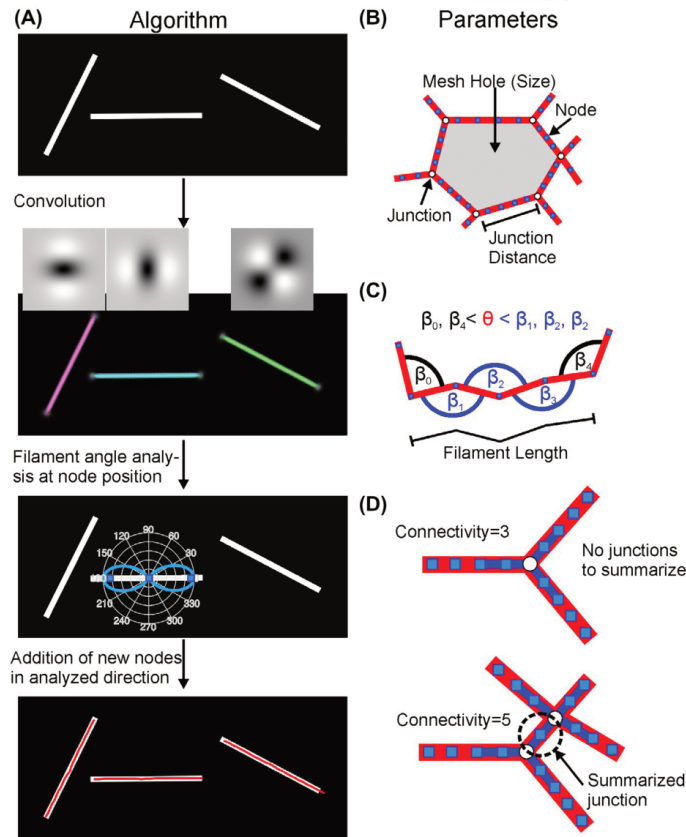
2.2 | Extracted parameters

The FiNTA provides information on at least eight of the most relevant parameters, which are: mesh hole size; circularity of each mesh hole; junction distance; filament density, filament length, connectivity of each unified junction, global angle distribution, and the persistence length.

The mesh hole size (MHS) is the measure of the network pore size, pore area, or hole size, or similar, and this is defined as the area of the pores or holes within the network (Figure 1B). The circularity is defined as $C_i = 4\pi (MHS) / P^2$, where P is the perimeter of a mesh hole. Consequently, the circularity is a measure of the fractal dimension of the mesh holes. The filament density is the total network length divided by the total mesh hole area. Furthermore, the junction distance as the length of a filament between two junctions (Figure 1B). The filament length is the distance between nodes before reaching a defined break-off angle θ within two adjacent connections (Figure 1C). The number of filaments that are connected to a junction is described with the term connectivity, which in three-dimensional (3D) data analysis is often referred to as the coordination number. As a value of two represents a single filament, the minimum value of the connectivity is three, while the maximum value is unlimited. For instance, in actin networks, the connectivity rarely exceeds six, and these filaments typically have a mean connectivity of around 3.4. Within a user-defined unification distance FiNTA identifies junctions that are close to each other and considers them as one junction (Figure 1D). This is needed since junctions often have an expansion larger than the filament diameter, which forces FiNTA to identify two junctions instead of one for example. The global angle distribution is defined as the angles of the connections between the nodes relative to the image orientation measured counter clockwise, where the left edge of the image represents 0° , respectively. The worm-like chain model approximation is used to extract the persistence length.²¹

FIGURE 1 Graphical illustration of four parameters implemented in the filament network-tracing algorithm (FiNTA).

A, Algorithm routine to trace filaments vectorially. Starting with the original image, followed by kernels and angle analysis that leads to tracing lines finally. Filament thickness: 12 px. B, A single mesh hole with several junctions. C, The filament length (FL) calculation. The break-off angle is θ (or smaller). The break-off angle assigned to the FiNTA is $0-180^\circ$ (as for all other angles), or larger. D, Implementation of the Connectivity condense the junctions along the unification distance shown as the thick blue line. In the upper example, within two nodes (blue squares) per filament no other junction (white circle) was identified by FiNTA. In the lower example, within three nodes per filament one other junction was identified. Since the unification distance was three (nodes) in this example, FiNTA summarizes both junctions to one leading to a connectivity of 5



To demonstrate which parameters are easier to extract with the FiNTA, we analyzed three scanning electron microscopy images of structurally different actin microfilament networks in cells. These were taken over the nucleus, in the perinuclear area, and in a lamellipodium at the cell edge, as shown in Figure 2A. We thereby determined the density and structure of the actin microfilament network, and how it differed between the different subcellular regions, according to 18 different parameters (Figure 2B). This broad parameter space leads to a high flexibility of FiNTA compared to other algorithms. Therefore, extracted parameters that are identical to DiameterJ or NeuronJ are presented in Supporting Information (Table S2).

2.3 | Biological sample preparations and imaging

The preparation of the biological samples and the imaging details are in the Supporting Information.

3 | RESULTS

3.1 | Filament density, filament angles, and mesh hole size

The filament density is commonly calculated by determining the length of the total traced network, and dividing by the image size. To quantify the quality of this analysis, a realistic range of values of filament packing/densities were tracked that were within an acceptable error (10% SD). An orthogonal grid of white filaments on a black background was digitally created. In this network, the number of filaments was then increased, from a filament density of 26% white and 74% black pixels, to 92% white and 8% black pixels, as shown in Figure 3A-D. The sizes and counts of the mesh holes in these images were then analyzed using the FiNTA, which were compared to the known sizes and counts of the designed mesh holes. The results with the FiNTA were similar to the known mesh hole sizes and counts (Figure 3E,F). This indicated that the FiNTA provided an accurate description of

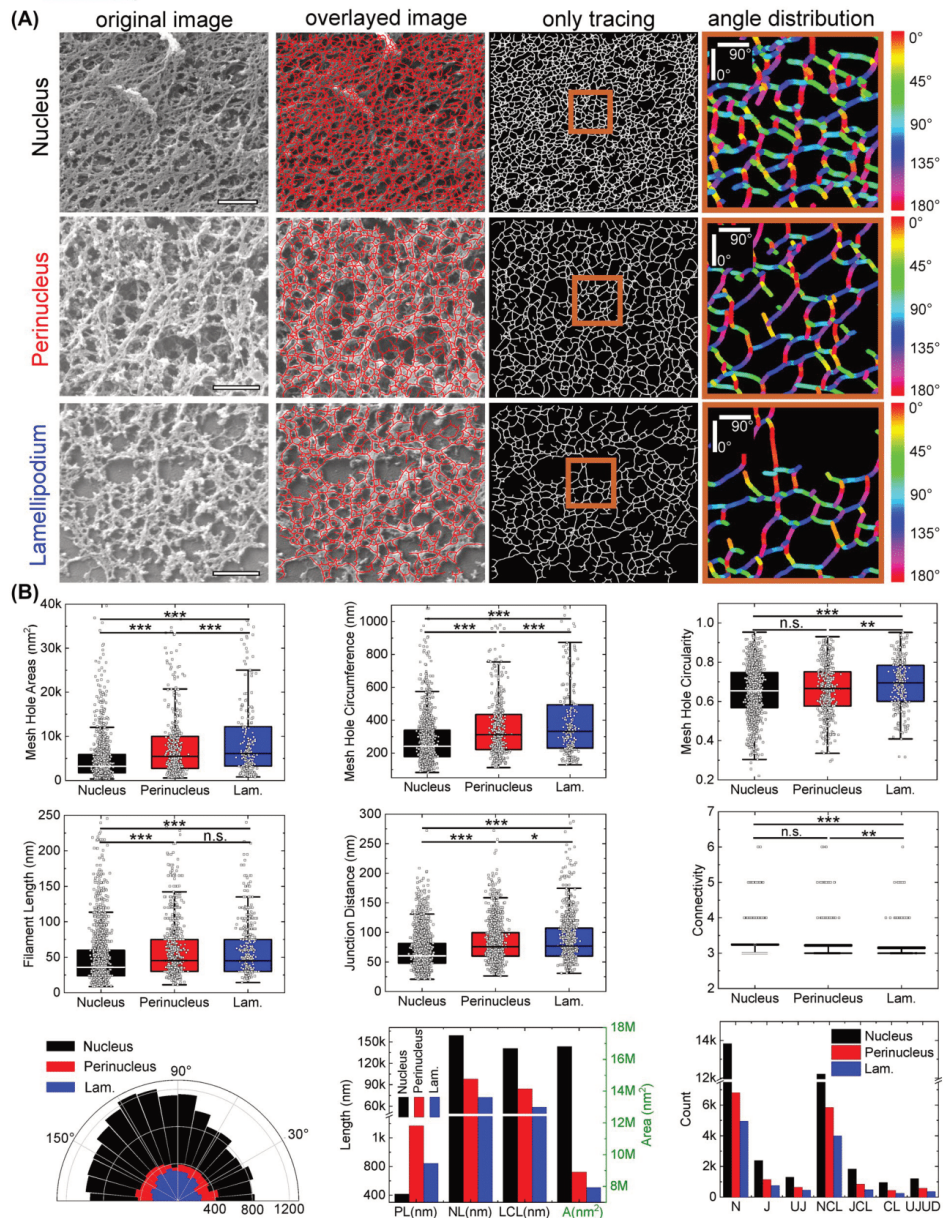


FIGURE 2 Scanning electron microscopy examples and parameters. A, Representative actin images showing the tracing and angle distributions of three different cell regions of RPE1 cells. Scale bars and edge length of angle distribution images: 500 nm. B, Quantification of 18 parameters extracted by the FiNTA. Lam., lamellipodium; PL, persistence length; NL, total network length (to calculate, eg, fiber density LCL, total network length of closed loops; A, total area of all loops; N, total number of nodes; J, total number of Junctions; UJ, total number of united junctions upon user defined unification distance used to calculate the connectivity; NCL, total number of nodes that contribute to closed loops; JCL, total number of Junctions that contribute to closed loops; CL, total number of closed loops; and UJUD, total number of united junctions of the network that only contain closed loops with the user-defined unification distance

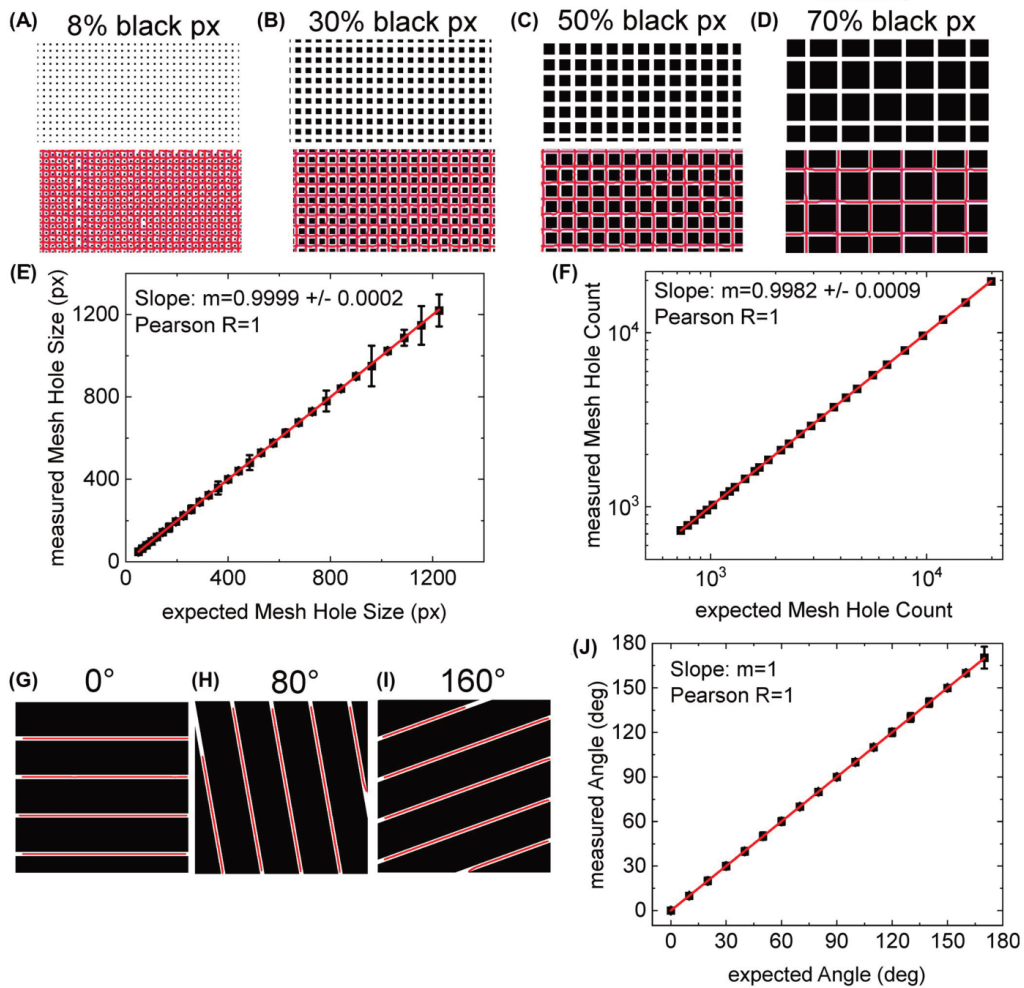


FIGURE 3 Fiber density and orientation quality tests. A-D, Cropped regions of exemplary images with increasing black pixel fractions (decreasing filament density), with tracing results in the bottom half. Line thickness: 6 px. E, F, Linear approximations of expected vs measured mesh hole size (E) and mesh hole count (F). G-I, Exemplary images of different global filament angles with a line thickness of 27 px, that lead to accurate tracing lines. J, Linear approximation of expected vs measured angles

these porous and dense networks, with detection of up to 92% of the filaments.

To quantify the accuracy of the FiNTA analysis of the global filament angles, 18 images were created with filament angles from 0° to 170° , in 10° increments (Figure 3G-I). The following FiNTA analysis of the filaments angles was very similar to the expected values, with a Pearson's correlation $R = 1$ (Figure 3J). This indicated that the FiNTA provided an accurate analysis of the global filament angles.

3.2 | Image resolution and noise level

Image resolution and the signal-to-noise ratio govern the quality of the various imaging methods. We thus determined how these features of images influence the FiNTA tracing of networks. For this, test images were initially created with a filament density grid of 74% black. To recognize different network types, the FiNTA detection of different grid sizes was also tested by analysis of lines of six different sizes of pixels.

For the signal-to-noise ratio, six digital noise levels were added, as infinite to zero signal-to-noise ratios, and the noise levels were calculated. The tracing quality of the FiNTA was then analyzed at these different signal-to-noise ratios by comparisons of the measured to the expected mesh hole size and count with the similarities expressed as percentage errors (Figure 4). Here, the higher the resolution of the image, the more noise was acceptable, and vice versa. Therefore, the FiNTA can trace images across a wide range of image resolution, and with various noise levels.

The typical signal-to-noise ratios of fluorescence and electron microscopy images of the cellular actin cortex are in the range of 5 dB to 15 dB.

3.3 | Connectivity

The connectivity (also known as coordination number or branching number) is rarely included in algorithms for segmentation-based network analysis, and to the best of our knowledge, it has not been included in vectorial-tracing algorithms. Nonetheless, it is an essential parameter that is important to include and describe in any comprehensive analyses of networks. Therefore, the connectivity is also determined in the FiNTA.

To determine the efficiency of the connectivity measured by the FiNTA, four black and white 2D test images were artificially created where the only connectivity values were three, four, five, and six. As a connectivity of two represents a line, the minimum value of the Connectivity is three.

The connectivity measured on the original images with the FiNTA was then compared to the expected values, as shown in Figure 5A-D. These FiNTA values matched those expected (Figure 5E, F), and therefore, the FiNTA can measure all of the predominant connectivities within 2D networks.

3.4 | Filament length

In addition to the mesh hole size and connectivity, the filament length is a crucial parameter in the characterization of networks. To include this parameter in the FiNTA, a user-defined break-off angle was implemented to detect and define a filament as a single filament (see Figure 1C). This definition and implementation to FiNTA allows “one filament” to cross junctions identified by FiNTA. This is crucial since in a two dimensional image it is often not possible to differ between a physical junction and an overlay of filaments above each other. Consequently, we implemented the break-off angle in order to be not limited by the identification of junctions. Even visual inspection of network images does rarely allow the identification of the beginning or end of a filament. Therefore, the filament length calculated by FiNTA is most likely not the real filament length, but a filament length close to the one that is identified by visual inspection.

To determine the accuracy of this filament length tracing approach, the artificially created test images for the connectivity were modified to show a homogenous distribution of filament lengths by removing the filaments at the

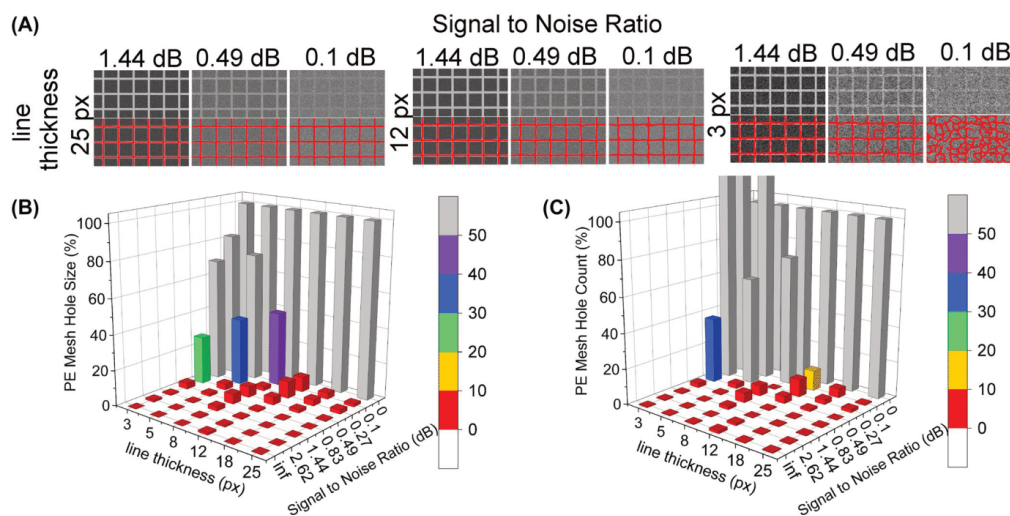


FIGURE 4 Mesh hole size by varying signal-to-noise ratio and line thickness. A, Exemplary images of traced mesh holes by varying signal-to-noise ratio and line thickness. B, Percentage errors (PE) of expected mesh hole size and count vs measured mesh hole size (B) and count (C), with dependence on signal-to-noise ratio and line thickness

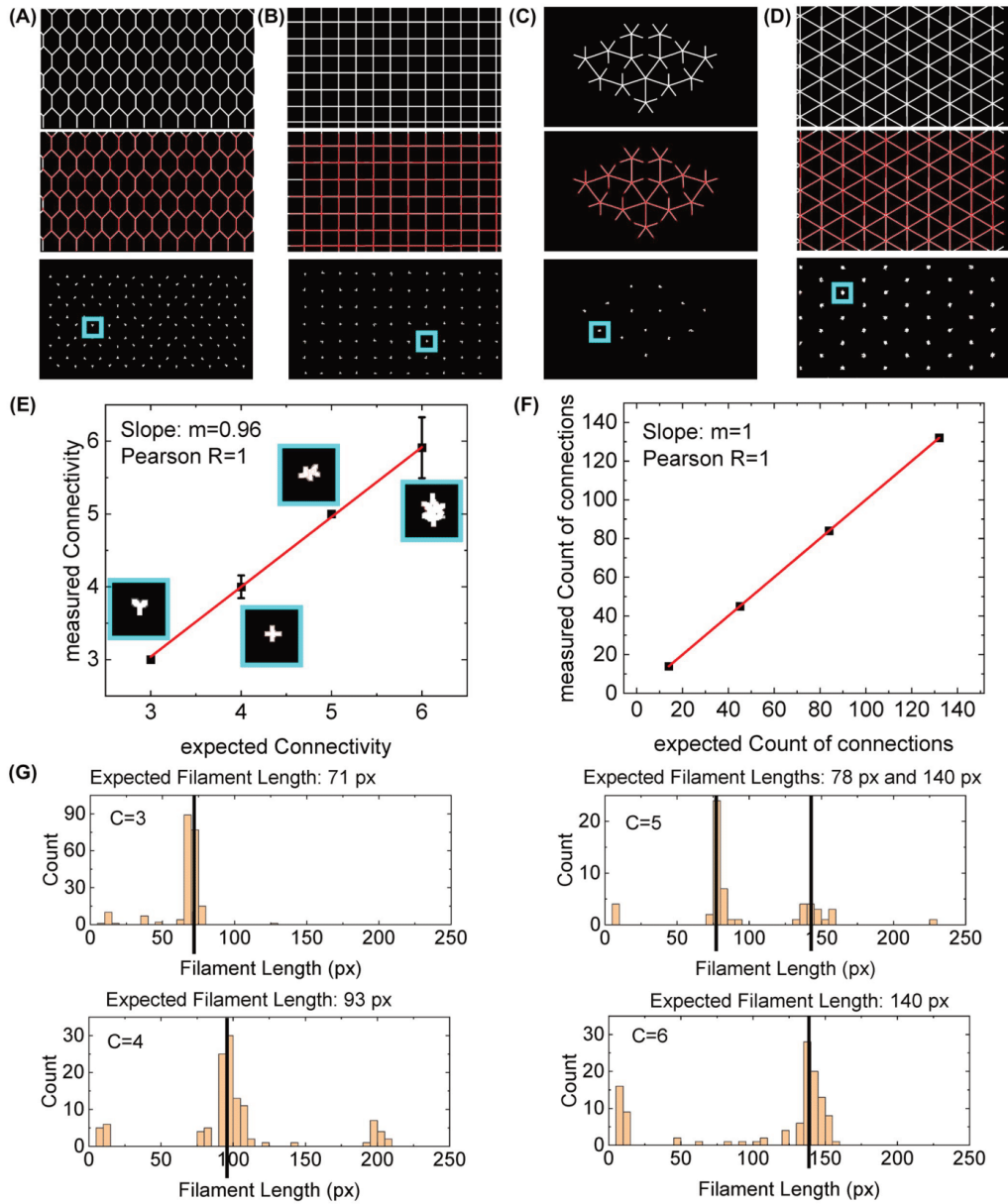


FIGURE 5 Connectivity and Filament Length tests. A-D, Exemplary images with discretely increasing connectivities as three (A), four (B), five (C), and six (D), as are traced in red (second row), and with branches/junctions extracted (third row). Junction connectivity was set to 6 (ie, all junctions that can be connected by 6 or less steps are unified to one junction). Line thickness: 9 px. E, F, Linear approximations of expected vs measured Connectivity (insets show corresponding third rows of (A-D)) (E) and counts of branches/connections (F). Red lines show the linear approximation. G, Filament length histograms of images (A-D) corresponding to the four connectivities from three to six. The break-off angle was set to $\sim 17^\circ$ (0.3 rad). Black vertical lines represent the expected filament length

edges of the images. This resulted in data with very similar filament lengths, as shown in Figure 5G for a break-off angle of $\sim 17^\circ$ (0.3 rad), where all of the filament lengths were within an accurate range of the expected lengths. However, the FiNTA also identified artificial filaments that were significantly shorter than those expected, and were localized to the branching/connection zones. Such very short filaments can be eliminated easily using a threshold value. We also performed a more detailed test of the filament lengths and their dependence on the break-off angle, as presented in Figure S2.

3.5 | Other extracted parameters

As the mesh hole size, connectivity, and filament lengths should be the most challenging parameters to implement, we mainly focused on testing these parameters in detail. Additional parameters that can be calculated based on the mesh hole size and from the tracing per se were also tested. The filament density can be calculated from the length of the total traced network divided by the image size. The junction distance (so-called fiber length in DiameterJ) was calculated forward from the known junction positions. The connectivities from the FiNTA were very accurate for both the quality and the counts, and thus the reliability of the analysis of junction distance was also accurate, as for the connectivity. The circularity is the fractal dimension of the mesh holes, and this was defined as proportional to the mesh hole size divided by the perimeter squared. The reliability of the analysis of circularity is therefore strongly depending on the mesh hole size, which was shown to be very accurate in Section 3.1.

3.6 | Tracing accuracy

The accuracy of the tracing determines the quality of all of the parameters that are extracted from any tracing software. To determine the tracing accuracy with the FiNTA, we analyzed electron microscopy images of actin filaments and a fluorescence confocal microscopy image of microtubules (Figure 6). For the quality of the analysis, the filaments traced with the FiNTA were then also traced manually in the same images. This thus determined the relative levels of false-negative and false-positive signals obtained using the FiNTA, as the relative proportions of nontraced filaments and nonexisting filaments traced, respectively.

For determination of the levels of false-negative signals, the relative lengths of nontraced filaments were calculated by dividing these by the total network length traced by hand including the nontraced filaments. For determination of the levels of false-positive signals, the proportion of false-positive filaments were defined according to the total network length traced by hand. On this basis, the FiNTA tracing for the electron microscopy images showed 8.55% false-negative filaments and 1.54% false-positive filaments. For the fluorescence image FiNTA tracing, there were 9.72% false-negative filaments, and 1.42% false-positive filaments. Therefore, the false-positive rates can be considered as negligible, and the false-negative rates are $<10\%$, which can be considered an acceptable value. The false-negative filaments arise because the FiNTA does not trace up to the edge of the image, to avoid any distortion of the mesh hole size. In the central parts of the images, almost all of the filaments that are not traced (ie, the false negatives) arise where the angle between two filaments is small.

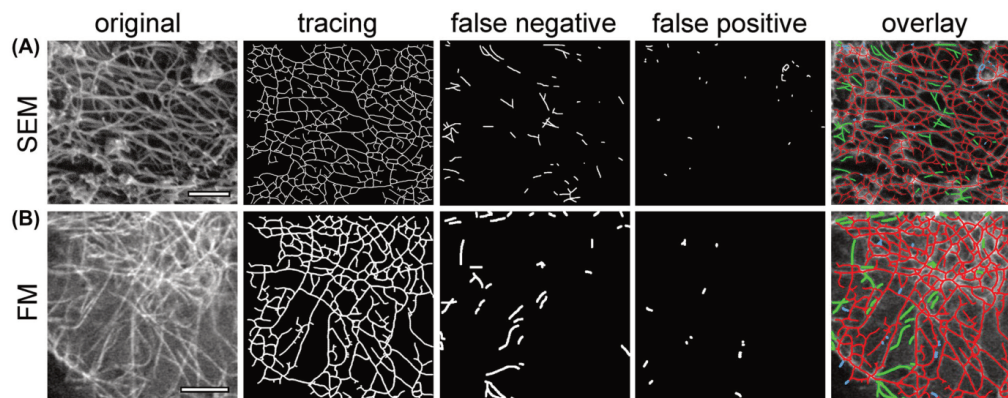


FIGURE 6 Tracing error tests. Representative images of actin filaments obtained using scanning electron microscopy (A; SEM) and of microtubules obtained using confocal fluorescence microscopy (B; FM), as traced with the FiNTA and compared to hand tracing. Nontraced fibers (false negative) and nonexisting filaments (false positive) that were traced are shown ($2\times$ fiber thickness of original tracing). Overlay of the correct tracing (red), false negatives (green), and false positives (blue) shown in the last column. Scale bars: 200 nm (A); 5 μm (B)

3.7 | Network separation

It is challenging to draw conclusions about spatial distributions in three dimensions from 2D images of 3D networks, both manually and automatically. For example, it is usually not possible to distinguish between a real junction and an overlay of two filaments. However, the FiNTA can reduce these events to a minimum. Here, this is based on the effect whereby the filaments closer to the camera (ie, at a higher level within the network) are brighter than the filaments that are further away from the camera (ie, at a lower level within the network). This is true for images from both electron microscopy and fluorescence microscopy. For this, the option was implemented to preserve traced nodes within a specified grayscale interval only, which can be chosen by the user. This approach can also be used to avoid over-exposed and under-exposed regions of a network.

To assess the quality of this approach, three different images were analyzed at high and low intensity levels (Figure 7). For electron microscopy images of actin networks, the high intensity areas, referred to as ruffles, provide no information about the network due to their overexposure. It might therefore be of interest to exclude these high intensity regions from the tracing, which is what the FiNTA does (Figure 7A).

To determine the quality of the FiNTA for other types of networks, an electron microscopy image of the hexagonal structure of a diatom alga was analyzed. The thresholding of the intensity values allowed the FiNTA to discern the hexagonal structures from the underlying network (Figure 7B). Furthermore, in fluorescence images of actin, the FiNTA can differentiate between high intensities (more fluorescein proteins) and low intensities (less fluorescein proteins) (Figure 7C). This allows the user to focus on the subcellular regions of a network, which can be useful if the user is interested in subregions, or parts of the intensity distribution within an image. Therefore, such intensity thresholding is a powerful method to separate networks for their detailed investigation.

3.8 | Tracing of cytoskeletal networks imaged by electron and fluorescence microscopy

To demonstrate the wide range of FiNTA applications, images of different cytoskeletal filaments were traced that were obtained by electron microscopy (Figure 2) and using different variants of fluorescence microscopy (Figure 8).

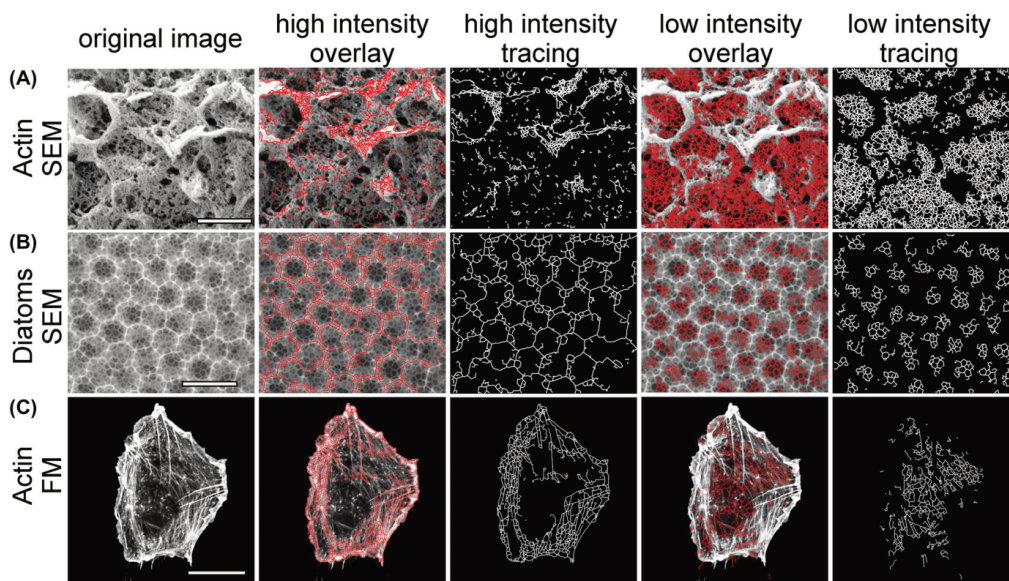


FIGURE 7 Network separation by intensity thresholding. Representative images for scanning electron microscopy (SEM) of actin (A) and a diatom (B) and fluorescence microscopy (FM) of actin (C), used to separate the networks by intensity. A, B, As used to eliminate unwanted areas (A, actin: high intensity) and analyze the remaining network (low intensity), or to separate a superior (B, diatom, high intensity) and an inferior (low intensity) network. C, As used to separate between high and low intensity signals that represent high and low amounts of fluorescent actin molecules. Scale bars: 1 μm (A), 4 μm (B), 20 μm (C)

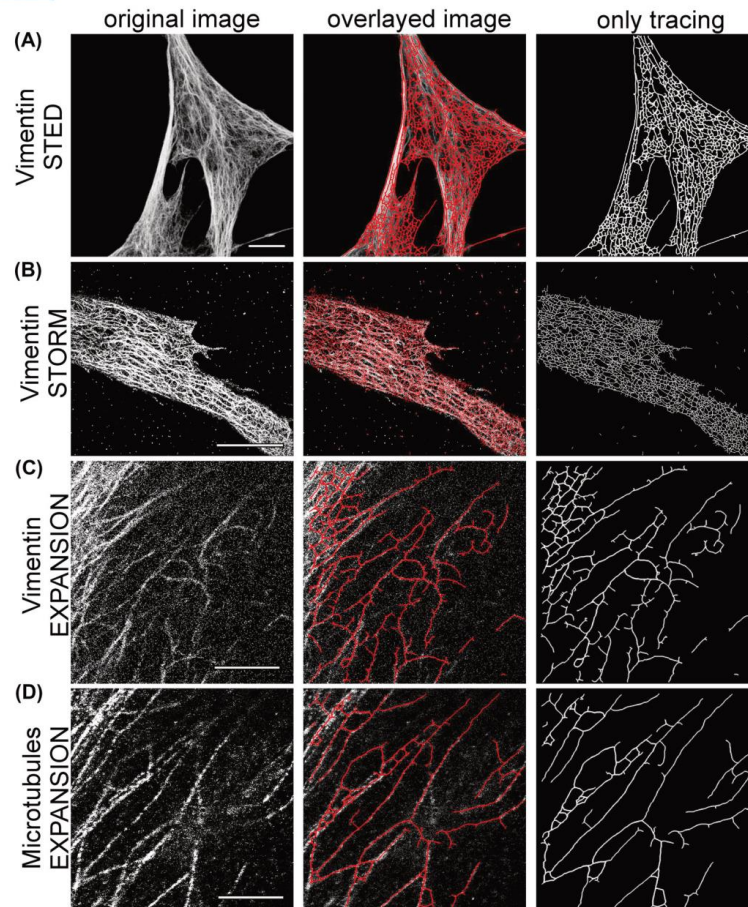


FIGURE 8 Representative images and exemplary traced fluorescence super-resolution networks. Vimentin was imaged and traced (as indicated) using stimulated emission depletion (STED) microscopy (A), 3D stochastic optical reconstruction microscopy (STORM) (B) and Expansion microscopy (C). D, Identical image section of cell vimentin in (C) is shown for microtubules in (D). Overlayed image: overlay of original and traced images. Scale bars: 10 μm (A, B) (expansion factor, 4.5); 2.38 μm (C, D)

We showed in Section 3.7 that the FiNTA can be used to analyze actin microfilament cytoskeletal networks imaged by confocal microscopy (Figure 7C). However, the resolution of confocal microscopy is often not sufficient to determine the fine structure of cytoskeletal networks, as more recently, super-resolution techniques are being increasingly used. To provide a useful tool for such studies, the reliability of the FiNTA was analyzed using images from super-resolution microscopy. Images of the intermediate filament protein vimentin were analyzed for various cell types that were provided by three distinct super-resolution microscopy techniques that are based on different approaches

and principles: stimulated emission depletion (STED) microscopy; stochastic optical reconstruction microscopy (STORM); and expansion microscopy. STED microscopy is a type of confocal microscopy where a homogenous signal along filaments is recorded. In contrast, STORM and expansion microscopy are techniques that create a pointillism-like signal along filaments. In STORM microscopy, this is achieved by the imaging technique itself, whereas in expansion microscopy, the structure under investigation is physically ruptured at the nanoscale level. These vimentin network images using each of these super-resolution techniques were indeed accurately traced by the FiNTA

(Figure 8A-C). This included the pointillism-like signals of STORM and expansion microscopy, as shown in the detailed pointillism test in Figure S3, and more indirectly in Figure 4. To further confirm this, Figure 8D shows the FiNTA tracing of a microtubule meshwork obtained using expansion microscopy. Consequently, we can conclude that the FiNTA can also correctly trace networks in images using super-resolution fluorescence imaging techniques.

As indicated in Section 2.2, the FiNTA can trace actin microfilament networks obtained using electron microscopy. To determine whether the FiNTA can also be used for electron microscopy images of other structures, we additionally investigated mushroom braid, eggshell, foam, and diatoms. With the exception of the foam, which showed high heterogeneity for the filament thickness and brightness, the FiNTA provided accurate tracing of these networks (Figure S5). Consequently, FiNTA is scale-independent and could be used for fundamentally different questions, such as cell-cell junctions (eg cell monolayers stained for E-cadherin) or even network-spanning organism (eg, *Physarum polycephalum*).

To further validate the FiNTA, other images were analyzed, including a picture of sticks of spaghetti obtained using a reflex camera, and different painted, biological, and written examples, which again resulted in consistently accurate tracing (Figure S6).

4 | DISCUSSION

In this study, we present the powerful, rapid, user-friendly, open-source vectorial FiNTA for grayscale images of different filament types and across a large variety of scales. This is shown by our analysis of the intracellular nanoscale actin microfilaments and vimentin cytoskeleton, and of other network forms using various imaging techniques.

A lot of the available software and plugins for analysis of networks require the raw data images in grayscale to be converted into binary images prior to analysis, such as the ImageJ plugin DiameterJ. The quality of the images will thereby greatly impact on the recognition of filaments by the software. With the FiNTA, grayscale images can be analyzed, which thus overcomes this problem.

The FiNTA allows analysis of the common network parameters, such as mesh hole size, circularity, junction distance, filament density, and others. Moreover, it provides a high level of quantification of challenging parameters, such as connectivity and filament length. The FiNTA can also be used to separate subnetworks in single images, through intensity thresholding. It has a high tolerance in terms of filament density and noise. Moreover, the FiNTA delivers good results regardless of the imaging technique used (eg, fluorescence microscopy, scanning electron microscopy, photographs), and of the substance investigated.

One limitation of the FiNTA relates to networks with small angles between the filaments. The FiNTA was also implemented for homogenous filament thickness. Although the FiNTA can be used where there are small variations in filament thickness, significant heterogeneity in filament thickness across a network can lead to nonideal tracing. Finally, heterogeneous intensity distributions along filaments can result in an increased false tracing by the FiNTA. In such cases, segmentation-based algorithms might provide more accurate tracing.

In summary, the FiNTA is an algorithm that can provide great benefits across a wide variety of scientific fields that involve analysis of images of networks.

ACKNOWLEDGMENT

The authors thank the Leibniz Institute for New Materials (INM), Saarland University, and the DFG (CRC 1027 (A10)) for financial support. The authors also thank the Weston Park Cancer Centre (University of Sheffield) the Fundação para a Ciência e a Tecnologia (FCT), the Portuguese Government (PEst-OE/QUI/UI0674/2013) and the Agência Regional para o Desenvolvimento da Investigação Tecnologia e Inovação (ARDITI), M1420-01-0145-FEDER-000005-Centro de Química da Madeira—CQM (Madeira 14-20). We thank Gaudenz Danuser (Texas, USA) for the hTERT-RPE1 cells stably expressing mEmerald-vimentin and mTagRFp α -tubulin, Matthieu Piel (Paris, France) for the hTERT-RPE1 cells stably expressing mCherry LifeAct, and William C. Hahn (Harvard Medical School, USA) for the BJ cell line. We thank Ana Lopez and Christa Walther, University of Sheffield, UK, for excellent technical support. We thank Guillaume Charras (London Centre of Nanotechnology, UK) for excellent ideas about the parameters extracted by the FiNTA. Universität des Saarlandes (US), Open access funding enabled and organized by Projekt DEAL

CONFLICT OF INTEREST

The authors declare that they have no conflicts of interest.

AUTHOR CONTRIBUTIONS

D.A.D. Flormann, M. Schu, and E. Terriac designed the study. D.A.D. Flormann and F. Lautenschläger supervised the work. M. Schu developed the algorithm. D.A.D. Flormann and M. Schu tested the algorithm. D.A.D. Flormann and M. Koch prepared the samples and provided the electron microscopy images, which were obtained at the Leibniz Institute for New Materials (INM), Saarbruecken, Germany. A.K.B. Gad prepared samples and provided the STORM images, which were obtained at The Wolfson Light Microscopy Facility, University of Sheffield, UK. D. Thalla prepared samples and provided fluorescent STED images of vimentin, which were obtained at the Leibniz Institute for New Materials (INM), Saarbruecken, Germany. L. Kainka prepared samples and provided confocal

images of microtubules, which were obtained at the Leibniz Institute for New Materials (INM), Saarbruecken, Germany. D.A.D. Flormann prepared samples and provided Expansion microscopy images of microtubules and vimentin, which were obtained at the Leibniz Institute for New Materials (INM), Saarbruecken, Germany. D.A.D. Flormann, A.K.B. Gad, and F. Lautenschläger wrote and revised the manuscript.

REFERENCES

- Xia S, Lim YB, Zhang Z, et al. Nanoscale architecture of the cortical actin cytoskeleton in embryonic stem cells. *Cell Rep. J.* 2019;28(5):1251-1267.e7.
- Zemel A, Rehfeldt F, Brown AE, Discher DE, Safran SA. Optimal matrix rigidity for stress fiber polarization in stem cells. *Nat Phys.* 2010;6(6):468-473.
- Bovellan M, Romeo Y, Biro M, et al. Cellular control of cortical actin nucleation. *Curr Biol.* 2014;24(14):1628-1635.
- Chugh P, Paluch EK. The actin cortex at a glance. *J Cell Sci.* 2018;131(14):jcs186254.
- Nasrollahi S, Banerjee S, Qayum B, Banerjee P, Pathak A. Nanoscale matrix topography influences microscale cell motility through adhesions, actin organization, and cell shape. *ACS Biomater Sci Engineer.* 2017;3(11):2980-2986.
- Maiuri P, Rupprecht J-F, Wieser S, et al. Actin flows mediate a universal coupling between cell speed and cell persistence. *Cell.* 2015;161(2):374-386.
- Yamaguchi H, Condeelis J. Regulation of the actin cytoskeleton in cancer cell migration and invasion. *Biochim Biophys Acta.* 2007;1773(5):642-652.
- Hall A. The cytoskeleton and cancer. *Cancer Metast Rev.* 2009;28(1-2):5-14.
- Cordes A, Witt H, Gallemí-Pérez A, et al. Prestress and area compressibility of actin cortices determine the viscoelastic response of living cells. *Phys Rev Lett.* 2020;125(6):068101.
- Hecht FM, Rheinlaender J, Schierbaum N, Goldmann WH, Fabry B, Schaffer TE. Imaging viscoelastic properties of live cells by AFM: power-law rheology on the nanoscale. *Soft Matter.* 2015;11(23):4584-4591.
- Svitkina TM. Actin cell cortex: structure and molecular organization. *Trends Cell Biol.* 2020;30(7):556-565.
- Gardel ML, Shin JH, MacKintosh FC, Mahadevan L, Matsudaira P, Weitz DA. Elastic behavior of cross-linked and bundled actin networks. *Science.* 2004;304(5675):1301-1305.
- Chugh P, Clark AG, Smith MB, et al. Actin cortex architecture regulates cell surface tension. *Nat Cell Biol.* 2017;19(6):689-697.
- Chen F, Tillberg PW, Boyden ES. Optical imaging. Expansion microscopy. *Science.* 2015;347(6221):543-548.
- Svitkina TM. Platinum replica electron microscopy: imaging the cytoskeleton globally and locally. *Int J Biochem Cell Biol.* 2017;86:37-41.
- Chikina AS, Svitkina TM, Alexandrova AY. Time-resolved ultrastructure of the cortical actin cytoskeleton in dynamic membrane blebs. *J Cell Biol.* 2019;218(2):445-454.
- Hotaling NA, Bharti K, Kriel H, Simon CG. DiameterJ: a validated open source nanofiber diameter measurement tool. *Biomaterials.* 2015;61:327-338.
- Meijering E, Jacob M, Sarria JC, Steiner P, Hirling H, Unser M. Design and validation of a tool for neurite tracing and analysis in fluorescence microscopy images. *Cytometry A.* 2004;58(2):167-176.
- Xu T, Vavylonis D, Tsai F-C, et al. SOAX: a software for quantification of 3D biopolymer networks. *Sci Rep.* 2015;5:9081.
- Su R, Sun C, Pham TD. Junction detection for linear structures based on Hessian, correlation and shape information. *Pattern Recogn.* 2012;45(10):3695-3706.
- Smith MB, Li H, Shen T, Huang X, Yusuf E, Vavylonis D. Segmentation and tracking of cytoskeletal filaments using open active contours. *Cytoskeleton.* 2010;67(11):693-705.

SUPPORTING INFORMATION

Additional Supporting Information may be found online in the Supporting Information section.

How to cite this article: Flormann DAD, Schu M, Terriac E, et al. A novel universal algorithm for filament network tracing and cytoskeleton analysis. *The FASEB Journal.* 2021;35:e21582. <https://doi.org/10.1096/fj.202100048R>

Supporting information

A novel universal algorithm for filament network tracing and cytoskeleton analysis

D.A.D. Flormann^{1,2†}, M. Schu^{1†}, E. Terriac², D. Thalla^{1,2}, L. Kainka^{1,2}, M. Koch², A.K.B. Gad^{3,4} and F. Lautenschläger^{1,2}

1. Algorithm method

1.1. Image analysis using the filament network-tracing algorithm

The aim of the filament network-tracing algorithm (FiNTA) is to trace filaments on grayscale images with increased precision and detail compared to classical segmentation-based algorithms. This was achieved by populating the images with variable numbers of starting nodes on the filaments. A circle was taken around each node. The FiNTA defines where the filaments are localized on the circle, using the second-order derivatives of the Gaussian kernel (Hessian matrix). At this location, a second node connected to the first one is set. This procedure is performed for every node, until the whole network is traced. In this way, each node can be connected to an arbitrary number of other nodes, which allows the branching of the traced network and the formation of closed loops.

1.2. Details of the tracing algorithm

Before the image convolution by the FiNTA, the image is converted into a 64-bit float image. To compute the smoothed second-order derivatives of the image brightness, the tracing algorithm works on the basis of the Hessian matrix of the Gaussian transform. The convolution with the three second-order derivatives of the Gaussian transform yields the Hessian matrix for each pixel. Using the Hessian matrix, the directional second-order derivative for any pixel and any direction can then be computed. Generally, negative second-order derivatives with large absolute values indicate the presence of a filament. This filament travels perpendicular to the direction of the directional second-order derivative. An automatic function sets several starting nodes. From these nodes, the FiNTA traces the whole network without multiple tracing of the filaments. The FiNTA is available at: <https://github.com/SRAent/FiNTA>.

1.3. Input parameters

One key feature of the FiNTA is that it is highly adaptable to a wide range and scale of images of networks. The eight input parameters create the flexibility that allows the user to adjust the FiNTA to a specific network of interest. Another advantage is that there is no need to define and potentially optimize any of the parameters choices, because the parameters are defined as in Table S1, with their suggested starting values that generally lead to correct tracing, for almost all cases investigated. Finally, the consequence of over-estimation and under-estimation of the individual parameters are also described in Table S1.

TABLE S1. Overview of the parameters assigned to the filament network-tracing algorithm (FiNTA).

Parameter	Definition	Starting value		
		Suggested	Too low	Too high
<i>conv</i>	Image smoothing and Hessian matrix is computed	Half the fiber diameter, in pixels	Multiple tracing of single fibers	Not all fibers traced
<i>smooth</i>	Smoothing of angle-dependent curvature of the fibers	0.5 radians ($0.35 < smooth < 0.8$)	Too many nodes are generated	Not enough branches, with small angles between fibers
<i>rmin</i>	Minimal distance around nodes	0 px (< half fiber diameter)	--	No tracing
<i>rmax</i>	Maximal distance around nodes	Fiber diameter in pixels	Many branches are not traced	Influence of surrounding fibers on tracing, and increased computation time
<i>rstep</i>	Distance between generated and new nodes	Half fiber diameter < <i>rstep</i> < fiber diameter, in pixels	Single fibers are traced more than ones, and increased computation time	Branches are not found, thus decreased tracing smoothness
<i>steps</i>	Number of angles for which new nodes can be generated	$100 < steps < 360$	Minor changes in tracing quality	Minor changes in tracing quality, and linear increase in computation time
<i>thresh</i>	Value above which the local maxima in the smoothed angle depending curvature are used to generate nodes	2.5	A lot of nodes in noisy areas	Less intense fibers are not found up to no tracing at all
<i>min_loop_length</i>	Minimal length of loops, expressed as number of nodes belonging to a loop	$5 < min_loop_length < 10$	Unwanted connections	Increasing number of almost closed loops

1.4. Comparison of FiNTA to DiameterJ and NeuronJ

Since DiameterJ or NeuronJ are potential and commonly used alternatives to FiNTA, we compared them to our algorithm. First, we show that FiNTA delivers a higher functionality than both ImageJ plugins in the sense of extracted parameters (derived parameters from “basic parameters” were excluded, such as the Circularity that depends on the Mesh Hole Area and the Mesh Hole Perimeter). Nonetheless, DiameterJ offers a broad range of derived parameters such as a more specific analysis of mesh

holes compared to FiNTA. Second, the workflow of FiNTA is faster than DiameterJ and NeuronJ due to batch processing ability of original images (Table S2). Third, FiNTA produces more accurate tracing results than any thresholding method implemented in DiameterJ. We demonstrate this using the “traditional thresholding”, since it delivers most accurate results for our SEM and FM images (Figure S1 A, B). Other thresholding methods, which are not implemented in DiameterJ, might lead to more accurate segmentations than “traditional thresholding”. However, all thresholding we tested led always to a more significant over- or underestimation of the real network compared to FiNTA. Nonetheless, for binarized images DiameterJ is very efficient in analyzing time, batch processing ability and functionality in terms of output parameters. Additionally, we compared FiNTA to NeuronJ. Since NeuronJ uses pixel-based center lines defined by hand (i.e. starting and end point of each filaments needs to be drawn by hand) it could be more accurate than FiNTA, depending on the accuracy of the user. However, the procedure is extremely time consuming and increases the risk of personal errors (Figure S2 C, D). We assume that network analyzing algorithms are mainly used to compare a minimum of two networks with each other in order to evaluate potential differences. FiNTA reduces personal errors since we highly recommend to use one set of input parameters for one batch of network images belonging to one specific study. In contrast, both, DiameterJ and NeuronJ require a personal decision per image or even per filament, which increases the risk of personal errors significantly compared to FiNTA.

In summary, we think DiameterJ is very useful and efficient, if binarized images are investigated. NeuronJ is efficient at the scale of single filaments compared to hand-drawing of the full fiber length. In contrast, FiNTA is independent of image binarization and personal identification of filaments with the ability for excellent tracing results and high functionality.

TABLE S2. Comparison of extracted comparable parameters and workflow between NeuronJ, DiameterJ and FiNTA.

Parameter	NeuronJ	DiameterJ	FiNTA
<i>Filament Lengths</i>	Yes	No	Yes
<i>Filament Brightness</i>	Yes	No	No
<i>Mesh Hole Area</i>	No	Yes	Yes
<i>Mesh Hole Circumference</i>	No	Yes	Yes
<i>Mesh Hole max Diameter</i>	No	Yes	Yes
<i>Mesh Hole min Diameter</i>	No	Yes	No
<i>Filament Diameter</i>	No	Yes	No
<i>Junction Distance</i>	No	Yes	Yes
<i>Absolute Angle Distribution</i>	No	Yes	Yes
<i>Junction Connectivity</i>	No	No	Yes
<i>Persistence Length</i>	No	No	Yes
Workflow			
<i>Grayscale image batch processing</i>	No	No	Yes
<i>Segmented image batch processing</i>	No	Yes	Yes
<i>Automatic filament recognition</i>	No	Yes	Yes

2. Further FiNTA testing

2.1. Details for Filament Length and Connectivity

To quantify the accuracy of the Filament Length tracing by the FiNTA, the artificially created Connectivity images were modified such that no filament reached the edge of the image, to create a homogenous Filament Length distribution. The original images, traced images, and resulting Filament Lengths are illustrated in Figure S2A-D. Each of the different colors corresponds to a slightly different Filament Length, which depends on the total Filament Length distribution. The Filament Lengths calculated by the FiNTA strongly depend on the break-off angle set by the user. Therefore, the length histograms are shown for the four investigated images from 6° to 115° (0.1-2.0 rad) in Figure S2E-H. Independent of the angles within the investigated networks, the optimal break-off angles were between 17° and 26° (0.30-0.45 rad). This universal range of break-off angles that lead to the correct Filament Lengths can be reasoned on the basis that the angle between each of two connected nodes defines the break-off angle. Consequently, the angle between the filaments is independent of the break-off angle for the calculation of the Filament Length. The drawback of this method is that it increases the short false filaments, which occur at the junctions. In addition, the junctions can be ignored as intended, which leads to Filament Lengths that are multiples of the histogram peaks. Consequently, we suggest that the resulting histograms are always investigated carefully and the Filament Length optimized by thresholding. The analogous argumentation is valid for the Filament Count, as demonstrated in Figure S2I-L.

Despite the explained weaknesses of the Filament Length calculations, the FiNTA can measure the real Filament Length independent of the Junction Distance. We conclude that the Filament Length calculation by the FiNTA has to be further investigated by hand for more accurate results, although the histogram analysis provides correct results.

Junctions close to each other frequently result in incorrect Connectivities. Therefore, we implemented summarization of junctions to one junction. For this, the user needs to specify a unification distance. The FiNTA unites all of the junctions that can be connected by the number of steps specified by the unification distance. These are interpreted as one junction. One step is considered to be the distance between two nodes that are connected to each other.

2.3. Pointillism tests

Many algorithms are dedicated to the analysis of images using a specific technique or even from a specific network. In contrast, the FiNTA can be used to analyze networks imaged with any of the existing imaging techniques, as long as the filament thickness and brightness are relatively homogenous (see filament thickness in section 2.4. below) and the image type is grayscale.

Some imaging techniques result in pointillism-like signals, such as STORM. Depending on the sampling and post-processing, the distribution of signal points can vary. We tested the tolerance of the FiNTA to pointillism by creating images with increased black pixels on white filaments, analogous to the noise tests in Figure 4. Therefore, we increased the amount of black pixels on the white filaments from 0% to 100% (Fig. S3A). In addition, we varied the line thickness (see Fig. S5), and used the Mesh Hole Size and Count as quantification parameters. By calculating the percentage errors between the measured and expected Mesh Hole Size and Counts, we show that the FiNTA traces pointillism filaments very accurately (Fig. S3B, C). The larger the filament thickness, the more pointillism is accepted by the FiNTA. We conclude that the FiNTA can be used for any imaging technique that creates pointillism-like structures of networks.

2.4. Filament thickness

Initially, the FiNTA was implemented to quantify filament networks with uniform filament thicknesses. Nonetheless, the FiNTA has a tolerance regarding heterogeneous filament thicknesses. For quantification of this tolerance, an image was artificially created with 13 lines of different filament thicknesses, from 1 px to 13 px, in 1 px steps. Each line was connected to the following thicker line once. The connection line had the thickness of the thicker line (see Fig. S4A). In total, 29 different filament thicknesses were assigned to the FiNTA, from 2 px to 30 px, in 1 px steps. Figure S4B-E provides examples for assigned filament thicknesses of 2 px, 10 px, 20 px, and 30 px. Three parameters were tested here: recognition of filament thickness; accuracy of the traced filament thickness; and accuracy of the traced connection thickness.

The filaments recognized by the FiNTA are defined as the filaments that are traced at least for 90% of their full length. The tracing line can be anywhere on the filament (including at the edges), while double tracing of one filament is prevented. Here, the FiNTA can handle roughly $\pm 90\%$ of the assigned filament thicknesses (Fig. S4F).

The accurately traced filament thickness is defined as the recognized filament thickness, under the requirement that the tracing line is not on the edge of a filament (except when close to the connection). The FiNTA leads to correct tracing of up to 100% thicker filaments than the assigned filament thickness, and about 70% to 80% thinner filaments than the assigned filament thickness (Fig. S4G).

The accurately traced connection thickness is defined as the filament thickness of a connection filament for which neither multiple filament tracing nor tracing of the background occurs. The FiNTA leads to correct tracing of roughly 20% thicker connection filaments than the assigned filament thickness above a 5-px filament thickness (Fig. S4H). Below the 5-px filament thickness, more or less none of the filaments thicker than the assigned filament thickness were correctly traced. In contrast, the FiNTA leads to correct tracing of filaments that are between 60% and 86% thinner than the assigned filament thickness (the only exclusion was an assigned filament thickness of 2 px, because the smallest filament was 1 px thick). Consequently, although depending on the heterogeneity of the filament thickness of interest, if all of the filaments are to be traced, we would recommend to tend to over-estimation of the filament thickness than to under-estimation. In contrast, this effect can be very useful to discern between filaments of different thicknesses, as long as the difference is in the range of the filament thickness itself.

3. Biological material and methods

Cell culture

Immortalized retinal pigmented epithelium (hTERT-RPE1) cells were grown in Dulbecco's modified Eagle's medium (DMEM)/F12 medium supplemented with 10% fetal bovine serum (Thermo Fisher, MA, USA), 1% glutamax, and 1% penicillin/streptomycin under 5% CO₂ at 37 °C, in cell culture flasks (Cellstar, Greiner Bio-One, Austria).

For fluorescent imaging, hTERT-RPE1 cells stably expressing mEmerald-vimentin and mTagRFPT- α -tubulin (a kind gift from Gaudenz Danuser, Dallas, TX, USA) or mCherry LifeAct (a kind gift from Matthieu Piel, Paris, France) were placed in glass-bottomed dishes (Fluorodish; World Precision Instruments, Germany) and left to adhere overnight. Live cells were imaged at 37 °C and 5% CO₂ using laser scanning confocal microscopy (LSM 980; Zeiss, Germany).

Bjhtert SV40T V12 H-Ras¹ cells were cultivated at 37 °C in 5% CO₂ in DMEM (Sigma-Aldrich, Germany) supplemented with 10% fetal bovine serum (VWR, Germany) and 1% antibiotic/antimycotic solution (Invitrogen, Germany). The cells were harvested at approximately 30% confluence.

Baby hamster kidney (BHK-21) cells were cultured in DMEM/F12 supplemented with 5% fetal bovine serum and 1% penicillin/streptomycin under 5% CO₂ at 37 °C.

4. Fluorescence protocols and imaging

4.1. Fluorescence microscopy

For fluorescent imaging, RPE1 cells that stably expressed mCherry LifeAct (a kind gift from Matthieu Piel, Paris, France) were fixed in 0.5% paraformaldehyde and mounted with Fluomount-G mounting medium, with DAPI (FisherScientific, Germany). If not stated otherwise, the imaging was performed using laser scanning confocal microscopy (LSM 980; Zeiss, Germany).

4.2. Stochastic optical reconstruction microscopy

Bjhtert SV40T H-RasV12 cells were seeded onto glass coverslips that were pre-cleaned, as described previously². After 48 h, the cells were washed in phosphate-buffered saline (PBS) at 37 °C, and the autofluorescence and paraformaldehyde were quenched. The cells fixed in PBS with 3.7% paraformaldehyde and 0.2% Triton X-100 for 15 min at 37 °C, blocked, and immunostained with a mouse anti-vimentin antibody (V9; 1:50), followed by anti-mouse IgG Alexa 647 (1:400), as described previously². GLOX buffer was used, where 1 mL contained: 0.1 g glucose (in 10 µL), 100 µL glucose oxidase (at 0.005 g/mL), 100 µL cysteamine/MEA (at 1 M cysteamine/MEA), in 790 µL Tris/NaCl buffer (at 50 mM Tris, with 10 mM NaCl). Images were taken with a 20-ms exposure time for the N-STORM (Nikon), for a resolution of ~50 nm.

4.3. Stimulated emission depletion microscopy

BHK-21 cells were plated on coverslips coated with poly-L-lysine. The cells were fixed with ice-cold acetone for 10 min at -21 °C. The samples were washed with PBS, blocked using 5% goat serum in PBS for 1 h, and incubated with the anti-vimentin antibody (V9; 1:200) for 1 h at room temperature. After a further wash with PBS, the samples were incubated with Abberior Star Red (1:500) for 1 h. The coverslips were washed with PBS and mounted using Mowiol, for 12 h at room temperature. Image acquisition with STED microscopy was then performed (SP5-STED; Leica, Germany).

4.4. Expansion microscopy

The preparation for Expansion microscopy was performed following the protocol for cell culture of Tillberg and co-workers³. In brief, hTERT-RPE1 cells stably expressing mEmerald-vimentin and mTagRFPT- α -tubulin were fixed in 0.5% paraformaldehyde. Anchoring with Acylol-X was followed by *in-situ* polymerization with a hydrogel. The addition of water after the digestion (including with proteinase K) physically increased the sample size by a factor of 4.5, in all spatial directions.

5. Scanning electron microscopy preparation and imaging

All of the scanning electron microscopy images were obtained using an environmental scanning electron microscope (Quanta 400; FEI, USA).

5.1. Actin cortex

The preparation of the actin cortex of hTERT-RPE1 cells for the electron microscopy was similar to the protocols of Svitkina, Chugh, and others^{4,5}. In brief, the cell membrane was disrupted with Triton X-100, and the cells were lightly fixed, at the same time. After stronger fixing with glutaraldehyde and other fixation agents, the cells were dehydrated using a series of increasing ethanol concentrations. Hexamethyldisilazane was used as the final drying procedure before the samples were sputtered with 6 nm to 7 nm platinum. Images were taken at 5 kV under high vacuum conditions, using secondary electrons, with an Everhart-Thornley detector.

5.2. Mushroom braid

Wet mushroom braid was dried under ambient conditions and visualized at 10-kV accelerating voltage under low vacuum conditions (water vapor, 100 Pa) using secondary electrons, with a large field detector.

5.3. Eggshell

A piece of an egg shell was placed on double-sided carbon tape with the outer surface on top. Secondary electron imaging using a large field detector was performed at 10-kV accelerating voltage under low vacuum conditions (water vapor, 100 Pa).

5.4. Foam

A small piece of foam packaging was cut using a blade and fixed using double-sided carbon tape. The surface analysis was carried out at 5-kV accelerating voltage, under low vacuum conditions (water vapor, 100 Pa), using secondary electrons, with a large field detector.

5.5. Diatoms

Diatoms were placed on double-sided carbon tape and imaged at 10-kV accelerating voltage under high vacuum conditions using secondary electrons, with an Everhart-Thornley detector.

References

1. Hahn WC, Counter CM, Lundberg AS, Beijersbergen RL, Brooks MW, Weinberg RA. Creation of human tumour cells with defined genetic elements. *Nature*. Jul 1999;400(6743):464-8.
2. Hari-Gupta Y, Fili N, dos Santos Á, et al. Nuclear myosin VI regulates the spatial organization of mammalian transcription initiation. *bioRxiv*. 2020:2020.04.21.053124
3. Chen F, Tillberg PW, Boyden ES. Optical imaging. Expansion microscopy. *Science*. Jan 30 2015;347(6221):543-8.
4. Chugh P, Clark AG, Smith MB, et al. Actin cortex architecture regulates cell surface tension. *Nat Cell Biol*. Jun 2017;19(6):689-697.

5. Svitkina TM. Platinum replica electron microscopy: Imaging the cytoskeleton globally and locally. *Int J Biochem Cell Biol.* May 2017;86:37-41.

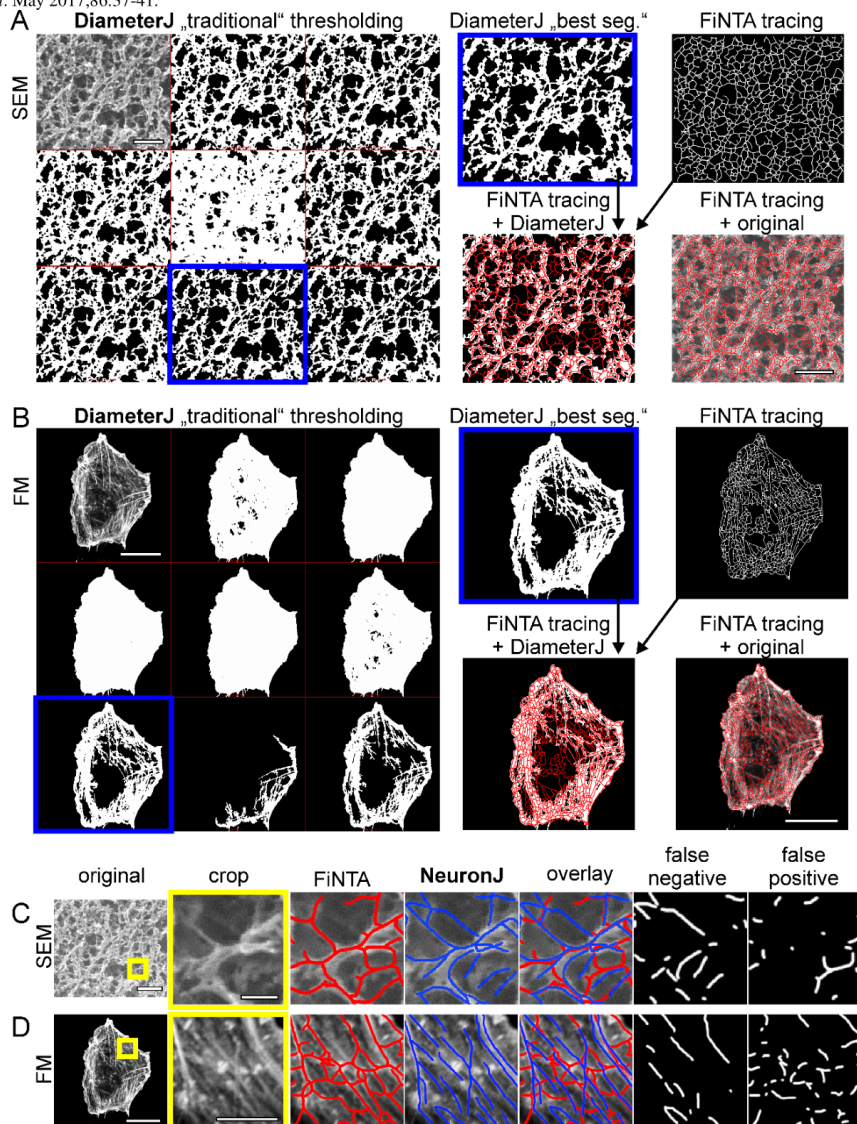


FIGURE S1. Comparison of DiameterJ, NeuronJ and FiNTA. (A, B) DiameterJ segmentation comparison with FiNTA tracing using the SEM image of Fig. 2A, Perinucleus, and the FM image of Fig. 7C. (C, D) NeuronJ comparison with FiNTA on the same images as in A and B. False positive and false negative refer to the differences in the FiNTA output compared to the one of NeuronJ. Scale bars: 500nm (A), 20µm (B), 500nm and magnification 100nm (C), 20µm and magnification 5µm (D).

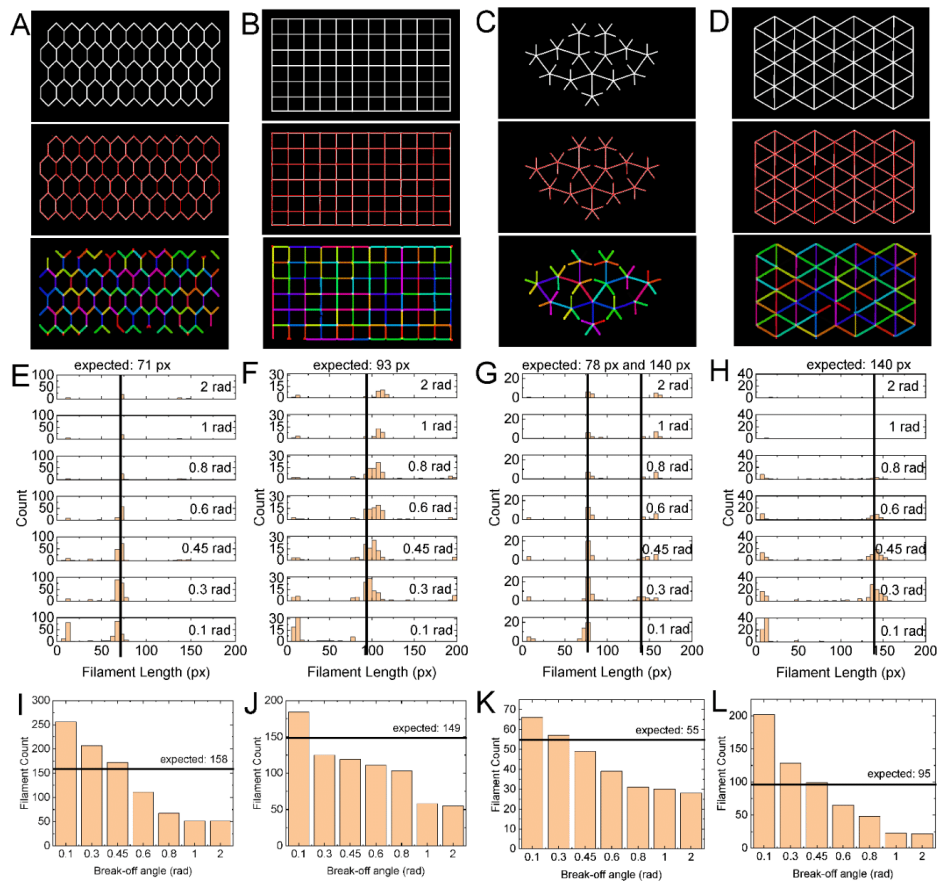


FIGURE S2. Filament Length tests. (A-D) The exemplary images used for the Connectivity tests (Fig. 4) were also used for these length tests, because of the high length homogeneity within each image. The traced images (second row) and color-coded lengths (third row) are also shown. The color coding was applied to better differentiate between the Filament Lengths. (E-L) Quantification of filament lengths (E-H) and filament counts (I-L) for each of the images in (A-D), respectively. Black lines, expected Filament Lengths (E-H) and Filament Counts (I-L).

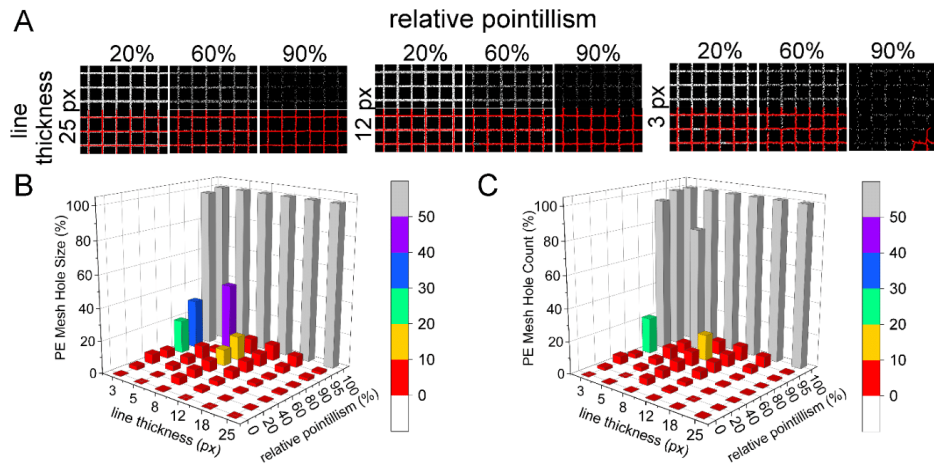


FIGURE S3. Mesh Hole Size determination by pointillism and line thickness. (A) Exemplary images of the traced Mesh Holes for the varied pointillism (amount of black pixels on white lines) and line thickness. (B, C) Percentage errors (PE) of the expected Mesh Hole Size (B) and Counts (C) *versus* the measured values, according to line thickness and signal-to-noise ratio.

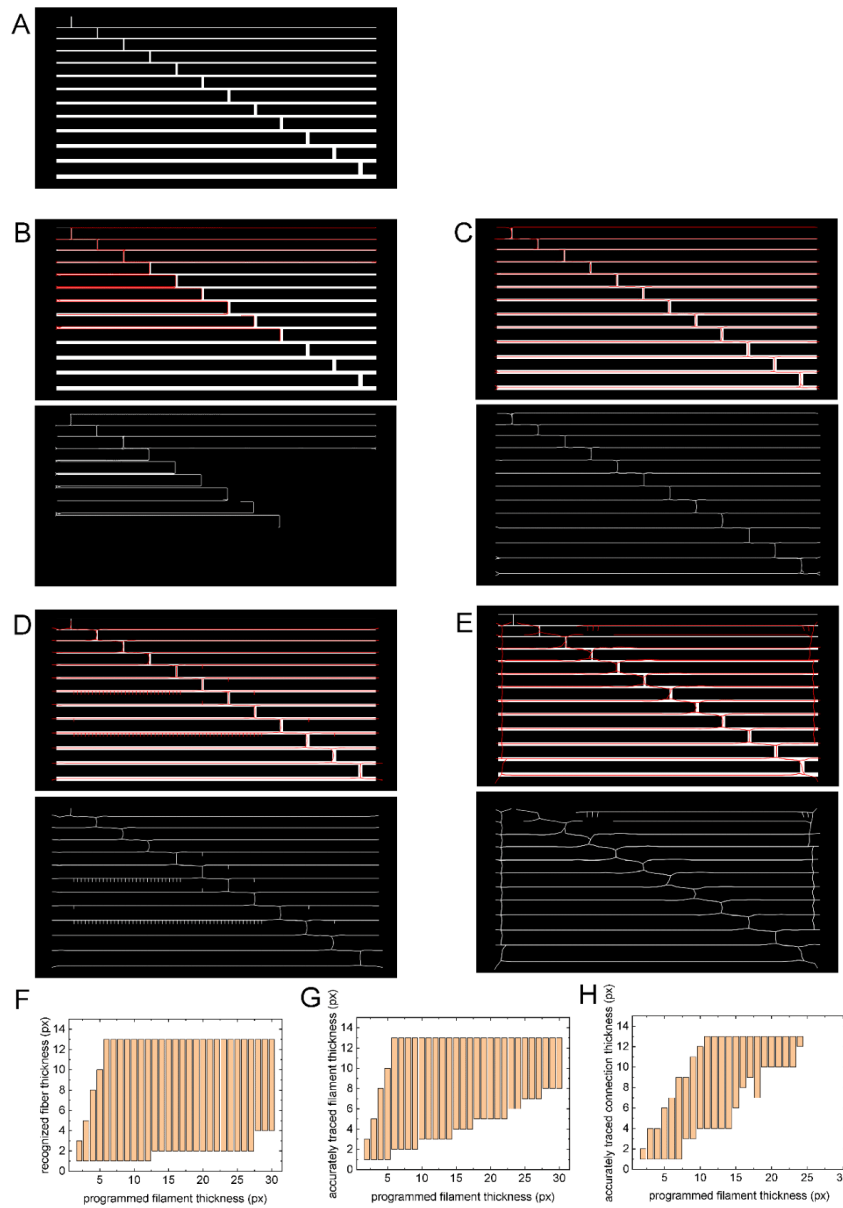


FIGURE S4. Filament thickness tests. (A-E) Exemplary images with lines ranging from 1 px to 13 px in 1-px steps (A), and their tracing (B-E). Each line is connected to the next thicker line by a connection with the thickness of the thicker line. (F-H)

Quantification of corresponding recognized fiber thickness (F) and the accurately traced fiber thicknesses (G) and connections (H).

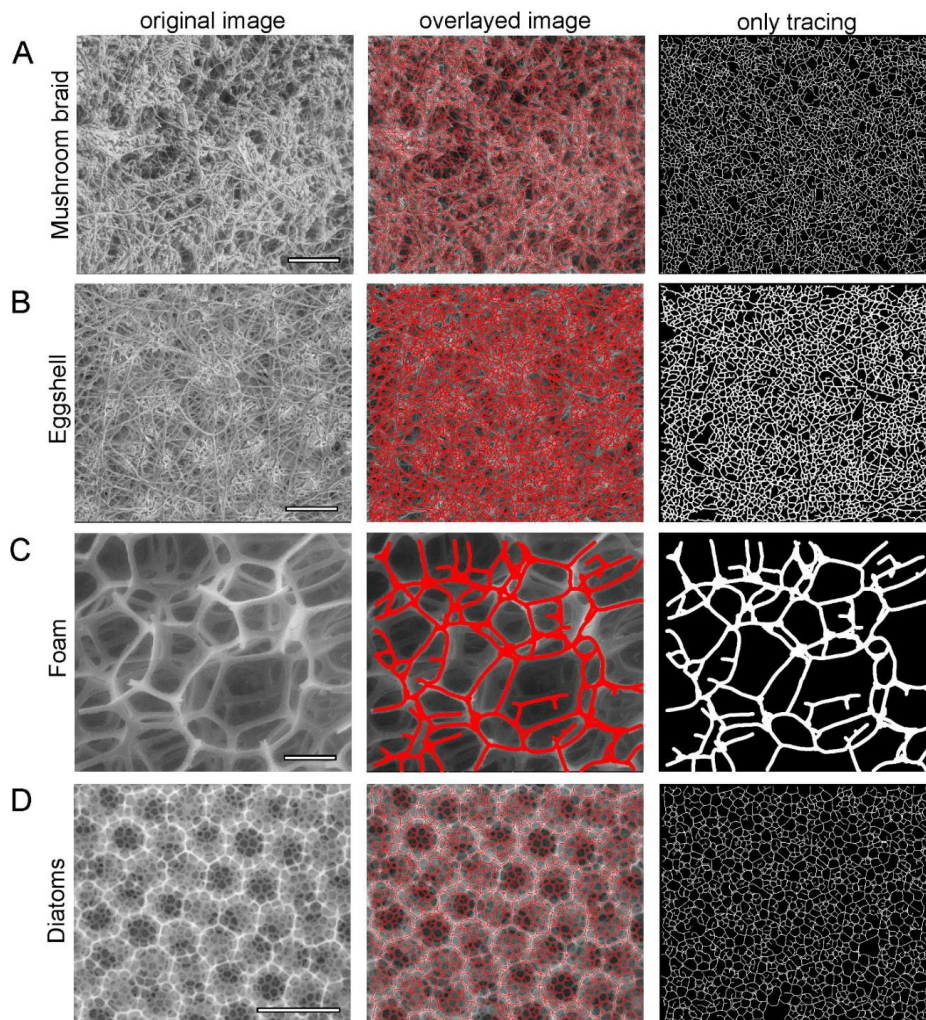


FIGURE S5. Tracing of various scanning electron microscopy images. Exemplary images and their tracing (as indicated) of mushroom braid (A), eggshell (B), foam (C) and a diatom (D). Overlayed image, overlay of original and traced image. Scale bars: 100 μm (A), 50 μm (B), 500 μm (C), 4 μm (D).

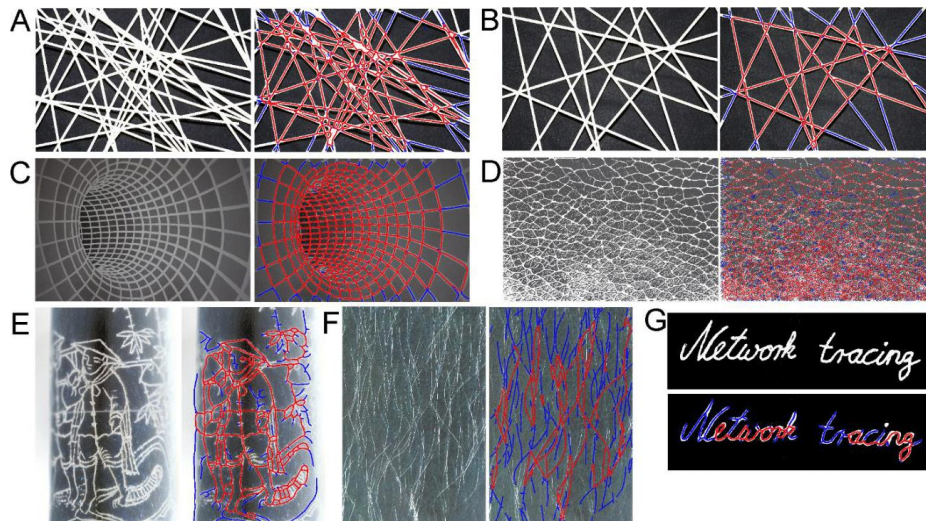


FIGURE S6. General examples of network tracing using the filament network-tracing algorithm (FiNTA). Exemplary images (left/top) and their tracing (right/bottom), for different kinds of networks using the FiNTA. All of the images were color modified for bright 'filaments' and dark backgrounds. The images shown are for: dense (A) and porous (B) networks of sticks of spaghetti; three-dimensional tunnel painted on a wall (C); the structure of leather (D); a line drawing of a person (E); human leg hairs (F); and handwriting (G). Red tracing, closed loops; blue tracing, open loops.